Thermal parameter optimisation for accurate finite element based on simulation of machine tools

By

Ayman Abuaniza

A thesis submitted to the University of Huddersfield in partial fulfilment of the requirements for the degree of Doctor of Philosophy

In the School of Computing and Engineering

Centre for Precision Technologies

October 2015

Copyright statement

i. The author of this thesis (including any appendices and/or schedules to this thesis) owns any copyright in it (the "Copyright") and he has given The University of Huddersfield the right to use such copyright for any administrative, promotional, educational and/or teaching purposes.

ii. Copies of this thesis, either in full or in extracts, may be made only in accordance with the regulations of the University Library. Details of these regulations may be obtained from the Librarian. This page must form part of any such copies made.

iii. The ownership of any patents, designs, trademarks and any and all other intellectual property rights except for the Copyright (the "Intellectual Property Rights") and any reproductions of copyright works, for example graphs and tables ("Reproductions"), which may be described in this thesis, may not be owned by the author and may be owned by third parties. Such Intellectual Property Rights and Reproductions cannot and must not be made available for use without the prior written permission of the owner(s) of the relevant Intellectual Property Rights and/or Reproductions

Abstract

The need for high-speed/high-precision machine tools is swiftly increasing in response to the growth of production technology that necessitates high-precision parts and high productivity. The influence of thermally induced errors in machine tools can have a much greater influence on the dimensional tolerances of the final products produced as compared to geometric and cutting force errors. Therefore, to maintain high accuracy of machine tool, it requires an accurate method of thermal error control or compensation using a detailed model.

The thermal errors of machine tools are induced by the propagation of heat through the structure of the machine due to excitation of internal and external heat sources such as belt drives, motors and bearings. There has been significant research effort to model thermal errors of machine tools in recent decades. The utilised techniques have proved their capabilities with excellent thermal prediction and compensation results but they often involve significant effort for effective implementation with constraints for complexity, robustness, and cost.

One of the most significant drawbacks of modelling machine behaviour using Finite Element Analysis (FEA) is the difficulty of accurately obtaining the characteristic of heat transfer, such as heat power of machine tool heat sources and the various boundary conditions.

The aims of this research to provide reliable techniques to obtain heat transfer coefficients of machine tools in order to improve the accuracy of FEA simulations. FEA is used to simulate the thermal characteristics of spindle system of small Vertical Machining Centre (VMC) using SolidWorks Simulation software.

Most FEA models of machine tools employ the general prediction technique based on formulae, provided by OEMs, to identify many of the boundary conditions associated with simulating thermal error in machine tools. The formulae method was used to identify the heat transfer coefficients of a small VMC feed drive system. Employing these values allowed FEA to be used to simulate the thermal characteristics of the feed drive model. In addition, an alternative efficient methodology, based on energy balance calculations and thermal imaging, was used to obtain the heat transfer coefficients of the same feed drive system. Then the parameters obtained were applied to the FEA model of the system and validated against experimental results. The residual thermal error was reduced to just 20 % when the energy balance method was employed and compared with a residual of 30 %, when the formulae method was employed.

The existing energy balance method was also used to obtain the heat transfer coefficients of the headslide on a small VMC based on thermal imaging data. Then FEA model of the headslide of VMC was created and simulated. There was significant reduction in the thermal error but significant uncertainties in the method were identified suggesting that further improvements could be made.

An additional novel Two Dimensional (2D) optimisation technique based on thermal imaging data was created and used to calibrate the calculated heat transfer coefficients of the headslide of a small sized machine tool. In order to optimise the heat power of various heat sources, a 2D model of surface temperature of the headslide was created in Matlab software and compared against the experimental data both spatially across a plane and over time in order to take into account time varying heat loads. The effectiveness of the technique was proved using FEA models of the machine and comparison with test data from the machine tool. Significant improvement was achieved with correlation of 85 % between simulated thermal characteristics and the experimental data.

Table of Contents

List of tables

List of figures

Acknowledgements

This thesis was written while I was sponsored by Libyan government to study a PhD degree in the Engineering Control and Machine Performance Group of the University of Huddersfield. I am very grateful to all of them for their financial and academic support. Without their support I would have been unable to write this thesis.

I would like to express my most sincere gratitude to my supervisors Dr. Simon Fletcher and Dr. Andrew Longstaff for supervising the project and providing me with support and guidance throughout the project period.

Additionally, I would like to thank all members of the Engineering Control and Machine Performance Group for providing assistance when required. Sincere thanks also to the laboratory staff who provided technical assistance.

Most importantly I would like to thank my family, especially my parents, my brothers and my sisters, for their constant support through what has been a busy and difficult journey.

Last, but not least, I would like to thank all my friends and colleagues who have helped in many ways, both professionally and personally.

Ayman Abuaniza

October 2015

Chapter 1

1 Introduction

In machining operations, the precision of the product dimensions depends on the accuracy of the relative position between the tool centre point and the workpiece. The most significant errors which affect machine tool accuracy can be categorized as (1) geometric errors, (2) thermal errors (3) Non-rigid body errors and (4) dynamic errors [1] and these will be described in more detail in the following sections. It is common practice in modern manufacturing industry that some form of geometric error compensation is applied which means that often the most significant are thermal errors, typically accounting for between 40 % and 70 % of the overall positioning errors [2]. Therefore the ability to understand and predict these errors through simulation is very important and motivates this work.

1.1 Geometric errors

Geometric errors are inaccuracies due to the mechanical imperfections of the machine tool structure and the misalignments of the machine tools elements, which affects the final production. These geometrical inaccuracies change steadily during the lifetime of a machine due to wear and settling of, for example, the machine tool foundations. This type of error can be quantified and compensated during the life time of machine tool [1]. The effect of the geometric imperfections is to cause errors such as squareness and parallelism between the machines moving elements which produce small, unwanted error motions of each of the moving elements.

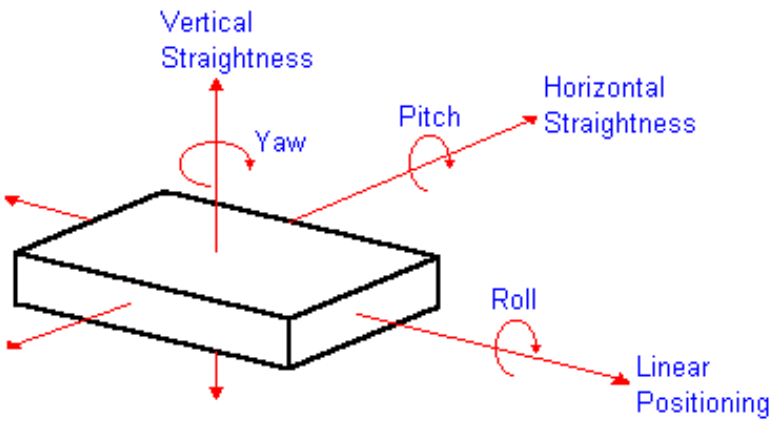

Figure 1-1 Six degrees of freedom of a machine tool axis

An ideal slide without unwanted movements would have only one degree of freedom to produce rectilinear motion. In practice, it will reveal movement in all six possible degrees of freedom causing three translational error components and three rotational components as shown in Figure 1-1. The translational error components are known as linear positioning error, horizontal and vertical straightness errors. The rotational errors are known as roll, pitch and yaw. Furthermore, for a standard three-axis machine tool, there are three squareness errors. This results in twenty one sources of error which are three axes with six degrees of freedom and three squareness, however, a few of the errors do not normally affect the positioning accuracy of three-axis machine tools [2].

1.2 Non-rigid body errors

Non-rigid body errors occur as a result of loading the machine structural elements [3;4] These errors can have an effect on the machine tool accuracy and have a number of causes:

- Weight of the workpiece, heavy workpiece on the machine table produces loading of the structure, which might cause deformations because of the movement during machining process.

- Machine axes movement, the machines own weight can be significant and movement of the machine axes causes a new weight distribution on the machine structure, resulting in distortion and an effective change in the geometric mechanical parts error.
- Cutting load, forces due to the cutting process present loading into the machine structure. Moreover, deep cuts of the workpiece can produce large errors.
- Inadequate machine tool fixture stiffness.

Fixtures stiffness is usually relatively high compared to the machine tool structure. However, this might not true for large or complex workpieces, as fixture design becomes intricate and a smaller amount of material is used for clamping.

1.3 Thermal errors

Due to the demand for tight tolerances on parts manufactured on machine tools, thermal errors become more substantial, in some cases accounting for up to 70 % of the total error of a machine tool [2].

While the geometric errors are mostly systematic and therefore relatively easy to compensate, the thermal problem is much more complicated as the amount of generated heat internally will vary significantly based on how the machine is used and external heat sources vary greatly depending on the environment in which the machine is located. This is compounded by the many different machine tool parts, materials, joints and arrangements. The distortions of several structural elements contribute to the total thermal movement in a particular axis direction. Each part may have different heat sources and has a different thermal time constant, causing different levels of non-linear distortion. All these factors contribute to the complexity of the thermal errors.

Thermal errors in machine tools result from temperature gradients in the machine tool structure. Variations in the temperature arise from heat sources which can be categorised into

internal heating, external environmental variations and radiation. In Figure 1-2 is shown an overview of the various heat sources. The temperature increase leads to non-linear thermal expansion of structural elements and ultimately a complex interaction between the tool and workpiece.

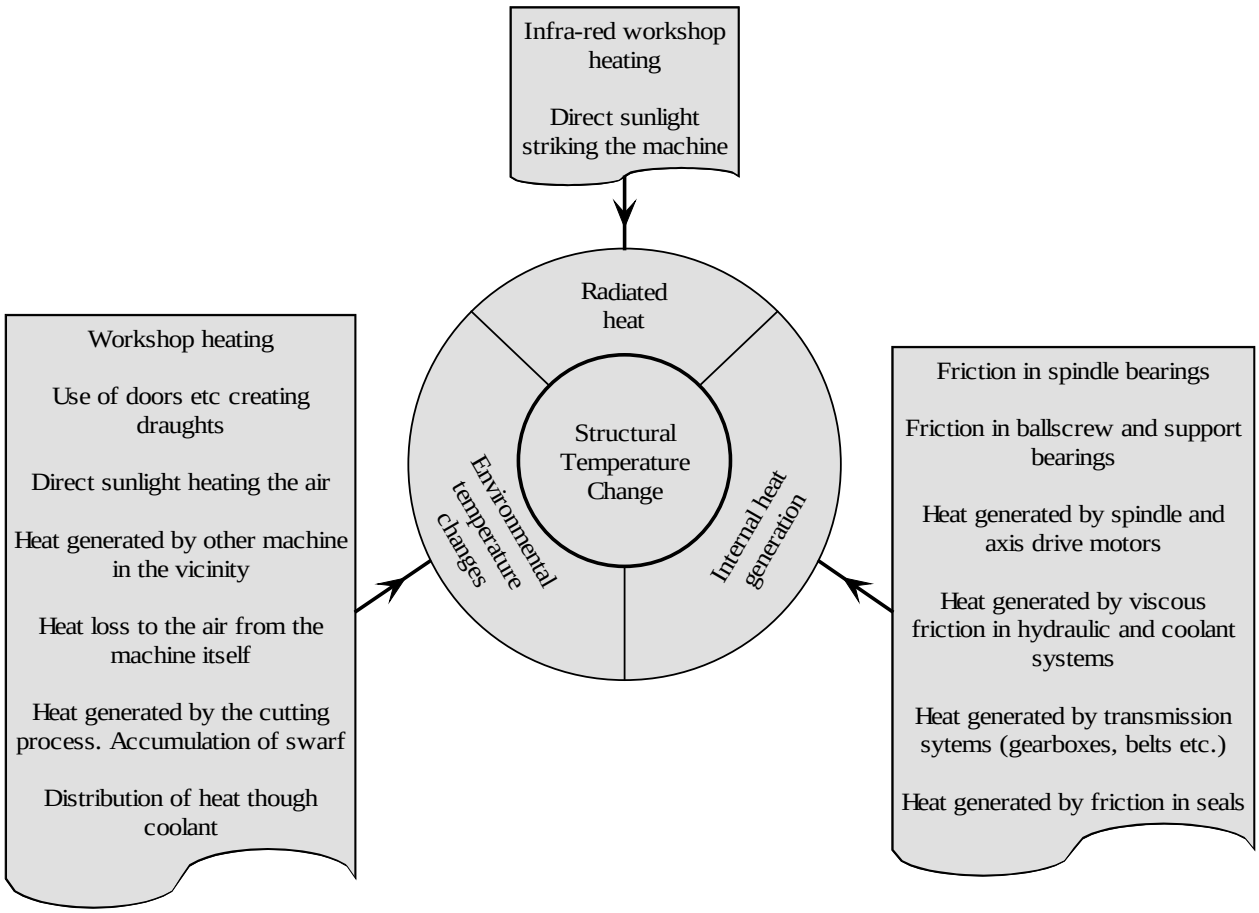

Figure 1-2 Machine tool sources of heat [5]

1.3.1 Internal Heat Sources

Internal heat sources are all sources that directly connect to the machine tool structure such as bearings, motors, auxiliary units and feed drives [6-8]. Heat generated in machine tool structure comes from power losses due to frictional and electrical effects. Figure 1-3 shows a headslide of machine tool and its thermal image due to internal heat source exciting.

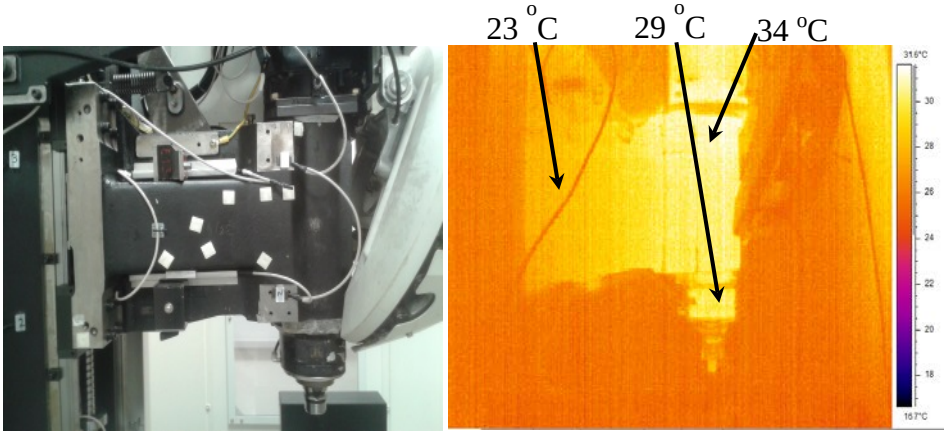

(a) (b)

Figure 1-3 (a) Headslide of machine tool, (b) Its thermal image

1.3.2 External Heat Sources

External heat sources are related to the environment in which the machine is located. The main effect on the machine is the change of the environmental temperature throughout the day and night cycle, also through seasonal extremes from summer to winter. Moreover, the spatial change is important, as the air temperature changes with the height above the ground [8], and it can also be influenced by machines in the vicinity, opening/closing of the machine shop doors and so forth. Radiated heat from workshop heaters and the sun can also seriously affect the machines structure temperature and environment. Such external heat sources and their effects may also require consideration for subsequent processes on high-precision parts such as in-process or post-process inspection. ISO standard 230-part three provides techniques to identify thermal effects on machine tools due to internal and external heat sources.

The thermal errors of machine tools are tackled in many different ways, which can be categorised into either 1) minimising heat generation, 2) minimising the effect of heat generation and loss, 3) error compensation. These three categories are discussed in more detail later.

1.4 Determination of thermal effects on machine tools

ISO 230, part 3 [2] provides three main test setups for the determination of thermal effects on machine tools:

- Environmental Temperature Variation Error (ETVE).
- Thermal distortion caused by rotating spindle. (spindle rotation)
- Thermal distortion caused by linear motion of axes.

It is required to measure the thermal effects over as wide a range of representative thermal conditions as the machine is expected to experience in its lifetime.

1.4.1 Environmental Temperature Variation Error (ETVE).

This ETVE test is intended to reveal the effects of environmental temperature changes on the machine and to predict the thermal error. It may also be used to assess the thermal error during other measurements, where the environmental temperature is in most industrial cases not constant. The environmental temperature should be controlled to the acceptable range that gives sufficient accuracy. A test setup example for a vertical spindle machining centre is shown in Figure 1-4 . Other setups for different machine types can be found in the standard [2].

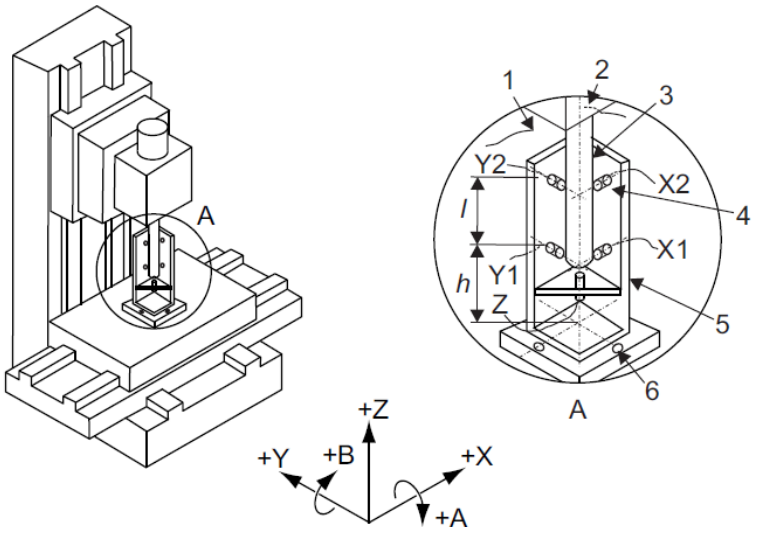

Figure 1-4 Measurement setup for thermal drift during ETVE and spindle rotation [2]

Key: 1 ambient air temperature sensor; 2 spindle bearing temperature sensor; 3 test mandrel; 4 linear displacement sensors; 5 fixture; 6 fixture bolted to table;

From Figure 1-4 it can be seen that there are five linear displacements sensors, and two temperature sensors. Three linear displacement sensors (X1, Y1, Z) are used to sense the translation in X, Y and Z which can be measured simultaneously. The additional two sensors (X2, Y2) can be used to compute the rotation about A and B. The results of displacements and temperatures could be plotted in order to analysis the results.

1.4.2 Spindle Rotation

This test is performed to measure the thermal distortion caused by the heat generated when the spindle is rotating. The same test setup for the ETVE test is used, shown diagrammatically in Figure 1-4 and in the photo on a large machine tool in Figure 1-5. The displacement sensors must not contact the test bar, therefore non-contact displacement sensors (NCDTs) such as capacitance or inductive sensors for example are used. This enables the thermal distortion to be measured while the test bar is rotating at high speed. In this case, the influence of test mandrel run-out has to be treated by using a low-pass filter. The test

regime is detailed in ISO 230-3, typically the test runs for about four hours, until the error does not vary more than 15 % during the last hour. This includes a period of running the spindle at constant speed or at varying speeds depending on the requirements and a period of cooling stage (spindle stopped) [2].

A typical constant speed result is shown in Figure 1-6 from a large machine located in an aerospace company. The development of the error has an exponential curve indicating a time constant for the machine where it stabilises. It is also quiet common for the machine to be symmetrical in at least one direction, in this case the X-axis direction which results in negligible error.

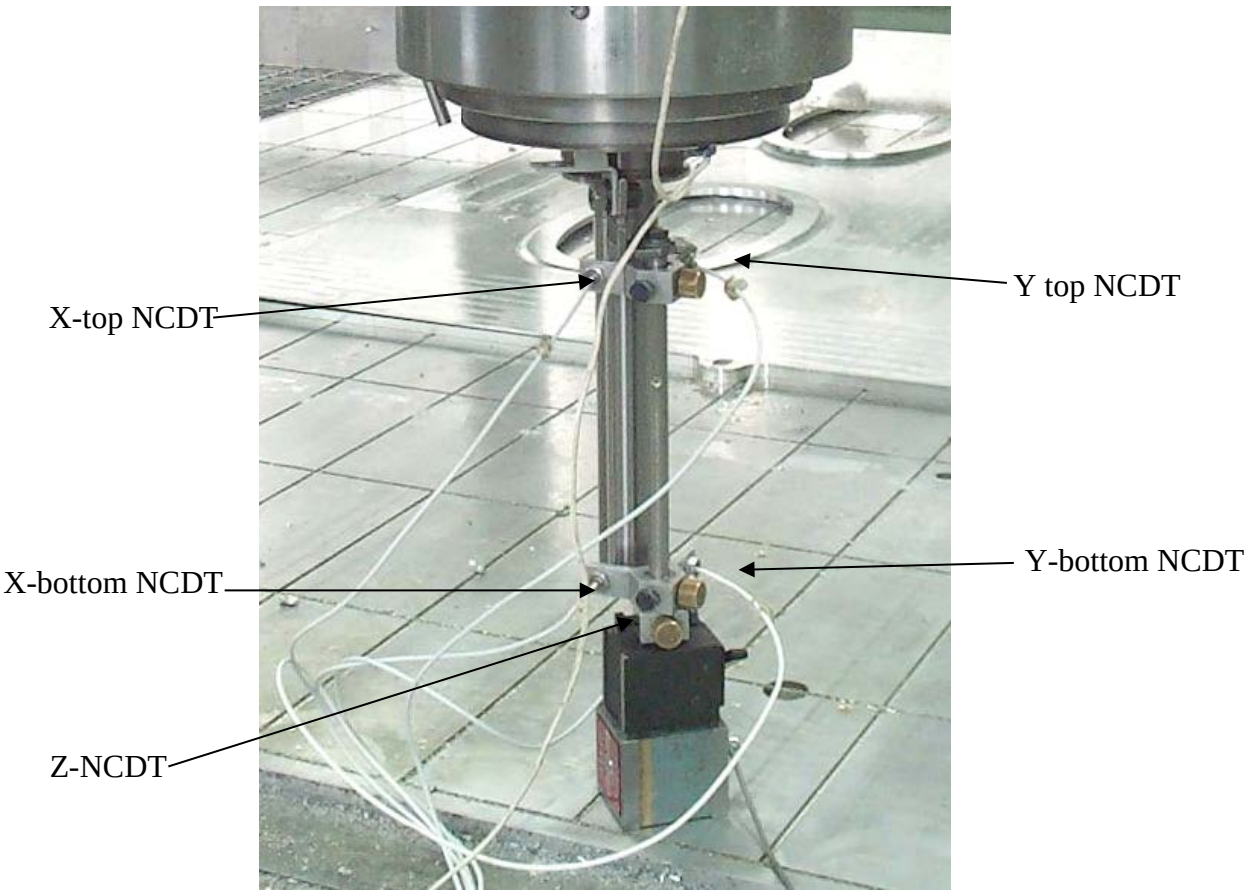

Figure 1-5 Spindle analyser set-up on long mandrel

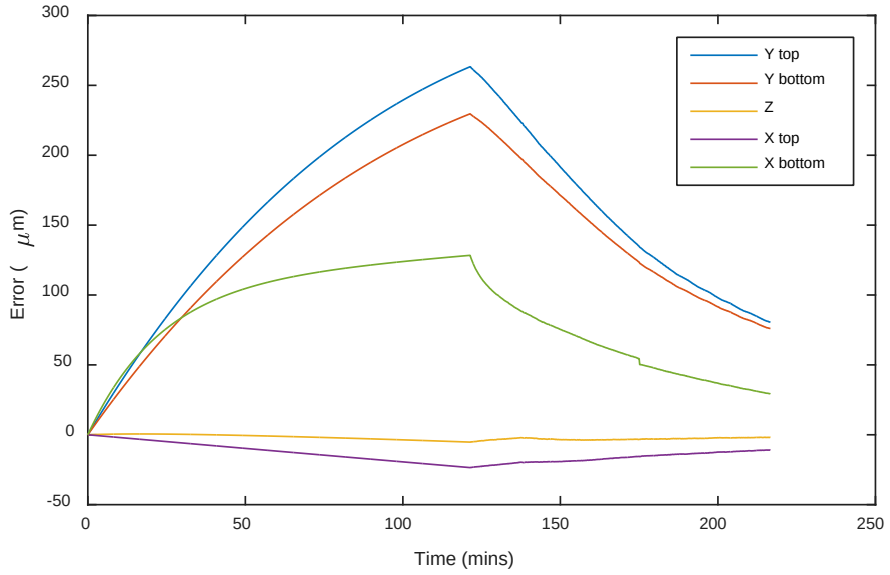

Figure 1-6 Example thermal error caused by spindle heating and cooling

1.4.3 Linear Motion of axes

When the linear axes move, the heat is generated by the machines positioning system which includes

- Support bearings
- Feed drives (motors)
- Ball screws
- Guideways

This test is performed at different axis positions in order to analyse the deformation of the machine structure due to the heat and elongation of the positioning system. A typical test setup is shown in Figure 1-7. It involves of two setups with five probes, in this case the thermal distortion can be measured at these two positions. Other measurement setups can also be found in the standard ISO 230-3 [2].

The guidelines for the duration of the test are the same as for the spindle rotation. The measurement starts at setup position P1 shown in Figure 1-7, where the machine stops long

enough to record the displacements. Then the machine shall move to setup position P2 shown in Figure 1-7, where again the displacements are recorded. Next the movement is reversed, towards setup P1, where again displacements are recorded. This cycle is repeated up to the end of the test duration. Temperature of the various heat sources changes with the feedrate and stop periods leading to different displacement measurements. Therefore these displacement figures have to be documented. To measure the cool down displacement, it is suggested to stop the machine in the middle of the movement and then readings are taken at both setups positions every five minutes. The machine tool displacement and temperature gradient can be recorded using other equipment such as laser interferometry (see Section 1.5.1).

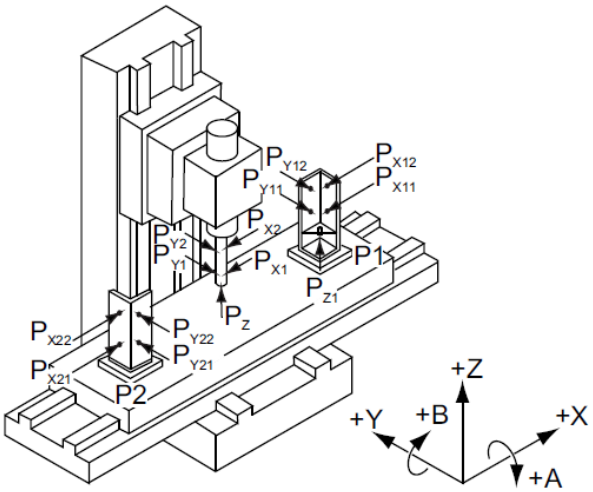

Figure 1-7 Measurement setup for the thermal drift during linear axis movement [1]

The measurement of thermal errors of machine tools as described above has two parts: temperature measurement and displacement measurement with the latter shown in the diagrams and occurring due to the aforementioned issues such as temperature increase and element motion. In order to understand the cause of the error, comprehensive and accurate temperature measurement is also important.

1.5 Thermal error and temperature measurement

Experimental tests provide practical and reliable data about the temperature gradient and thermal error of machine tools which can be used for thermal error modelling and compensation. The temperature gradient of machine tools structure may be under taken using thermal imaging camera.

1.5.1 Thermal error measurement

During machine tool thermal error testing, the aforementioned non-contact displacement sensors including the capacitance sensor, laser triangulation, eddy current sensor, etc. are the most used instruments [10]. The tests set up and sensors locations are explained in Section 1.4.1, 1.4.2 and 1.4.3. [9;10]

A laser interferometer system is also used to measure machine tool deformation [11;12]. The system provides a number of different measurement options, such as: linear positioning accuracy, angular pitch and yaw of an axis.

For machine axis thermal error, the most common measurement performed is linear measurement with the laser interferometer. The advantage is that intermediate positions can be measured to detect in more detail the effect of temperature on the accuracy. The linear measurement set up is shown in Figure 1-8 [13].

This equipment and methodology was used extensively in this work and entails 5 main parts: (1) laser head (2) linear optics kit together with linear interferometer and linear reflector (3) environmental compensation unit for air humidity, air temperature, air pressure and material temperature measurements (4) data logger software (5) data link cable. Typical accuracy of this measurement device is ± 0.5 ppm during a time of 1 min. This indicates that the uncertainty of displacement measurement of laser interferometer is ± 0.01 µm.

During set-up, the laser beam is aligned to avoid dead path and cosine errors. To obtain precise results, the laser interferometer readings must be amended for air humidity, air

temperature and air pressure which affect refractive index of the medium (air), which in turn influence the wavelength of the laser beam. The sensor output is read by computer automatically and computing the environmental compensation for acquired laser data. The Edlen's equation is used for compensation:

$$\mathrm{CLR} = \mathrm{LDR} + \mathrm{K_t}(\mathrm{T_m} - 20) - \mathrm{K_p}(\mathrm{P_m} - 760) + \mathrm{K_h}(\mathrm{V} - 10) \qquad 1.1$$

Where CLR is the Corrected Laser Reading, LDR the Laser Display Reading, K_t the coefficient of refractive index change due to environment temperature (0.93 ppm /8C), T_m the mean air temperature, K_p the Coefficient of refractive index change due to environment pressure (0.36 ppm/mm Hg), P_m the air pressure, (mm Hg), K_h the coefficient of refractive index alteration due to environment humidity (0.05 ppm/mm Hg), V the Partial pressure of water vapour, (mm Hg).

Throughout X-axis linear positioning error measurements, the linear interferometer was attached to spindle while reflector was mounted on the table, see Figure 1-8. The machine was programmed to travel in equal intervals (equal distance) in designated axis direction and dwelled for sometimes (seconds) to measure machine's linear displacement (positioning) errors. Measurement cycle of Computer Numerical Control (CNC) machine tool part program entails a sequence of moves beginning at one limit of the axis in forward direction, extending to the opposite limit, and going back to the beginning position in reverse direction (r). Linear positional errors as well as the temperature and air pressure/humidity readings were documented during laser measurement cycles [11]. Figure 1-9 shows feed drive displacement measured by the sensor nest shown in Figure 1-7, whereas Figure 1-10 shows the additional detail captured using the laser interferometer by recording the error at multiple positions along the axis, it is possible to determine the error caused by structural deformation and expansion of the feedback device such as ball screw or linear scale.

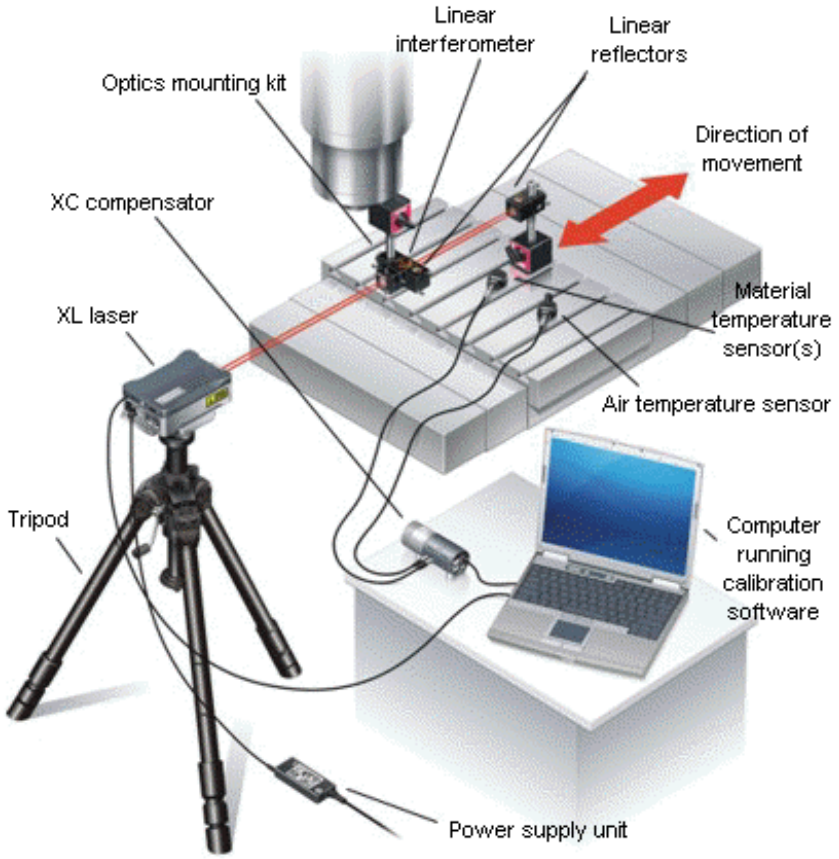

Figure 1-8 Laser interferometer linear measurement set up [12]

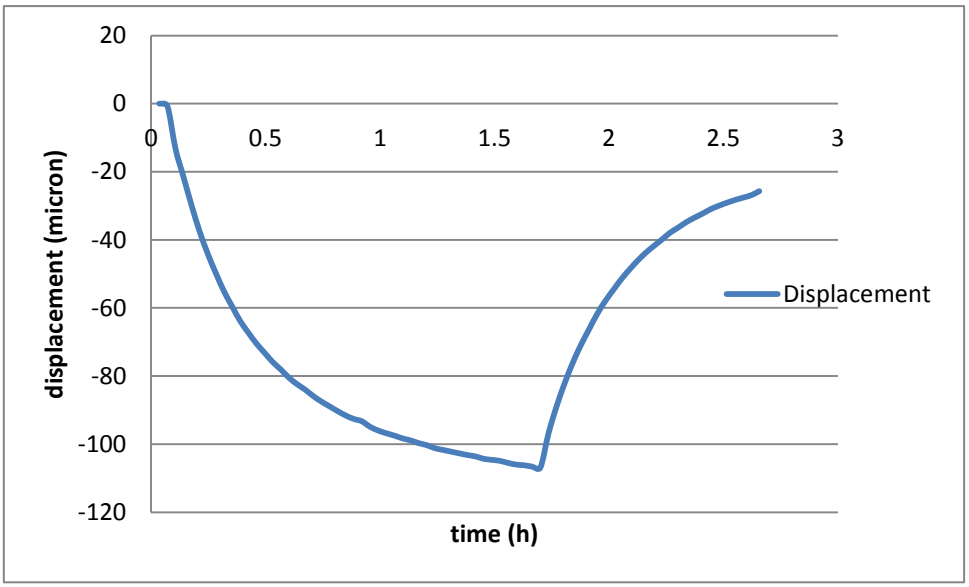

Figure 1-9 Feed drive displacement measured by sensor nest

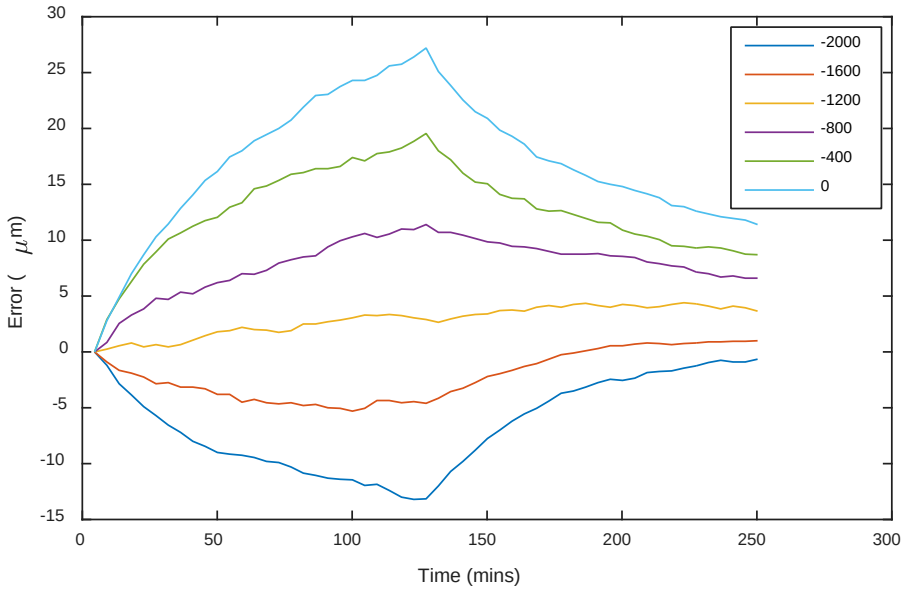

Figure 1-10 Feed drive displacement measured by laser interferometer

1.5.2 Temperature measurement of machine tool

The most common method to measure surface temperature of machine tools is using contact temperature sensors, such as resistance thermometers (Pt100, Pt1000) and thermocouples [15]. These sensors are attached on the surface of the machine tools to record the temperature gradient. However, these sensors are contact measuring devices, which means that these sensors must be positioned on the machine tool structure. This becomes inconvenient and dangerous on moving components on the machine tool such as the axes and impossible on rotating parts such as the spindle or ball screw [10]. In order to maintain normal operation of the machine, cables may need routing through axis drag chains and this can be difficult to achieve and can cause signal interference depending on the type of sensor used.

Non-contact temperature measurement methods such as infrared pyrometry or thermal imaging become a common method to measures surface temperature gradient on moving/rotating parts of the machine. A Flir Therma CAM S65 thermal imaging camera was used in this research as it can observe higher spatial temperature distribution within the structure and locate the heat sources [13]. This camera has a thermal sensitivity of 0.08 °C

and an accuracy of ± 2 °C however; much higher accuracy of about ± 0.5 °C can be attained with careful set-up. Therefore, uncertainty in the temperature gradient measured in this research is ± 0.5 °C. The Flir camera is shown in Figure 1-11 [16].

An infrared camera measures and images the emitted infrared radiation from any object. This radiation is a function of object surface temperature which makes it possible for camera to calculate and display temperature. The emitted radiation measured by the thermal imaging camera does not depend only on the surface temperature, it depends on many other parameters such as emissivity, humidity, distance between the camera and object and environment temperature. The most important parameter to set correctly is the emissivity. The emissivity is a measure of how much radiation emitted from an object compared to black body [17].

Infrared thermography is a non-destructive analysis method that can be broadly used due to the outstanding advantages that it offers in a number of applications and specifically in the assessment of structural materials [18;19]. Thermal imaging cameras have been broadly used for condition monitoring of machinery [20-23]. Rumsey et al [24] indicates that thermal imaging camera can be used for condition monitoring of wind turbine structures to avoid early failure of the turbine blades throughout operation. Picazo-Ródenas et al [25] used thermal imaging camera to measure a motor temperature gradient and then the infrared data was used to build a thermal model. Fletcher et al [16] reported that thermal imaging is an important temperature assessment that solves many practical problems associate with rotating parts. A thermal imaging system was used to capture images on a time basis while the heat sources of machine tool are excited. The numerical analysis of thermal imaging camera data can enables accurate determination of the temperature of a point or a region.

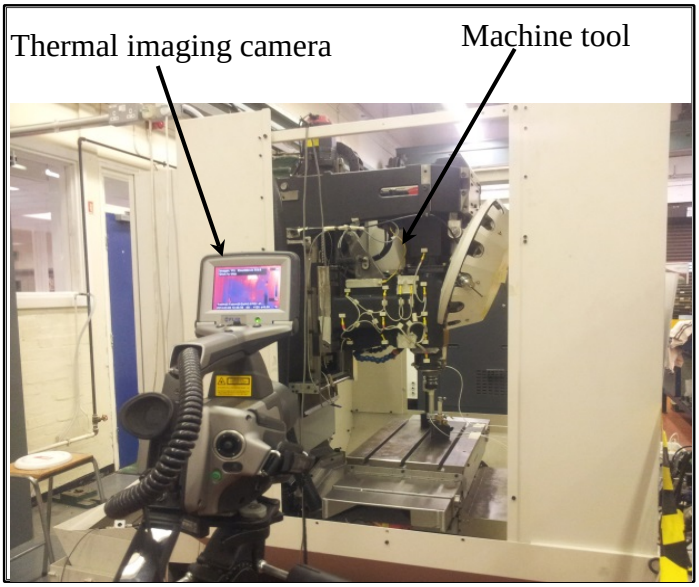

Figure 1-11 Infrared thermography using a Flir S65 thermal imaging camera

Thermal imaging camera can be used as an effective tool on time basis to monitor temperature gradient of machine tool for real-time with non-contact way. It provides pertinent information regarding the temperature rise which is very important to calculate machine tool displacement using numerical methods.

1.6 Thesis organisation

This thesis is laid out as follows:

Chapter 2- This chapter will present previous work to minimise thermal errors in machine tools components. Number of methods to minimise thermal error of machine tools is discussed. In general, thermal error reduction can be divided into three categories: 1) Thermal error avoidance which can be implemented in the design stage such building machine tools from material that has low expansion coefficient. 2) Thermal error control. This method can be used to reduce thermal error in exciting machine tools by heating up or cooling down machine tool component. 3) Thermal error compensation. This method is widely used as it not as costly as the first and second method. Prior to compensation, thermal error has to be modelled. Number of thermal model methods discussed such as Artificial Neural Networks

(ANN), Multivariable Regression Analysis (MRA) and Finite Element Analysis (FEA) method. The research aim and objectives discussed towards the end of this chapter.

Chapter 3- This chapter explains the heat transfer modes: conduction, convection and radiation which take place once an object is heated. Then a methodology of calculating heat power of heat sources was discussed. Two methods were presented to calculate heat power of heat sources: formula method and energy balance method. In formula method, heat sources are computed using equation provided by manufacturer while in energy balance method, heat power is calculated based temperature gradient and material properties of an object. The temperature gradient can be measured using thermal imaging camera. The different methods to calculate Thermal Contact Resistance (TCR) at machine tool joints were explained as well.

Chapter 4- This chapter present single and assembly benchmark simulation in order to check the reliability of heat power and TCR calculation methods. It also presents the Computer Aided Design (CAD) model of machine tools and the heat sources of machine tools were identified. The CAD model was meshed using suitable mesh as preparation for simulations.

Chapter 5- In this chapter the experimental set up and simulations of primary internal heat sources for a typical machine tool which are the axes and main spindle discussed.

It started with X-axis heating experiment set up as due to the practicality of installing sensors and monitoring the drive system components with the thermal imaging camera. The heat power calculated using formula method and energy balance method. After that A CAD model of the X-axis was created and simulated twice using parameters from formula and energy balance method.

The spindle heating experiment set up was conducted and heat power calculated utilising energy balance method as it gives good correlation. A CAD model of the headslide created

and simulated using. Good correlation was obtained between the simulated and experiment data.

Chapter 6- A novel optimisation method to optimise heat power of heat sources is presented in this chapter. The method was checked for reliability by set up a test rig which comprises steel plate, temperature controllers, thermocouple sensors, relays, power supply and thermal imaging camera. The temperature gradient of the plate was extracted as an array. This data was used to fit Two Dimensional (2D) heat transfer model which created using second order of heat transfer differential equation, in order to minimise error the sum-of-the-squares error between the experimental data (thermal images data) and simulated data (2D model). This method was applied on a headslide of machine tool to find the optimal heat power of its heat sources.

Chapter 7- Outlines the conclusions drawn and the suggestions for future work.

1.7 Summary

Reduction of machining accuracy is one of the most significant problems that machine tools users face under precision machining conditions due to geometric, non-rigid and thermal deflections of the machine tool structure. Previous research and publications have indicated the significance of thermal errors over the past decade and as electronic compensation for geometric errors becomes standard, the prevalence of temperature related accuracy problems will increase. It is therefore essential both practically and theoretically to study how to accurately simulate the thermal error of the machine tools and thermal error reduction and control is a major challenge accepted all over the world.

In order to identify the machine tool thermal error, the temperature increase and displacement of the tool relative to the workpiece must be measured. In the literature various techniques

can be employed to measure both of them, such as infrared thermal imaging camera and capacitance sensors.

Manufacturers of machine tool have been attempting to reduce the thermal displacement typically through careful design and more recently using electronic compensation employing various methodologies in order to improve the machine tool accuracy. In the next chapter, the previous research work performed to reduce these thermal errors will be reviewed as well as reviewing results obtained as part of this work on thermal errors and specifically the capability of thermal compensation installed on some new machine tools. This provides both the academic and industrial perspective on progress on thermal error reduction.

Chapter 2

2 Literature review

It has been stated that thermal errors represent the largest proportion of errors within the machine tool, about 70 % [2]. This figure has been quoted for many years but has been found to be reasonable based on results obtained during this work and previous research. Thermal errors in most cases produce nonlinear deformations due to uneven temperature gradients through machine structural elements.

Thermal errors in machine tools can therefore be significant and complex in nature and this has led to a variety of different ways of error analysis and reduction tactics being developed. A number of these methods are based on years of empirical design development, and others are based on mathematical and computing techniques. Thermal error reduction methods may be divided into the following methods [14]:

a) Thermal error avoidance.

b) Thermal error control.

c) Thermal error compensation.

2.1 Thermal error avoidance.

This method is intended to decrease the generation of the heat in the machine tool structure or minimise the effect of heat generated, there are some techniques to conduct this:

- Modifying the machine tool structure.
- Minimising the heat flow rate from heat sources to machine tool structure.
- Controlling the ambient temperature changes in work shops.

2.1.1 Modifying the machine tool structure.

At the machine tool design stage, its structure can be modified in order to minimise the effect of structural temperature change. Techniques used are:

- Building machine tool elements from materials with low expansion coefficient. Structural expansion coefficient can be reduced by building machine tool with materials with low coefficients of thermal expansion such as Zerodur, Invar, and carbon fibre. However, the cost of these materials is often expensive [15].
- Adding symmetry to the structure. This can be very effect if the point of interest such as a cutting tool is centrally located and the effect of expansion is balanced. This is often seen on C-Frame machine tools and Figure 1-6 shows an example result of this and such as structure is illustrated in Section 4.2.
- Locating the bearings axially at one end of the spindle only, the bearings at the other end are free to slide i.e. they support radially only. This is to avoid thermal expansion of the spindle or overloading the bearings. Making sure that the clamped bearings are close to the spindle nose. This means that maximum spindle expansion does not produce relative movement between the tool and workpiece [15].

2.1.2 Minimising the heat flow rate from heat sources to machine tool structure

The heat flow from heat sources to the structure can be decreased at the design stage and during operation of the machine. Examples include:

- Heat sources should be mounted outside of the machine tool structure such as motors, belt drives and hydraulic power packs. Therefore the heat dissipates to the air by convection and radiation and conduction into the structure is reduced.
- Insulating the machine tool structure to control the heat flow rate of workshop environment [9].

- Constructing the machine tool structure from materials with low thermal conductivity and high specific heat capacity such as polymer concrete [10].
- Swarf should be removed as quickly as possible from structural elements such as the machine table or bed of the machine tool to prevent heat flow from the cutting process to the machine tool structure.
- Reducing swarf as much as possible.

2.1.3 Controlling the ambient temperature changes in work shops

Discussed in the external heat sources Section 1.4.1.

2.2 Thermal error control

Another common method of reducing the thermal error is to control the amount of heat flow in to the machine tool structure or to avoid the generation of the non-uniform heat flow in the structure, for example:

- A number of designs use cooling jackets around the spindle bearings. A cooling liquid, oil or water, is circulated continuously through these jackets and a refrigeration unit. This removes heat before it reaches the main machine structure [15].
- Some other parts of machine tool are cooled, such as ball screw feed drive systems. A liquid is usually pumped through the ball screw and to a heat exchanger, where heat is removed through transfer to air directly, or via a cooling liquid. A controller is necessary to make sure the coolant flowing in the machine tool structure is at correct temperature [16-18]. Cooling systems require changes to the machine tool structure and can therefore be costly.
- Some researchers proposed controlling the heat flows by insertion a layer of thermal insulation between the spindle shaft and the inner race of the spindle bearings [15;19].

- Applying heat pipes and thermal actuators are other method to distribute the temperature evenly around machine tool structure [9;19;20].

Good design can decrease but not usually eliminate the effect of structural temperature change. Some of these design requirements can also be uneconomic to implement, especially on small to medium sized machine tools where such costs cannot easily be absorbed by the OEMs. Another disadvantage of this technique is the difficulty of applying it to machines already in use i.e. it is difficult to retrofit such methods. As a result, one of the most broadly studied techniques for reducing the effect of structural temperature change is electronic compensation.

2.3 Thermal error compensation

Compensation is a technique where the thermal error occurring at a particular time are known and the machine modified by adjusting the position of the tool and workpiece, usually using the machine axes [26]. Thermal error compensation is more convenient and can be less expensive compared with the other two methods [10]. This is because it does not need extensive hardware such as the heat pipes and cooling systems or advanced materials, and it can be employed at any stage of the machine tool life from design to build and retrofit by the end user, while the other methods cannot be employed easily after the machine tool has been built or installed [33]. Essential the application of compensation is usually very similar in that the axis positions are modified either through part program modification, internal software such as Programme Logic Control system PLCs or by an external system interfaced to the NC Numerical control by Ethernet for example. However, there have been many ways devised to calculate how much compensation to apply i.e. determine what is the magnitude of the thermal error in the machine tool. These ways can be divided into two main categories:

- Measuring thermal error directly within the machine tool.

- Measuring thermal error indirectly within the machine tool.

2.3.1 Measuring thermal error directly within the machine tool

This method is based on systems where compensation values are determined by making direct measurements of the error and involves in-process measurement of some part of the machine or component. Often the normal machining process is stopped and a probe is utilised to measure a datum on the machine or a reference surface on the component. Direct measurement can be very effective at correcting for thermal errors [34]. A number of researchers have utilised this technique.

Allen et al [21] proposed a direct method to measure and correct thermal errors of the linear scale using an invar bar equipped with a non-contact displacement transducer sensors. The methodology was successfully applied to CNC lathe where the remaining residual error was about 10 % of the original error of 120 µm. Chen et al [22] used probing method for calibrating and compensating thermal error both in real time and under static conditions. This was carried out in real time by probes and an artefact throughout machining process and found that thermal errors in real cutting were different from those in air cutting. Yang et al [23] suggested a method of measuring both thermal and geometric errors throughout machining process using two spherical balls and a touch trigger probe. The data recovered from these was fed into a neural network.

Direct measurement of machine tool accuracy has improved the accuracy of the machines. However, there can be some obstacles associated with their implementation. Installation of measuring systems close to the point of interaction is often not feasible on machine tools. Probing methods involve interruptions during machining process for thermal checks. In addition, interruptions can also pose uncertainty of the obtained compensation data due to the

amount of cool down during the probing cycle, and introduce issues such as machine downtime.

2.3.2 Measuring thermal error indirectly within the machine tool

In this technique errors are calculated from measurements made of a variable or variables other than the actual error between the tool and workpiece. For this to work, the relationship between these variables and the error must be known therefore the general process of the indirect thermal error measurement is to analyse and study the heat flow and the thermal errors of the machine tool experimentally, theoretically and numerically. Establishing the thermal error models, which describe the relationship between temperature gradient and thermal errors, based on analysing the test results. Although there are many computational methods available, the most widely used thermal error modelling methods are the following:

- Artificial Neural networks.
- Multi-regression analysis.
- Finite element analysis.

2.3.2.1 Artificial Neural Networks (ANN)

Artificial Neural Networks (ANNs) generally consist of two basic elements: artificial neurons which process input information and the network which connects the artificial neurons and which has weightings that evolve as the network learns. They can easily be used to correlate temperatures and thermal errors in a multiple-input and multiple-output configuration which suits the thermal problem of multiple temperature sensors and resulting three dimensional errors. Typical structures of ANNs are feed forward networks, where the input directly leads to the output or middle layers which include feedback loops in order to apply an internal state and time interval into the neural network, see Figure 2-1.

To compute the weight between the nodes, a training algorithm is used. The training algorithm was then used with ANN to create the desired output for a particular input. For thermal error compensation of machine tools, feed forward networks are usually used. A great number of researchers have been using ANNs to model machine tool thermal error [24-26].

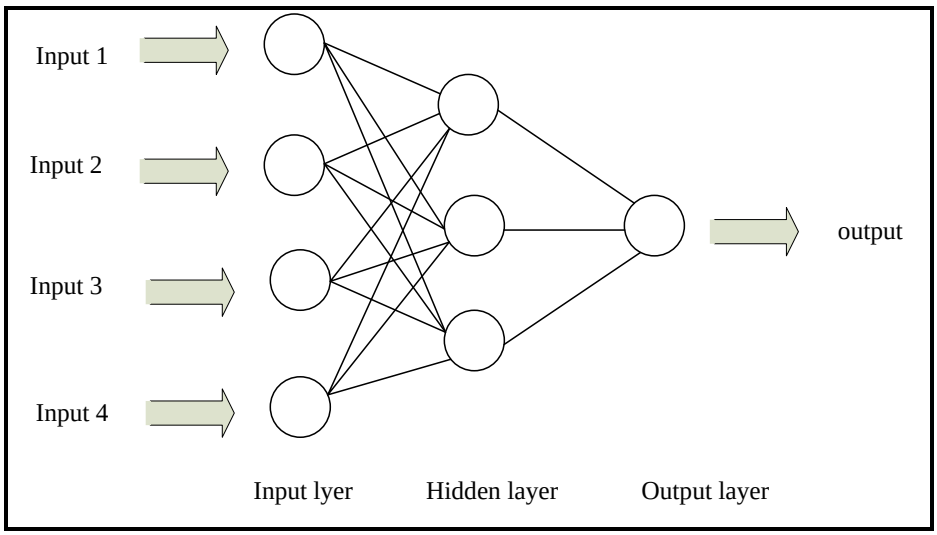

Figure 2-1 Structure of ANN network

Chen et al [27] reported that ANN models can considerably compensate thermal errors as the interaction influence between outputs are well considered in ANN models. The authors employed an ANN method with 15 input layers, 15 hidden layers, and 6 output layers to compensate thermal errors due to the spindle and lead-screws on a vertical machining centre. The network was accomplished by a training set of 540 training pairs. A new cutting process which is not one of the collected training pairs was utilised to validate the forecast accuracy of the ANN model. The results of experiment show that 70–80 % reduction in thermal errors can be achieved after compensation. ANNs are usually equipped with more than ten temperature sensors which are required in order to capture different time constants as the fast elongation of the spindle and the slow bending of the column, as the heat flow in the spindle [27-30].

Consequently a lot of research has been done to decrease the number of sensors and find the best location. Vanherck et al [31] reported that the number of temperature sensors can be reduced from 14 to 4 when used as inputs for the ANN model. The number of required temperature sensors can be identified by algorithm methodology which automatically determines the least possible number of sensors needed [32;33]. Typically the preliminary measurements are done with a large number of sensors mounted around the machine such as on scales, bearings, other heat sources and the machine tool structure. Then a back propagation algorithm checks which sensors have the maximum transfer behaviour from the input to the output. The final number of sensors is specified either by a desired target error or maximum number of sensors which can be employed on the machine tool. Weck et al [32] were able to reduce number of sensors from 40 to 6 sensors. A different method was used in [34] where the ANN utilised cutting data, spindle speed and so forth as additional input data. One temperature sensor was used to capture the environmental temperature. The estimated and experimental results were compared and exposed that 70–80 % of the thermal errors can be minimised after compensation. A number of modified ANN models were suggested thereafter.

Tseng et al [35] proposed a neural-fuzzy model to improve the of a CNC machining centre accuracy . The results exposed that thermal error of the CNC machining centre can be minimised from 80 μm to 3 ± 2 μm. Ramesh et al. [36] proposed a Hybrid Support Vector Machines (SVM)-Bayesian Network (BN) model. The aim of BN model was to divide the error into groups subject to different operating conditions and SVM model was to utilise plotting temperature and thermal errors. The predicted result was plotted against the experiment data measured using the interferometer. The predicted error for both models is able to minimise the trend in the actual error to about 10 ±2 μm.

While some researchers report that thermal error can be significantly reduced using ANN and modified methods of ANN, others state that this is only likely when the ANN is employed to the training data or data that is closely correlated to the training data and human intervention is often required in selecting the useful data set needed in order to train the model. In addition, the requisite experiments required to obtain the training data can take a significant amount of time which is costly as a result of machine down time.

2.3.2.2 Multivariable Regression Analysis (MRA)

Regression analysis is a statistical technique to find the relation between one dependent and independent variables. It is therefore widely used in estimation and forecasting values of the dependent variable. In the case of thermal errors on machine tools the dependent parameter is the displacement of the Tool Centre Point (TCP) and the independent parameters are usually temperatures, measured by thermal imaging camera or surface temperature sensors applied to the machine tool structure. MRA model equations take the following form [37-39]:

$$y = a_{11}T_1 + a_{12}T_2 + \cdots + a_{1n}T_n + b_1 \qquad 2.1$$

Where y_1 is a thermal error, a_{11},a_{12},……,a_{1n} are coefficients for temperature, T_1,T_2,……,T_n are temperature inputs, $b_1$is the constant for the thermal-error model. Equation 2.1 can be also written as following

$$Y = AT \qquad 2.2$$

Where

$$Y = [y_1\ y_2, \dots\dots, y_m]^T \qquad 2.3$$

$$A = \begin{bmatrix} a_{11} & a_{12} & \cdots & a_{1n} & b_1 \\ a_{21} & a_{22} & & 2_{2n} & b_2 \\ \vdots & & \ddots & \vdots & \\ a_{m1} & a_{m2} & \cdots & a_{mn} & b_m \end{bmatrix} \quad 2.4$$

$$\mathrm{T} = [\mathrm{T}_1\ \mathrm{T}_2, \ldots \ldots, \mathrm{T}_\mathrm{m}]^\mathrm{T} \quad 2.5$$

Where A is the Coefficient matrix, Y is the displacement matrix, and T is the temperature matrix. The relationship between thermal errors and temperatures can be established by least square method. A number of researchers have been used the MRA [37;40-42].

Chen et al. [37] used a MRA model to minimise thermal errors for a horizontal machining centre. The results indicated that the spindle thermal error reduced from 196 to 8 μm. The MRA model was also carried out by Yang et al [40] to build an error synthesis model which entails both the thermal errors and geometric of the NC twin-spindle lathe. Their results showed that the thermal error could be decreased from 60 to 14 μm. Pahk et al [41] used MRA model to compensate the thermal errors produced by the spindle and feed axis of a CNC machining centre. The results indicated that the accuracy of machine tool can be improved four to five times.

Huang et al [43] analysed the thermal displacement of a ball screw feed drive system using MRA method. Three temperature increases at front bearing, nut and back bearing were selected as independent variables of the analysis model and recorded by thermocouples. The estimated and experimental results were compared and exposed that 73–83 % thermal errors can be minimised. Tseng et al [44] proposed a non-linear MRA model to estimate the thermal errors of a high-precision CNC lathe. Their results revealed that 40 % of thermal errors could be decreased by their linear MRA model and 60 % of thermal errors could be decreased by their non-linear model.

MRA cannot model internal states of heat flow that define machine tool behaviour. This is an important drawback, particularly as thermal errors largely rely on their history. In a similar way MRA methods require accurate sensor placements selections as incorrect sensor placements may result in unreliable relationships between the thermal error and temperature. In addition, to find best place to mount sensors require re-testing which lead to machine tool down time.

2.3.2.3 Finite Element Analysis (FEA)

The concept of FEA is to replace any complex shape with the summation of a large number of relatively simple shapes such as triangles (2D) or tetrahedrons (3D) that make up the model of the original part correctly. Finite Element Analysis (FEA) can produce an accurate simulation of the three dimension temperature gradient in a machine tool structural element and from this calculate the thermal deformation of machine tool. This is done by simulating the heat flow in machine structure. Typically the technique is referred to as either the Finite Element Method (FEM) or Finite Element Analysis (FEA). These are interchangeable but in this thesis, FEA will be used.

Heat flow in all parts of machine tool can be modelled using FEA. The machine tool structure is typically split into smaller elements subject to significant temperature variation. The heat flow into and out of these elements can be estimated using heat conduction, convection, and radiation equations. Primary internal heat sources for a typical machine tool are the axes and main spindle. There has been significant previous research on simulating machine tool axes and spindles.

2.3.2.3.1 Spindle simulation

There has been significant research on machine tool spindles as they contribute significantly to overall thermal error, especially the axial thermal error which is in the direction of the

cutting tool and typically the Z-axis of the machine [45-47]. Li et al [45] simulated the spindle of a machine tool using FEA and they concluded from the simulated results that the thermal error of the spindle is not just determined by spindle temperature rise due to internal heat sources. It was demonstrated that the thermal error of the spindle is determined by multiple variables such as the temperature from internal heat sources, the historical spindle temperature, environment temperature, the spindle rotation speed, the historical thermal error, and the time lag between the present and previous times. It can be easy to use multivariable parameters as inputs in the FEA simulation technique. Moriwaki et al and Han et al [48;49] built a thermal model of a tool holder using FEA. They used a fine mesh at points of higher thermal gradient to maximize the simulation accuracy with a slight increase in computation time. A good agreement was achieved between the model and the measured data (80 %).

Haitao et al [50] modelled the thermal error of a machine tool spindle using FEA to estimate the thermal error of a CNC machine spindle. The actual machine spindle has many diameters; however the spindle's model was simplified in order to minimise computation time. They postulated that this simplification, if done carefully, does not adversely affect the accuracy of results. A heating up and cooling down test was run for 4 hours until the thermal error stabilised. Axial and radial errors were measured during the heating up and cooling down cycles. A verification experiment was conducted on a CNC turning centre, the results illustrate the simulation results are sufficient to replace the experiment results. When the simulated data was plotted with experimental data, there was good correlation between them (about 80 %). This is not true for the whole machine. Presumably, it occurred because the test of the machine structure was omitted.

Creighton et al [51] also used FEA to simulate a micro milling machine's spindle to determine the thermal error. The model was meshed using both hexagonal and tetrahedral elements which results in good trade-off between solution time and simulation accuracy. The

experiment lasted 2 hours; one heating up and one cooling down cycles which were repeated at different spindle speeds. The thermal error was 6.6 μm which was both axial expansion and tilt. By using a compensation system, the thermal error was reduced to 10 μm. Zhu et al [52] used the FEA to predict the thermal error and hot bending module of machine tool spindle based on temperature data which obtained by thermocouples. Thermal deformation was reduced by 75 %.

Although the results are reasonable, the method reliability subject to the knowledge of boundary conditions. Mian [13] modelled the entire machine tool structure but the focus was on predicting the thermal characteristics of the spindle by FEA. Only internally generated heat from the main spindle was included in the simulation but the inclusion of the full machine structure was included to provide a more complete prediction of the resulting error as heat conducted into the headslide and column of the machine. An efficient method of energy balance was employed to calculate heat power of internal heat sources without requiring very detailed information, for example from engineering drawings, of the specific bearing size and types installed. A good agreement of 70 % was obtained between simulated and experimental results. Residual error was 10 μm for the validation cycles.

However, in the methods employed the structure is split into regular shaped sections each having a heat source and the difference between heat loss and generation balanced based on temperature change, convection and specific heat capacity. This has a high level uncertainty if the conditions are not stable as it assumes no heat transfer through conduction from the sections of the spindle. This uncertainty can also increase as the running conditions of the machine (feeds and speeds) vary compared to the conditions used to perform the balance calculations.

2.3.2.3.2 Ball screw feed drive system simulation

Recirculating ball screw feed drive systems are commonly used in machine tools and are one of the major heat sources which cause considerable thermal displacement in CNC machine tools. Finite Element Analysis (FEA) has been used successfully in the past to model the thermal characteristics of machine tools with promising results.

Yang et al. [53] developed an FEM-based thermal model to resolve the temperature change and distribution that was causing the thermal deformation of the ball screw. Simulations were carried out to appraise the effects of cooling enhancement on thermal deformations by replacing a solid ball screw shaft with a hollow shaft. The deformations, however, obtained from the FEM predictions and the experimental results were in good agreement. These methods add cost, are time consuming and may not be retrofit table onto existing machines. Kim et al. [54] used FEA to build thermal model of ball screw drive system. Their results show that FEA gives good estimations of the rising pattern and axial distribution of temperature. Min et al [55] developed a systematic thermal model using FEA to study the thermal characteristics of a ball screw feed drive system, specifically the characterization of heat generation caused by the friction in moving components. However, the heat generation due to the friction in ball screw and ball nut pairs, bearings, and guideways were determined theoretically. The experimental results obtained from an actual measurement of a feed drive of vertical machining centre showed good agreement with the simulated results 75 %. Closer agreement of results of 83 % was also obtained after modification of heat convective coefficient from 37.4 $W/m^2/°C$ which was calculated from the model to 187 $W/m^2/°C$. The authors report that the calculated value of convection is lower than the actual figure as the shaft spiral grooves on the heat transfer property was neglected. However, the modified convective figure seems to be very high for this case. Wu et al [56] also applied FEA to simulate the thermal behaviour of the ball screw feed drive system of a machine tool. The

ball screw expansion was studied at different preloads. Heat transfer inverse analysis which has the same principles of energy balance method was applied to estimate the heat power of the heat source from the measured temperature profile. A simplified model (FEA) of the ball screw was created and the calculated heat power from experimental data was applied in the FEA model. Numerical simulation results were compared with measured data which showed agreement of 89 %. These results heavily depend on the magnitude of the feed rate and the traverse range of the axis. Gostimirovic et al [57] used the inverse method to determine a cutting zone temperature field and heat power generated due to friction between tool and work-piece. Based on temperatures measured by thermocouples located within a work-piece and giving the heat flow function, the inverse method allows determination of a temperature gradient in the cutting zone as well as the heat flow distribution on the work-piece/tool interface. The technique was not applied however to the machine structure.

Applying pretension to the ball screw i.e. stretching the ball screw is a common method used on the feed drive systems to increase rigidity and also absorb some ball screw thermal expansion. Fletcher et al [58] measured the displacement of a ball screw feed drive system due to thermal error five times, each with different levels of pre-tension applied (0, 22.4, 28.2, 36.3, 48 μm/m). Experimental results show that the amount of reduction in error is actual quite limited, even with high levels of pre-tension. It can be seen that the reduction in error is approximately 20 % when using 22 μm/m of pre-tension. The results from the five tests are shown in Figure 2-2.

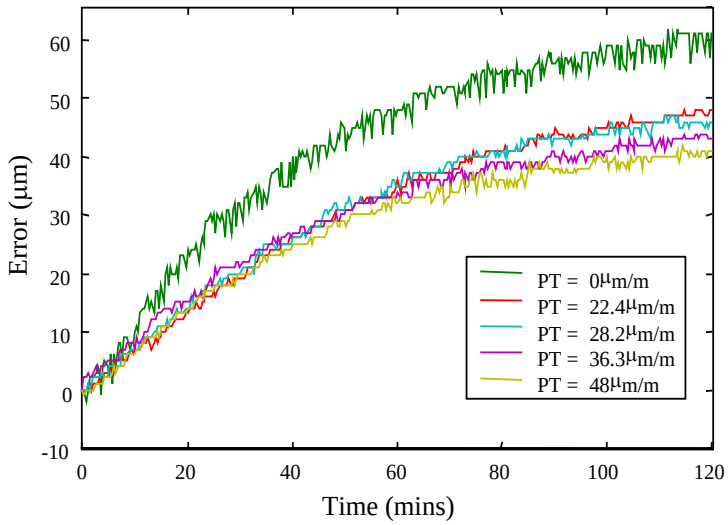

Figure 2-2 Effect of applying pre-tension on positioning error during a heating cycle [58]

Based on the performed literature survey, it is evident that a relatively small amount of research has been conducted on using FEA to simulate the entire machine tool.

2.3.2.3.3 Simulation of the entire machine tool

There have been some researchers who have studied the entire machine tool temperature field, thermal deformation modelling and simulation to improve the accuracy of the thermal simulation of machine tools.

Wang et al [59] simulated the entire structure of a crank press machine in order to find the temperature gradient and thermal error. The internal heat sources such as ball bearings and the ambient temperature were considered. The heat rate was calculated using heat transfer equations depending on the machine's speed, friction torque, coefficient of friction and normal force of contact. The simulation and experiment results are in good agreement (80 %).

It is expected that this result can be improved if the energy balance method was used instead of, or in addition to, the formulae method provided by manufacturer to calculate heat power of heat sources due to the uncertainties in the parameters. Section 3.6 contains research work performed using this method.

Mian et al [60] presented a novel offline environmental thermal error modelling method using FEA. This approach reduces the machine downtime needed for the ETVE test from two weeks to 12.5 hours. The modelling approach was tested and validated on a CNC machine tool over two ‘1 week’ periods, one in the summer and one in the winter and found to be very robust given the difference in the environmental conditions. The simulated and measured results of summer test revealed correlation of 60 % in Y-axis and 63 % in Z-axis. In addition the simulated and measured results of winter test revealed correlation of 63 % in Y-axis and 67 % in Z-axis.

Huo et al [61] Modelled the thermal characteristics of the whole structure of a grinding machine using FEA. The measured temperature data was utilised to calculate the heat power. The machining procedure was simulated to attain the temperature distribution within the cutting zone and its influence on the machine. Depending on the temperature inputs, the machine structure displacement was obtained. The actual machine displacement was not measured and no accuracy percentage can be deduced. Environmental temperature effects were not considered.

Kim et al [62] simulated a machine tool equipped with linear motors traversing at high speed. The linear scale was simulated and then the whole machine without the linear scale. Thermal error combined from linear scale simulation and simulation of entire machine tool without linear scale. The separation of thermal deformation of a linear scale, which is the dominant thermal error element, was to permit simple and fast simulation which is easy to analyse. The machine temperature increase was obtained by thermocouple sensors and displacement sensors were used to measure the thermal error. They found that the experiment and simulation results showed correlation of 80 %. In order to improve the simulation accuracy of machine tool, the thermal contact resistance at mechanical joints should be considered. This is an important thermal boundary on machine tools because of the number of mechanical

joints located near to heat sources and Section 3.7 includes work performed in this research to obtain such values efficiently.

Simulating the thermal characteristics of machine tools using FEA can yield promising results and the technique is used widely in a variety of research activities. Although good correlation between simulated and experimental data is often obtained, most of the research only focuses on a single aspect of the machine tool such as the main spindle, however, relatively few research has been done on simulating whole machine tool. Furthermore, a large number of FEA models were based on assumed heat power values as inputs to simulate temperature distribution in the structure. One of the most significant drawbacks of modelling machine behaviour using (FEA) is the difficulty of accurately obtaining the characteristic of heat transfer, such as heat power of machine tool heat sources and the various boundary conditions.

This research provides reliable techniques to obtain heat transfer coefficients of machine tools in order to improve the accuracy of FEA simulations. FEA is used to simulate the thermal characteristics of spindle system of small Vertical Machining Centre (VMC) using SolidWorks Simulation software.

2.4 Summary

Significant research has been carried out and various methods developed and implemented with regard to the control, modelling and compensation of thermal errors of machine tools.

A number of methodologies for controlling machine tool structural temperature are mentioned which can be applied at the design stage of the machine such as heating or cooling of the machine tool structure, selection of low thermal expansion materials, controlling ambient temperature. These techniques if employed will have substantial control on the

machine tool structural temperature rise however they are generally costly and difficult to implement, particularly as a retrofit solution.

Techniques used to compensate the thermal error, are divided into direct and indirect categories. Direct techniques of thermal error in machine tools are measured using special, purpose made, equipment such as artefacts and probes. In this technique the normal machining process is stopped and a probe is utilised to measure a datum on the machine or a reference surface on the component which can cause uncertainty in collected data. Furthermore, contamination or damage of sensors in the hostile machining environment is another prime issue which can extremely deteriorate the performance of a direct measurement system.

Indirect thermal error measurement is widely studied using a variety of modelling techniques to predict thermal errors of machine tools. ANNs and MRA models revealed high correlation between experimental and simulated data however these techniques require several hours of machine downtime to train the model under various working conditions. Sensor placements are very important to efficiently train these models model. Also, these models might not be transferred to other machines and if they transferred, a lot of modification is need.

A very good agreement between measured and simulated thermal characteristics data of machine tools was also achieved using FEA technique. The development of an FEA model can be quicker in comparison with the empirical approaches. Moreover, a big difference with FEA is that once the parameters and boundary conditions are well understood, the models can be changed /modified to support the design process. The others do not i.e. ANN and MRA only really for compensation. In addition, large number of FEA research used formulae provided by OEMs to calculate heat thermal parameters and some researchers used assumed thermal parameters in FEA model simulation.

The aforementioned advantages of FEA to support design as well as support model development for compensation mean that there is significant advantage from more accurate FEA. This research will create thermal error models of the machine tool feed drive system and the whole machine tool model will be studied by FEA method. The literature review showed that the method used by Mian [13] to obtain the heat power of the spindle bearings is very efficient and may be applicable to other elements if the uncertainty is managed somehow. The thermal parameters of the FEA model are calculated by an energy balance method but the uncertainty in the conduction across the elements needs addressing by a new optimisation method. In addition, the Thermal Contact Resistance (TCR) is generally obtained through experimentation but this may not represent accurately the machine joint therefore it would be an improvement if it can be obtained from the machine i.e. if it can be calculated utilising thermal imaging information instead of carrying out an experiment. Consequently, more accurate thermal parameters may be obtained, which in turn leads to more accurate FEA for machine tool thermal error prediction.

2.5 Aims and objectives

2.5.1 Project aims

The review of thermal characteristics has showed a variety of modelling methodologies for calculating the thermal errors in machine tools. In spite of the machine tool accuracy improvements, certain issues can be improved and made more efficient such as efficient thermal parameter calculation methodologies, consideration of all significant heat sources in the machine tool and optimisation of calculated thermal parameters. This research will deal with all those issues in detail. The project aims are therefore to:

- Develop a general purpose FEA model for the prediction of thermal errors, which can be applied to common machine tool types and configurations.

- Employ the use of thermal imaging data to determine thermal contact resistance in machine tool joints.
- Optimise the thermal parameters of machine tools to improve the FEA model accuracy.

2.5.2 Project objectives

In order to achieve these aims, the main project objectives are,

- Utilising the energy balance method to calculate thermal parameters of machine tools and applying to new structural / heat generating elements.
- Off-line thermal characteristics simulation of feed drive system of machine tool under various conditions by SolidWorks.
- Off-line simulation of machine tool spindle thermal errors under various conditions by SolidWorks.
- On-line measurement of actual thermal errors of feed drive system of machine tool.
- On-line measurement of actual thermal errors of machine tool spindle.
- Analysis of experiment thermal data and applying them off line in the CAD model.
- The ease with which the thermal parameters can be determined where applicable.
- Develop an optimisation technique utilising thermal imaging data in order to tune the calculated boundary condition parameters.

2.6 Identified novel aspects of the work

Due to the potential for variation in the boundary conditions in machine tools due to the way they are used, the environments in which they operate and changes due to wear, parameters estimated or calculated from, for example, OEM formulas or bench tests can become inaccurate. This research therefore will focus on how to have more accurate heat power and boundary conditions of heat transfer in machine tools, and the novelties were the following:

- In line calculation of Thermal Contact Resistance (TCR) instead of bench tests or similar experiments to determine the coefficients.
- New method of TCR calculation for complicated surfaces/interactions such as interface between ball screw nut and ball screw shaft.
- Comparison of parameter identification methods which shows that the energy balance method gives more accurate heat power than the formula method applied to a typical machine tool axis.
- Creation of a 2D optimisation technique based on thermal imaging sequences to optimise the energy balance calculation of the heat power of the machine tool spindle.

Chapter 3

3 Thermal study of the machine tool

Heat flow has three different modes: conduction, convection and radiation. This chapter describes the heat transfer process subject to internal and external heat sources in machine tools.

3.1 Conduction

Conduction can be defined as the flow of energy from the more energetic to the less energetic particles of a material as a result of interactions between the particles [63]. Conduction takes place in machine tools structure elements and through the gaps from one element to others. For the one-dimensional plane having a temperature distribution T(x) illustrated in Figure 3-1, the heat power rate, which is named in Finite element software thermal load, can be calculated by following Fourier's equation [63].

$$Q = -KA\frac{dT}{dx} \qquad 3.1$$

Where Q is the heat power rate (W), K is the thermal conductivity (W/(m.k)), dT is the temperature difference (k), is the dx length (m), A is the cross section area m^2.

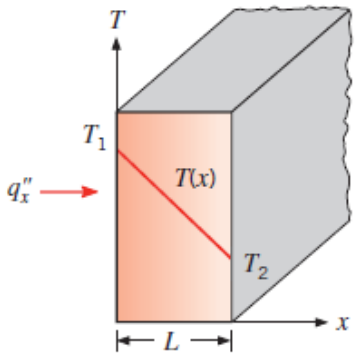

Figure 3-1 One dimensional heat transfer by conduction

A material's thermal conductivity is a temperature dependent property, for example carbon steel's thermal conductivity decrease at the temperature range of 400 °C to 1000 °C. However for machine tool application, the temperature amounts are less significant and this change can be neglected [64].

3.2 Convection

Convection is a mode of heat transfer which occurs due to energy transferred by the bulk or motion of the fluid (coolant, oil, air). Figure 3-2 shows an illustration of the convection process.

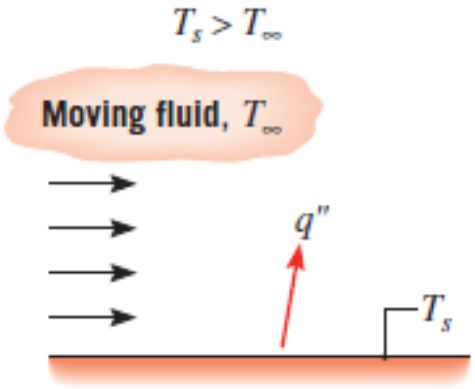

Figure 3-2 Heat transfer convection process [63]

Key: T_s is the surface temperature (°C), T_∞ air temperature (°C), q'' heat rate (W)

Heat transfer by convection can be classified into two kinds: Free convection and forced convection. Free convection takes place when energy releases to the surrounding without any force applied on the fluid adjacent to a surface. An example of this is a stationary fluid in a pipe or a structure in a close room. Forced convection takes place when flow occurs which may be caused by external means such as fans. Regardless of the nature of heat transfer convection process, energy loss by convection can be determined by Newton's cooling law [63].

$$Q = hA(T_{surf} - T_{air}) \qquad 3.2$$

Where Q is the heat power rate (W), h is the coefficient of convection (W/(m^2.k)),$T_{surface}$ is the surface temperature (℃), T_{air} is the ambient temperature(℃).

In machine tool applications, convection occurs in a range of modes for instance forced convection will be the primary heat transfer method between the cutting tool and the coolant, and natural convection occurs between stationary machine tool elements and the bulk ambient air surrounding the machine. Section 3.5 includes the calculation of this coefficient.

3.3 Radiation

Thermal radiation is a process where a body at a temperature emits thermal energy. This type of energy is transported by electromagnetic waves (photons). Conduction or convection requires a material medium to transfer in, however, radiation does not. In fact, radiation transfer can occur in a vacuum. Figure 3-3 shows a sketch of a radiation process.

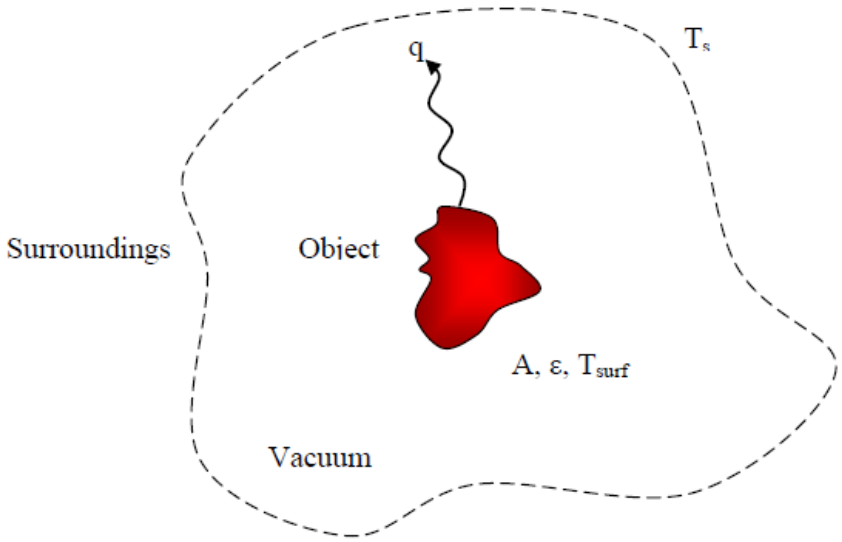

Figure 3-3 Radiation process [64]

Energy loss by radiation can be determined by Stefan-Boltzmann law [63] and some surface parameters as shown in the equation below.

$$q = A\varepsilon\sigma(T_s^4 - T_{surf}^4) \quad 3.3$$

Where A is the area (m^2), σ is the Stefan-Boltzmann constant ($5.67*10^{-8}$ ($W/(m^2.k)$), T_s is the temperature of the surrounding (℃), T_{surf} is the surface temperature (℃), q is the heat power loss by radiation (W), ε is the emissivity.

Emissivity is a radiative property of a surface. Its values are in the range $0 \leq \varepsilon \leq 1$, and provides a measure of how well a surface emits energy relative to a blackbody (a blackbody is an ideal emitter with $\varepsilon=1$). It depends on the surface material and finish, and representative values of selected materials are provided in Table 3-1 [65].

Table 3-1 Emissivity of some materials of machine tools

Material	**Emissivity**
Aluminium (heavily polished)	0.038 – 0.06
Aluminium (heavily oxidised)	0.28 - 0.31
Cast Iron (oxidised at 1100°C)	0.64-0.78
Cast Iron (rough, strongly oxidised)	0.95
Steel (roughly oxidised)	0.81
Oil Based Paint – all colours	0.92 – 0.96
Water	0.96
Masking tape	0.96

When a small vertical machine tool is used, its structural temperature does not usually exceed 70 ^{o}C even on bearing housing and assemblies. The energy lost due to radiation, according to equation 3.3, is therefore negligible at these relatively low working temperatures [64]. However, it plays a very important role for infrared thermography and its parameters should be identified accurately in order to use this method to measure temperature of surfaces.

3.4 Thermal imaging

In order to calculate heat power of any object, some parameters should be obtained experimentally, such as initial temperature, machine tool structure temperature gradient and environment temperature. On the other hand, the other parameters, such as heat transfer convective coefficients, heat power of the heat sources and Thermal Contact Resistance (TCR) across mechanical joints can be calculated either depending on the heat source nature or structure temperature gradient. This research utilises infrared thermography, specifically thermal imaging, to measure temperature flow in the machine structure. Exploitation of the high spatial resolution provided by the 2D thermal image has been used to some extent [13;21] but will be extended to further parameter identification in this research.

In order to ensure the temperature data is as accurate as possible, the aforementioned emissivity must be known as well as some additional environmental parameters such as distance to the object, ambient temperature, transmittance of external optics, etc. In this research, a Flir S65 thermal imaging camera, designed for science and research applications, was used which includes an interface where these parameters can be entered. The general accuracy specification of the camera is + /-2°C which is quite poor for this kind of works but does include some acceptance that the emissivity will not be well known. Work done by Fletcher [66] showed that the application of masking tape on the machine surfaces in

combination with some averaging can dramatically increase the accuracy achievable to better than +/ -0.5°C. These techniques have therefore been used in this research.

3.5 Computation of the convection coefficient of heat transfer

Calculating the convective Heat Transfer Coefficient (HTC) (h) at different locations on the machine tool is important to ensure accurate results of the heat power and FEA simulations. There are two different values of h required: free convective coefficient and forced convective coefficient (see Section 3.2) depending on the surface being analysed. The forced convective coefficient should be calculated for the parts of the spindle and test mandrel when they are rotating and on surfaces of the machine tool axes while they are traversing rapidly. The second free convective coefficient is for all remaining surfaces and for the aforementioned moving surfaces when the machine stops. These 'h' values were used during heating cycle simulations to represent the heat transfer at the rate expressed by the coefficient. For a rotating ball screw for example, the forced convection coefficient can be computed by heat transfer equations of air flow along a horizontal cylinder [50;63].

$$\overline{N}_{u_D} = CRe_D^m Pr^{1/3} \qquad 3.4$$

Where $\overline{N}_{u_D}$ is the average Nusselt number, C and m are constants, Re_D is the Reynolds number, Pr is the Prandtl number.

$$\overline{N}_{u_D} = \frac{\overline{h}\ d}{k} \qquad 3.5$$

Where $\overline{h}$ is the average convection coefficient (W/m^2.℃), d is the ball screw diameter (m), k is the thermal conductivity (W/(m.k)). The Reynolds number Re_D is calculated using:

$$\mathrm{Re} = \frac{\mathrm{ud}}{\vartheta} \qquad 3.6$$

Where d is the ball screw shaft diameter (m), ϑ is the kinematic viscosity (m^2/s), u is the velocity of the flow (m/s). The velocity of the flow can be calculated from the following equation:

$$u = \frac{\pi dn}{60} \qquad 3.7$$

Where d and n are the ball screw shaft diameter (meter) and its speed (rpm) respectively.

At normal ambient temperatures, the Prandtl number of the air is 0.701, the kinematic viscosity of the air is $16*10^{-06}$ m^2/s, the values of constants m and C in equation 3.4 are m=0.5, C= 0.683 at normal ambient temperature (20 ^oC) [63].

In contrast, since the other parts of the machine tools are stationary the natural convective coefficient of 6 $W/m^2.℃$ was applied based on previous experimental work [13;50]. This is an average value as it is accepted that there will be variation about this value depending on the orientation of the surfaces

3.6 Heat generation calculation methods for machine tool heat sources

The magnitude of the heat power in machine tool structures due to internal and external heat sources can be identified using a series of equations that calculate friction with parameters associated with lubrication, pre-load, speed etc. This method will be termed the ‘formulae method’ and the uncertainties associated with this method will be reviewed in the next section. A second solution, introduced in Section 2.3.2.3.1, involves the ‘energy balance method’ which will be used to calculate the same parameters and the resulting simulation accuracy compared with measured data.

3.6.1 Formulae method

The heat power of heat sources can be calculated based on the established literature [50;67]. Heat sources of machine tools are;

- Heat generated between the ball nut and ball screw shaft of the machine tool axes.
- Heat generated by spindle and ball screw support bearings due to the friction between the balls and races.
- Heat generated by the rolling elements in the guideways.
- Heat generated by spindle motor and belt drive if existing.

3.6.1.1 Heat generation due to friction between the ball screw shaft and ball nut

To maintain accuracy and high rigidity, suitable preload must be applied to the ball nut system. As a result of applying preload, heat will be generated due to the increase in friction caused by the preload in addition to the viscous friction from ball screw rotation. Tenjitus et al [68] reported that heat generation can be calculated by the following equation.

$$P = 0.12\pi nM \tag{3.8}$$

Where P is the heat power (W), n is the rotational speed (rpm), M is the total frictional torque (N.m), which entails friction torque M_d and resistance torque M_{pl}.

$$M_d = T_d(1 - \varepsilon) \tag{3.9}$$

$$M_{pl} = \frac{F_p L}{2\pi\varepsilon}(1 - \varepsilon^2) \tag{3.10}$$

Where T_d is the driving torque (N.m), F_p is the preload (N) and ε is the efficiency of a ball screw, a typical value of which is 0.95 for precision ball screws used in machine tools [68]. T_d can be calculated using

$$T_d = \frac{FL}{2\pi\varepsilon} \tag{3.11}$$

Where F is the axial load (N) and L is the lead of the ball screw (mm).

3.6.1.2 Bearing heat generation

Heat generated in the angular contact rolling element bearings due to friction is influenced by speed, preload, and lubricant and can be calculated by the following equation [50].

$$H_b = 1.047 * 10^{-4} * n * M_t \quad 3.12$$

Where n is the rotational speed, M_t is the total torque of the bearing (N.m). The total torque is the sum of the load torque and viscous friction torque.

$$M_t = M_l + M_v \quad 3.13$$

Where M_l is the load dependent friction torque, which can be calculated from the following equation

$$M_l = f_1 p_1 d_m \quad 3.14$$

Where f_1 is a factor depending on bearing design (N), p_1 is the relative bearing preload (N) and d_m is the mean diameter of the bearing (mm). For angular contact bearings:

$$f_1 = 0.001\left(\frac{p_0}{c_0}\right)^{0.33} \quad 3.15$$

$$p_1 = 1.4f_a - 0.1f_r \quad 3.16$$

M_v is the viscous friction torque and can be empirically expressed as [55]

$$M_v = 10^{-7} f_0 (\vartheta_0 n)^{2/3} d_m^3 \quad 3.17$$

If $\vartheta_0 n > 2000$

$$M_v = 160 * 10^{-7} f_0 d_m^3 \quad 3.18$$

If $\vartheta_0 n < 2000$

Where f_0 is a factor that depends on bearing type and lubrication type.

3.6.1.3 Heat generated by the guideway

The guideways are also one of the possible heat sources in the machine tool, particularly for high speed machining and where hydrostatic systems are used. In this case, for common rolling element bearings, heat generation of the guideways can be calculated by the following equation [55].

$$q_g=\mu*F*V \quad 3.19$$

Where q_g is the heat power rate (W), μ friction coefficient, F is the normal load (N) which may include the weight of the workpiece, V is the velocity of the axis (m/s).

3.6.1.4 Heat generated by the spindle motor

The heat power of a motor can be obtained from the difference between motor mechanical power and motor electrical power. The motor mechanical power (P_{mec}) (W) provided by the motor, can be calculated from the motor mechanical torque T (Nm) and the rotational speed v (in rad/s). On the other hand, the motor electric power (P_{elec}) (W) can be obtained from motor current and voltage. Finally, motor power losses (P_{losses}) (W) were calculated from the difference between mechanical and electrical power [69].

$$P_{mec}=T*v \quad 3.20$$

$$P_{elec}= I*V*\text{power factor} \quad 3.21$$

$$P_{losses}= P_{mec}- P_{elec} \quad 3.22$$

The equations in this formulae method will be applied to a small vertical milling machine in Section 5.4 and the parameters used in the FEA for comparison with the energy balance method described next.

3.6.2 Energy balance method

Heat power rate of all heat sources in the machine tools can be calculated using the following equation based on temperature data from a thermal imaging sequence and estimates of the convective heat transfer coefficient. It is evident that there can be difficulties in practice to 'see' some of the machine heat sources with thermal imaging camera but for many machines most of the guarding is easy to remove.

For a structural element that has small net heat transfer through conduction, the following equation provides the heat rate for the element [13].

$$Q = \frac{mc_p(T_2 - T_1)}{t} + hA(T_{surface} - T_{air}) \quad 3.23$$

Where Q is the heat power rate (W), m is the mass (kg), (T_2-T_1) is the surface temperature difference (℃), $T_{surface}$ is the average surface temperature (^oC), T_{air} is the air temperature (^oC), t is the time (second), C_p is the specific heat (j/(kg.℃)), h is the heat transfer convective coefficient (W/(m^2.℃)), A is the area (m^2).

This method will be compared to the formulae method in Section 5.4.

3.7 Thermal Contact Resistance (TCR)

Whenever two solids are joined, the mechanical interfaces are imperfect. This occurs because the surfaces, nominally machined flat, are not perfectly smooth and flat. A mechanical joint entails abundant discrete micro contacts that may be scattered in a random pattern over the apparent contact area and interfacial fluids and contaminants can also exist. The TCR occurs at mechanical joints and depends on surface roughness, surface flatness, contact pressure, number of contact points, size and shape of contact points, size of voids, type of interfacial fluid in voids and material hardness [70]. A number of researchers have explored this topic to find out the TCR values but typically these are for specific applications such as a joint in machine tool or specific joint material.

Thermal Contact Resistance (TCR) affects the heat conduction across mechanical joints, therefore, the amount of heat conducted throughout joints decreases as the surface quality decreases. Min et al [71] modelled machine tool bearings by FEA. They reported that the accuracy of simulated FEA model was increased by considering TCR by about 25 % as shown in Figure 3-4. Attia et al ([72] cited in white [73]) reported that the range of heat flow through a joint in a machine tool can vary between 3.5 and 9.5 kW/m^2.

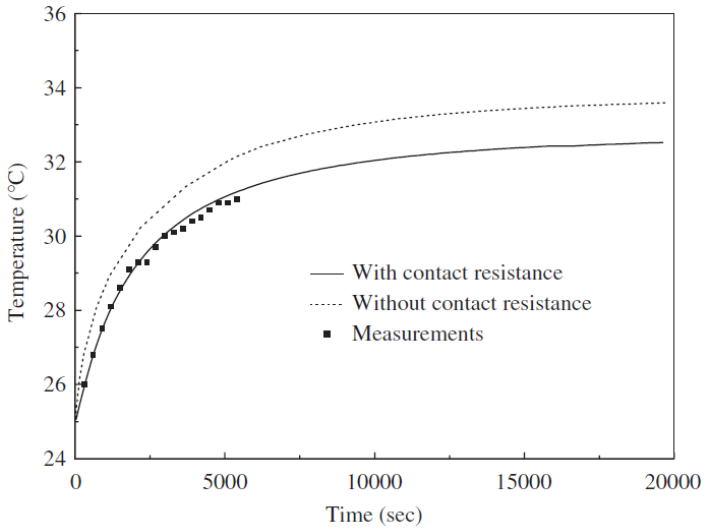

Figure 3-4 Comparison of temperatures with TCR and without TCR [71]

Mian et al [13] conducted two experiments to identify TCR of surfaces representing a spindle flange. Two rectangular plates of similar dimensions were used. Four digital temperature sensors in sets of two were embedded into the plates to ensure high accuracy measurement of the core temperatures. TCR experiments were conducted in two phases, first with cleaned dry plates and then with oiled plates. The results of two experiments show difference in the TCR figures which were 0.0004 $m^2.^oC$ / W and 0.0005 $m^2.^oC$ / W respectively when the two plates clamped by force of 100 KN, see Figure 3-5. The values of TCR were applied in FEA software to simulate machine tool. The simulation results were improved by about 20 %. Although improvements were made, the process of creating experiments to represent actual machine joints may not always be feasible and the condition of the actual joints is not always well known.

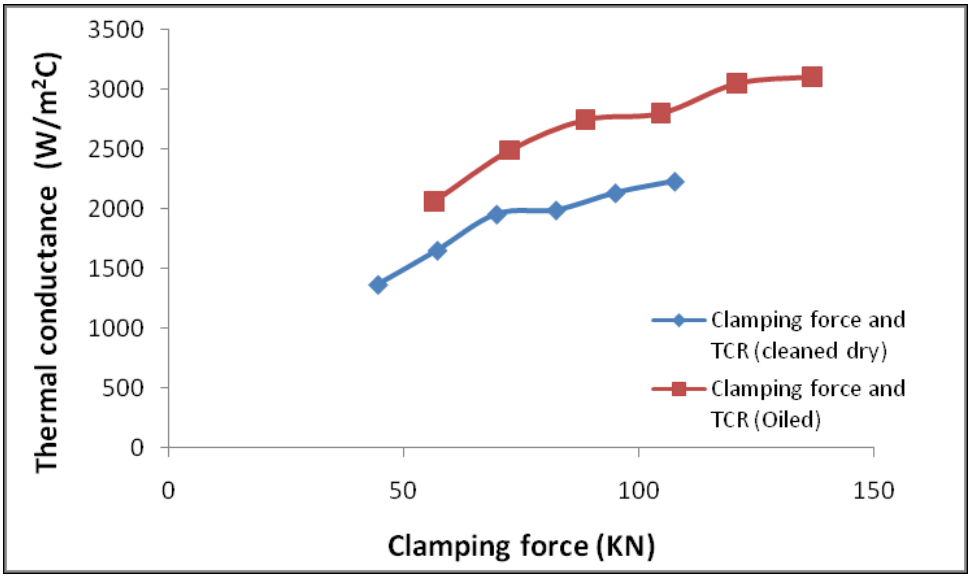

Figure 3-5 Thermal contact conductance values of oiled and dry joint [13]

3.7.1 In-line determination of TCR

Due to the potential difficulties with performing experiments to obtain good TCR, an alternative was researched. TCR is the resistance of heat flow between two solids in contact that results in a temperature drop across the mechanical joint.

By measuring this drop an indication of the resistance may be obtainable. It can be difficult to install sensors between, or even near to, a machine tool joint such as the spindle bearing housing. Thermal imaging is more convenient and at the machine tool joints, it is possible to find out the average temperature on the two connected parts for example the upper and lower sections of the spindle bearing housing which is shown in Figure 3-6.

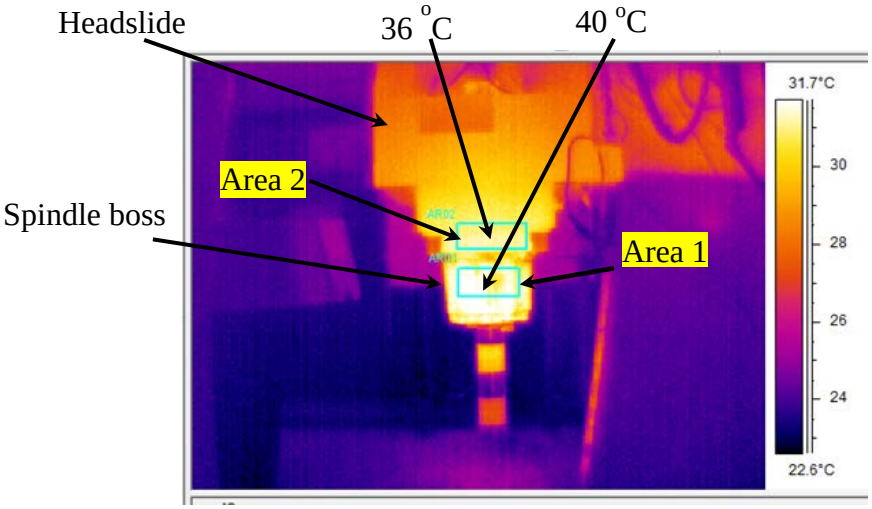

Figure 3-6 Thermal imaging of spindle boss and headslide of machine tool

In the shown areas in Figure 3-6 there is a noticeable temperature difference across the mechanical joint due to TCR. Figure 3-7 shows the temperature variation during a heating and cooling cycle.

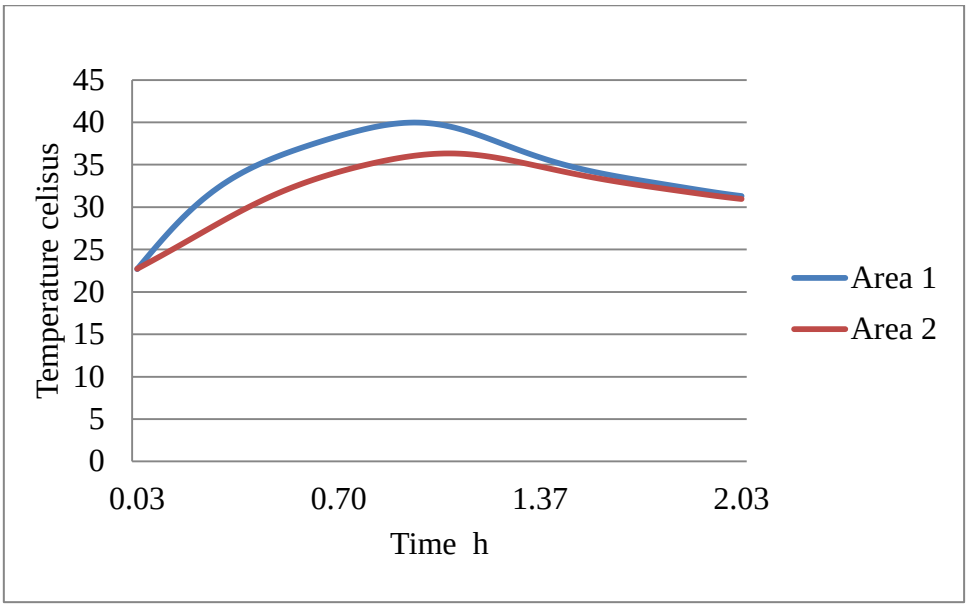

Figure 3-7 Temperature difference spindle boss and headslide joint

Thermal contact resistance can be calculated from the following heat transfer equation,

$$\frac{1}{h_c} = \frac{A(T_2 - T_1)}{Q} - \frac{X_1}{K_1} - \frac{X_2}{K_2} \qquad 3.22$$

Where 1 / h_c is the TCR ((m^2.k) / W), A is the joint cross section area (m^2), (T_2-T_1) is the temperature difference (℃), Q is the heat power rate of source (W), (K_1,K_2) thermal conductivity of the material on either side of the joint (W / (m.k)), X_1,X_2 is the distance of the centres of areas 1 and 2 from the joint (m).

The TCR magnitude of 0.0002 (m^2.k)/W was obtained using the above equation and applied as the boundary condition in the FEA model during simulation of a spindle heating and cooling cycle. This value 0.0002 (m^2.k)/W is similar to the ones obtained experimentally.

In order to validate this methodology the effect of TCR was studied using FEA. An assembly block of 3 parts was simulated to obtain the TCR at the joints, see Section 4.1.3.

The limitation of this work is that this method might not work if the two joined parts have heat sources as the heat flow to the cooler part should be constant and not effected by other heat source.

3.8 TCR of ball screw nut and ball screw shaft.

Heat is generated inside the ball nut and therefore is difficult to measure a differential temperature across the interface using thermal imaging. The mechanical interface is very complicated to simulate, for example using FEA, due to the uncertainty in the amount of lubrication and the Hertzian contact between the ball bearings and the curve race of the ball screw. The TCR between the ball screw nut and ball screw shaft will have a different magnitude due to this complicated surface contact and the pre-load in the nut. A typical cross section is shown in Figure 3-8.

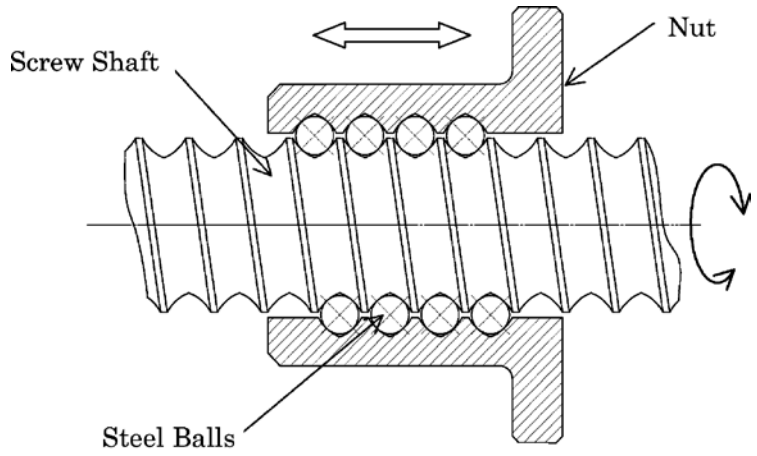

Figure 3-8 Ball screw cross section [74]

Using a long strip of digital temperature sensors embedded inside a specially made hollow ball screw enabled the, heat transfer from the nut to the screw to be measured. The nut was rapidly heated at one position on the screw using a small cyclic movement at one end of the traverse range of the axis then, for cooling, moved to a part of the screw not yet affected by the heat i.e. negligible heat transfer through conduction along the ball screw (which was 1m long). At this new position, with the nut stationary, any heat entering the screw must have transferred by conduction from the nut through the rolling element bearings and lubrication. The measured temperatures were then used to calculate a heat transfer coefficient.

Figure 3-9 shows the temperature of the nut and the screw shaft under the nut (the length of the contact area of the nut completely covers 2 temperature sensors in the hollow ball screw) during the transition from heating to cooling. The slope of the curve calculated from H and L equates to the heat transfer. For the recorded data, the heat transfer value is 66 Watts/m^2.^{o}C when the contact area between the nut and the screw is estimated to be 0.017 m^2.

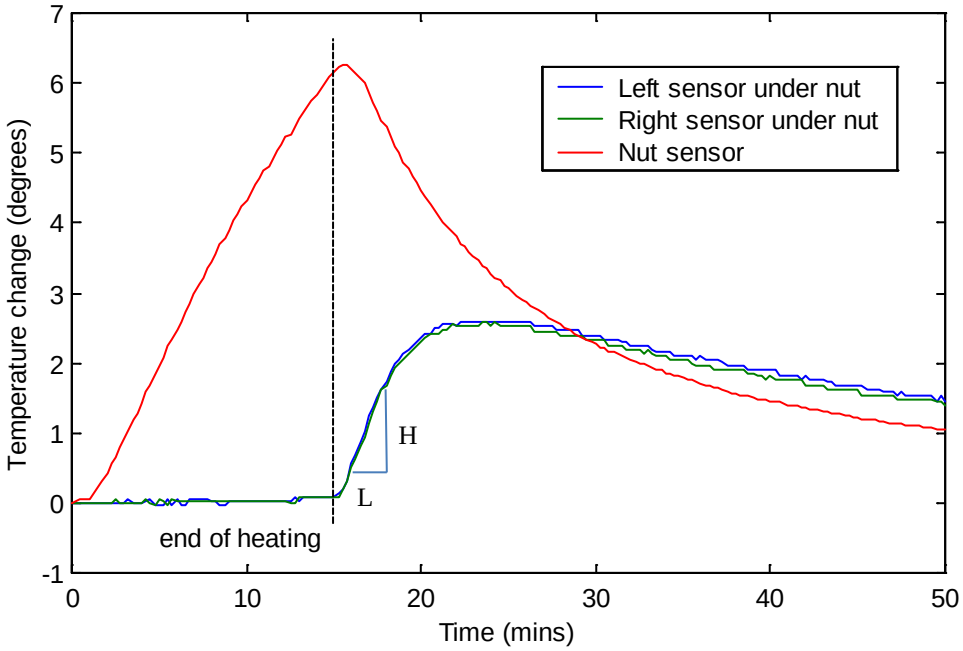

Figure 3-9 Graph showing heat conduction from nut to screw sections under nut

Throughout the feed drive thermal error modelling experiment, the table was moved 500mm. therefore, the contact area is changed to 0.0314 m^2 and TCR between the ball screw nut and ball screw shaft is 0.028 $m^2.^oC$ / Watts. These figures of TCR were used in a 1-D finite element model, programmed in Matlab, at the relevant joints, i.e. joints between the ball screw nut and ball screw shaft.

3.9 Implementation of the research

The aims of this research are to study the thermal characteristic of the machine tool based on FEA simulations, and create an offline technique to predict the thermal distortions in the machine tool structure. Creation of the 3D Computer Aided Drawing (CAD) models of the machine tool structural components was conducted from actual machine tool component measurements using the SolidWorks software. This software was selected due to its short learning curve and ability to execute the most commonly needed finite element analyses. Other software packages could be chosen to this work such as Abaqus and Ansys however, this software were not available to be used and could be more complicated than

SolidwWorks. The research was conducted on a small three axis C-frame milling machine tool located in the engineering workshop and shown in Figure 3-10.

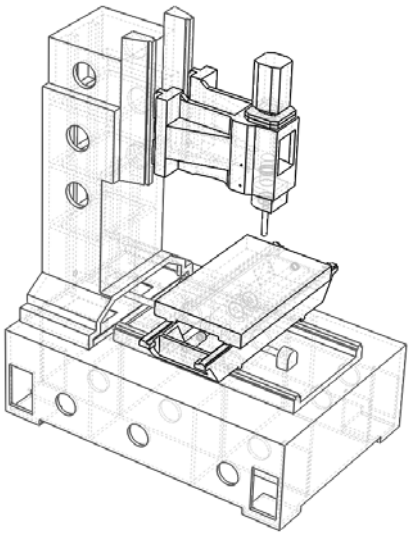

Figure 3-10 Small C-frame machine tool

The 3D CAD assembly of all the structural and heat generating components on the machine tool was generated and simulated using FEA software and subjected to internal and external heat sources. The magnitudes of TCR were applied at the model joint surfaces. The effect of varying TCR across a joint is shown in the assembly benchmark work conducted in Chapter 4. To progress the existing research performed on using the energy balance method, new work was performed on applying the technique to the X-axis of machine tool and its spindle. Internal heating tests were carried out on the X-axis and spindle of the machine tool to investigate thermal behaviour of the main heat sources of the machine tool. The internal heat sources of X-axis are front and rear bearings, ball screw nut and guideways. The modelling approach of machine tool and the practical study carried out on the machine tool when subject to internal heat sources, which were calculated by formulae and energy balance method, and its simulations will be discussed in Chapter 5. Whereas the internal heat sources of the spindle are upper and lower spindle bearings and spindle motors.

The modelling approach of machine tool and the practical study carried out on the machine tool when subject to internal heat sources, which were calculated by energy balance method, external environmental temperature fluctuations and its simulations will be also discussed in chapter 5. Then, a novel 2D optimisation technique utilising thermal imaging data in order to tune the previously calculated boundary condition parameters will be discussed in Chapter 6.

3.10 Summary

The three modes of heat transfer, conduction, convection and radiation, occur in machine tool structures and their significance and propagation are discussed in this chapter. Conduction and convection are considered in the subsequent thermal analysis of the machine tool. Radiation can be neglected as a significant heat transfer mechanism due to the relatively low temperatures occurring in the machine tool structure which typically do not go beyond 50 ^{o}C.

The heat power of internal heat sources can be obtained by formulae method or by energy balance method. For the formulae method, equations were developed based on the heat source type i.e. bearings, motor, and ball screw nut, while the energy balance method depends on measuring temperature gradients of the machine tool structure.

In addition, the heat flow in machine tools is affected by TCR which takes place at mechanical joints. From thermal imaging data, the TCR can be obtained in some case i.e. the joint between spindle boss and head slide as the temperature gradient can be recorded in detail by the thermal imaging camera. This is a new technique developed to reduce the need for TCR experiments. Conversely, the TCR in the ball screw and ball nut had to be calculated experimentally due to the difficulty in recording the ball screw shaft temperature gradient and complex contact area.

Chapter 4

4 Modelling of machine tool, meshing and heat sources position identifications

The creation of 3D CAD models of all the main structural elements on a small Vertical Machining Centre (VMC), required to perform detailed FEA simulations, will be discussed in this chapter. Dassault Systemes Simulation (Part of the Solidworks suite of software) was selected due to its short learning curve, ability to execute the most commonly needed finite element analyses and its ability to simulate large geometrically complex problems. It also allows the application of spatial boundary conditions that includes time varying parameters including environmental temperatures.

A small C-frame vertical milling machine was chosen for this research as it represents a common configuration of machine used in a broad range of manufacturing industry. Just as important was the machine availability for performing a broad range of thermal tests which was generally very good.

4.1 Bench mark simulation

Bench mark simulations were performed to validate the reliable application of thermal parameters and define the accuracy of the software simulation compared to hand calculation. Both single block and an assembly of blocks will be simulated to include all the relevant heat transfer components.

4.1.1 Single block

The application of this research was on the prediction of thermal behaviour in a 3-axis VMC by FEA software. It is necessary to find the best thermal parameters and simulation

methodology to obtain an optimised thermal characteristic of the machine tool. Therefore benchmark simulations are undertaken to be used as points of reference.

The SolidWorks software provides the thermal characteristics feature where an object is simulated for its thermal behaviour. The software provides two types of heat power to an object. 1) Surface heat flux is the input applied to the surface of an object. 2) Heat power rate is the input applied to a body generating heat within itself and, depending on boundary conditions, dissipating to other material attached to it. For example, heat power rate can be applied to bearings as they are considered a significant heat source that dissipates heat into the bearing housing and other supporting structure. Heat power rate was used extensively in this research as a convenient way to represent the machine tool heat sources, the magnitude of which is estimated from the measured surface temperatures. A thermal transient analysis of the single block of the benchmark is carried out.

A model of a cubic steel block of dimensions (100mm*40mm*40mm) was created in the software and simulated thermally using a transient analysis based on temperature gradient and its material properties (see Table 4-1) for one hour. The transient simulation was chosen as it represents the actual temperature gradient of the object. To ensure the results of the block thermal simulation are reliable, hand calculation of the heat power rate was conducted iteratively at small time interval of 100 seconds to ensure reasonable accuracy using equation 4.1, assuming a block temperature rise from 20 to 25 °C, see Figure 4-1. After calculating the heat power, the values were applied in the FEA to obtain the change of the block temperature and compared with calculated temperature. The progressive error was very small (see Figure 4-2).

Table 4-1 Block material properties and boundary conditions [75]

Property	**steel**
Density Kg/m^3	7800 ± 10 %
Specific heat ($\frac{j}{kg.^{\circ}C}$)	500 ± 13 %
Thermal conductivity $(W/m.k)$	30
Mass (kg)	1.25
Area (m^2)	0.0192
Transient simulation duration (mins)	60
Iteration step size (°C)	0.14
Number of steps	360
Ambient temperature (°C)	20 ± 0.5 %
Convection coefficient ($W/m^2.°C$)	6

$$Q = \left(\frac{mc_p(T_2 - T_1)}{t}\right) + hA(T_{surf} - T_{air}) \qquad 4.1$$

The calculation of first iteration is the following

$$Q = \left(\frac{1.25 * 500 * (20.28 - 20.14)}{100}\right) + 0.0192 * 6(20.14 - 20) = 0.9 \pm 0.75\ W$$

The calculated heat power rates were used in the software to obtain the thermal behaviour of the simple bench mark block. The result was accurate to within 0.05 °C.

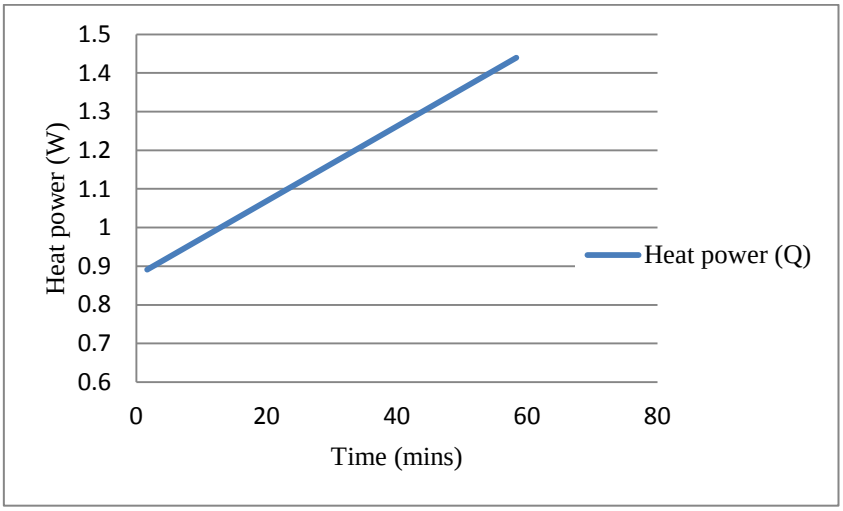

Figure 4-1 Calculated heat power of single block

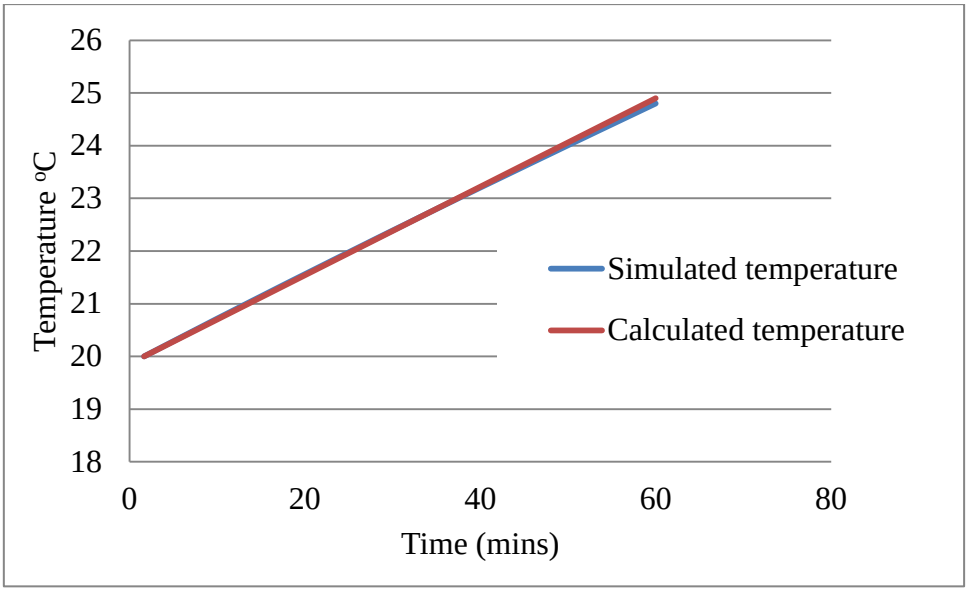

Figure 4-2 Simulated and calculated temperature gradient of single bench mark block body

4.1.2 Bench mark assembly

This benchmark is carried out to confirm the following objectives:

- Approving the reliability of the mathematical relationship used to calculate heat power for predicting temperature flow in an assembly and to simulate heat flow from heat sources in complex structures, for example, spindle bearing temperature.
- To validate the effects of the TCR on heat flow across the joints.

The benchmark assembly simulation was conducted using three steel blocks, as shown in Figure 4-3. The middle block had the dimensions of (40 mm x 40 mm x 40 mm). Both attached blocks on the ends have dimensions of (40 mm x 40 mm x 20 mm).

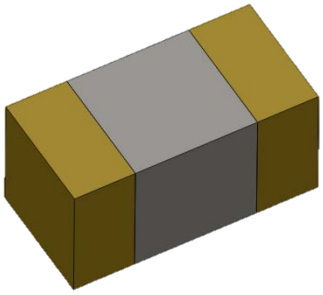

Figure 4-3 Model of assembly block

New heat power figures were calculated iteratively as before using Equation (4.1) for the middle block which is considered to be a heat source that raises the temperature of the whole assembly by 5 ^{o}C. The blocks are assumed to be made from steel with mass and area of 1 kg and 0.0224 m^{2} respectively. The calculated heat power rates of the assembly were used in the simulation of the assembly. Figure 4-4 shows the simulated assembly block for one hour. In this preliminary simulation, the TCR at the assembly block joints was not included.

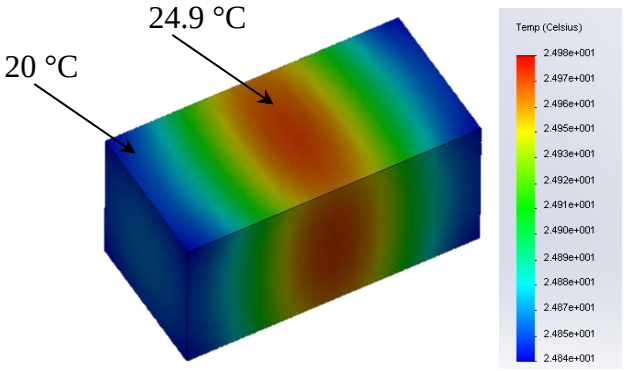

Figure 4-4 Simulated assembly block with negligible TCR

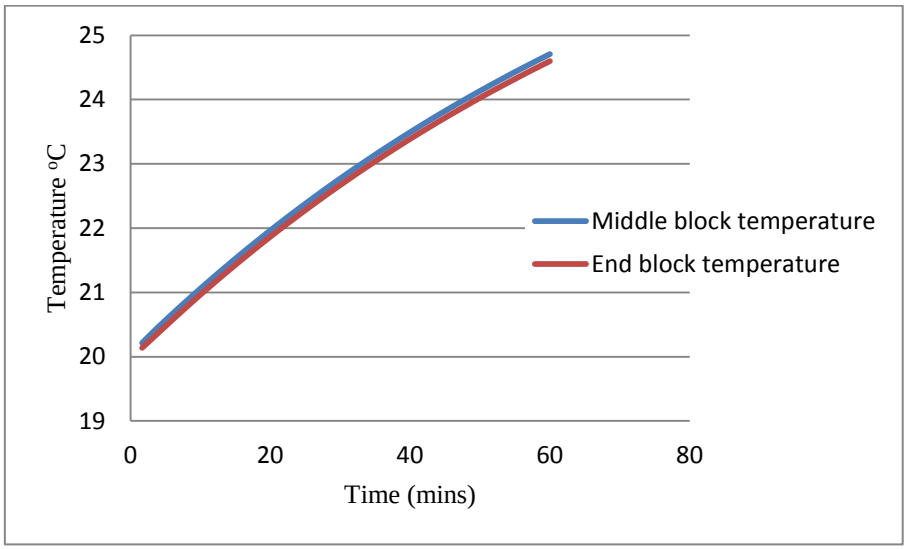

Figure 4-5 Simulated temperature of assembly block

From Figure 4-5, it can be noticed that the assembly block temperature rises to 24.9 ± 0.5 ^{o}C at the middle of the block and at the end block the temperature is a fraction lower due to conduction. The temperature increase was due to the fact that the TCR parameters at block joints were not included to achieve negligible resistance to the heat flowing at the assembly joints to observe if the calculated heat power can generate the targeted temperature of 25 °C.

The results of single and assembly block simulation confirmed the application of the thermal characteristics simulation technique and giving a good correlation to within 0.05 ± 0.5 °C.

4.1.3 Effect of thermal contact resistance

The assembly bench mark was simulated using different values of TCR at the joints in order to observe its effect on the simulated heat flow. These figures are 0, 0.1, 0.01 and 0.001$m^2.^oC)/W$, see Figure 4-6. These benchmarks were targeted towards machine tools joints where the TCR value is not known with a high level of certainty.

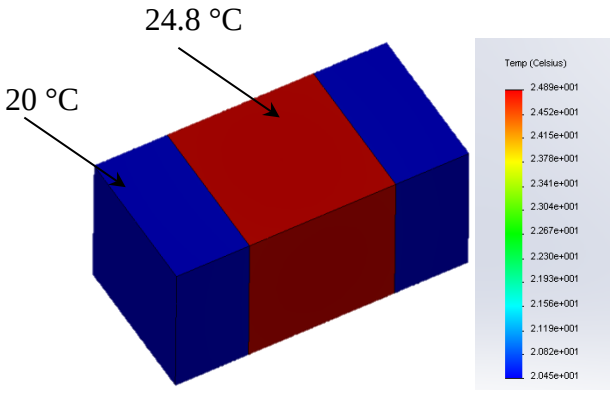

Figure 4-6 Simulated assembly block with 0.1 of TCR

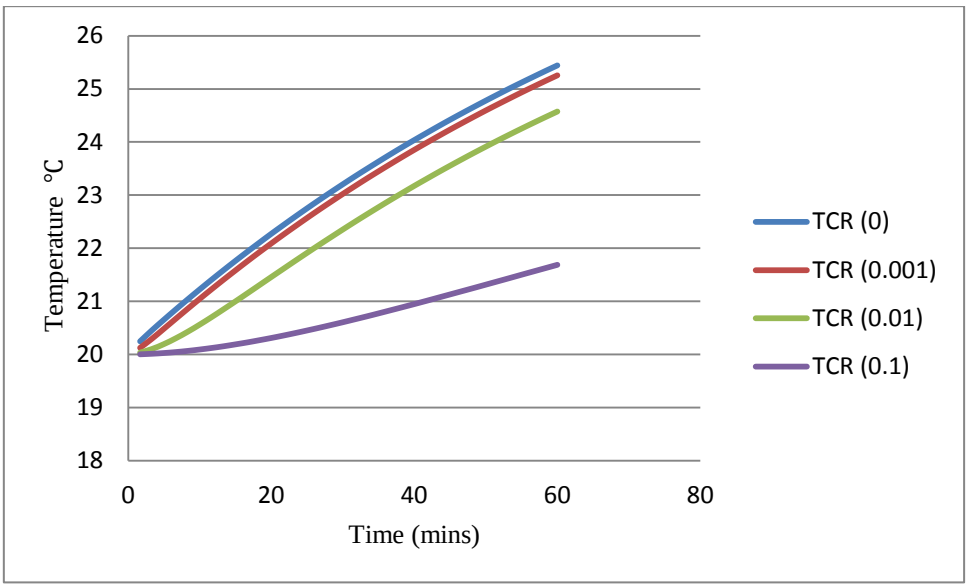

Figure 4-7 TCR effects on heat flow in the assembly block

As expected, Figure 4-7 shows the reduction in heat flow due to the increased TCR values at the joints.

These simple benchmark simulations confirm the methodology of calculating and applying heat power and the associated boundary conditions including convection and accurate TCR parameters should be applied in FEA models at the mechanical joint to ensure the high level of simulated data accuracy.

4.2 Machine CAD modelling

3D CAD models of all the main structural elements of a small vertical machining centre (VMC) were created from manual measurements of the small VMC using the SolidWorks software. The main structural components such as column, base, headslide, etc., were created based on internal and external dimensions obtained from a tape measure, since engineering drawing were not available and then assembled. It is recognised that the accuracy of the reading will be in the order of +/-1mm but the effect of this uncertainty on this work is expected to be negligible. It was not possible to measure the hidden, or partially hidden, parts such as bearings, however for most of theese components the dimension and specification was obtained from the OEM using the serial numbers. In order to find an effective compromise between the simulation and accuracy of the mesh, the geometric model of the VMC is simplified using standard techniques to shorten the computation time for finite-element simulations. These simplifications include elimination of small holes, curvature, chamfers, bolts and bolt holes [21]. Such simplifications are commonly applied and do not adversely affect accuracy. Further reductions may have been possible but was not the focus of this research.

The VMC model was meshed utilising different mesh size (3000, 1500, 750, 150 and 75 mm^3) in order to improve the simulation accuracy. The largest mesh size of the VMC model was 3000 mm^3. The simulation takes long time if the mesh size was 75 mm^3 or less. Figure 4-8 shows comparison of experimental and simulated data of the VMC that meshed with different element size in order to improve the simulation accuracy. The results show that

there is small accuracy improvement in spite of meshing the FEA model with small element size. Therefore, a course mesh was chosen for the simulation as the accuracy is not adversely affected and the simulation time is minimised. The assembly of the machine is shown in Figure 4-9. The individual CAD models are shown in Appendix A.

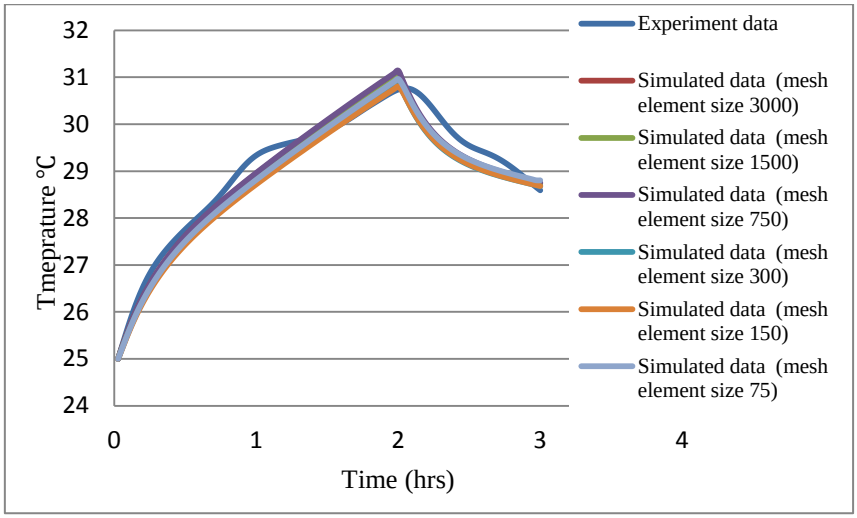

Figure 4-8 FEA model simulation using different mesh size

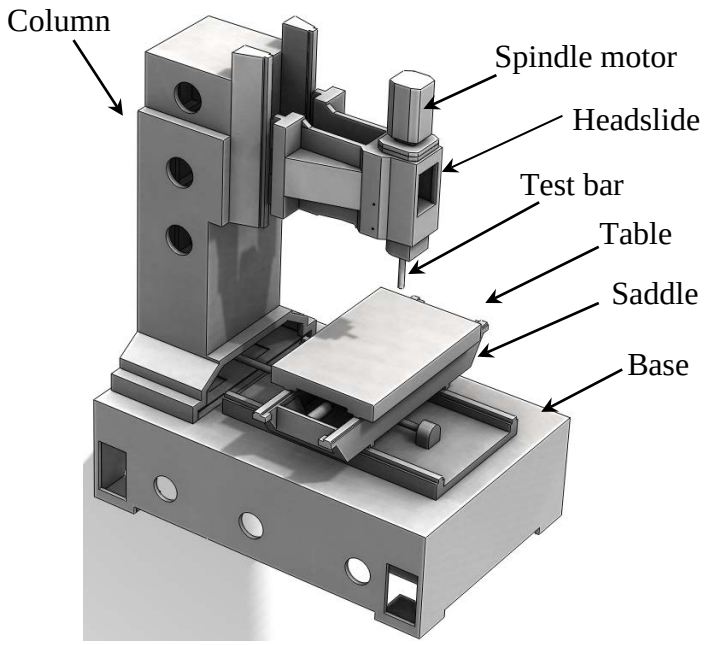

Figure 4-9 Assembly of the machine tool

4.3 Meshing the VMC model and application of the constraints

There are two options for meshing in the software package: standard mesh and curvature mesh. Curvature mesh was chosen as it is suitable for complex CAD models as it automatically optimises the mesh density, within some specified limits, based on the shape of the structure, adding more elements around holes and on curved surfaces. These limits were tightened to obtain a higher density mesh for the spindle, carrier, table, saddle, ball screw nut and shaft compared to the rest of VMC structure following best practice of meshing introduced in [71;76] and to ensure sufficient nodes for extracting data of high spatial density for post processing and comparisons with thermal imaging. A total of 24244 elements were used. Figure 4-10 shows the meshed assembly of the VMC.

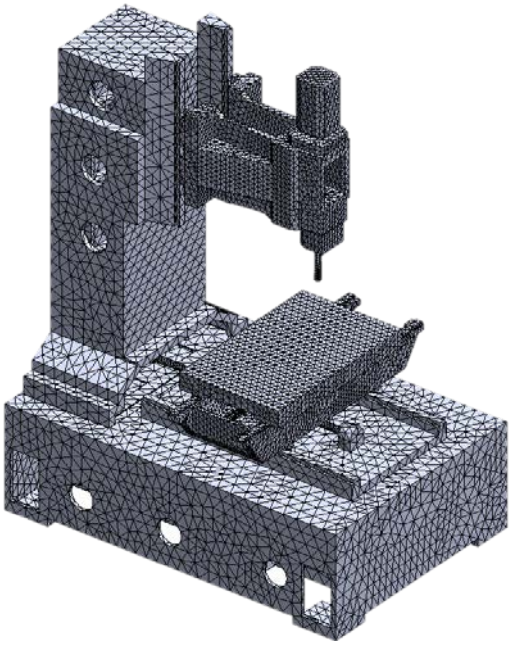

Figure 4-10 Meshed model of small VMC

The base of the VMC was fixed at four locations across the bottom where the machine would normally be attached to the foundations using displacement constraints. The initial temperature of 20 ± 0.5 °C was applied to the whole VMC structure based on experiment

data. Furthermore, ambient temperatures were applied to all of VMC structure, which exposed to air, based on measured data.

The small VMC was tested twice using different duty cycles: the first involved simulated air cutting to heat up the main spindle and the second involved rapidly moves the X-axis to heat up the feed drive system. These tests align with the ISO 230 part 3 standard. The machine was tested when the structure temperature is approximately the same ambient temperature to avoid thermal history. As described previously in Section 1.5.1 and 1.5.2, the structure temperature gradient was recorded using the thermal imaging camera and the displacement was monitored by Non-Contact Displacement Transducer NCDT sensors and laser interferometer.

4.4 Location of modelled heat sources in the FEA model

The X-axis and spindle of the machine tool were studied in this research for their thermal characteristics. The lower spindle bearing, upper spindle bearing, spindle motor, X-axis front support bearings (driven end), X-axis rear support bearing, ball screw nut and guideways of the X-axis are considered to be internal heat sources. The bearings are angular contact ball bearings and they are loaded both axially and radially except for the X-axis ball screw end support bearing which is loaded only radially to allow ball screw expansion. Figure 4-11 shows the main regions of the FEA model considered as heat sources for applying heat power.

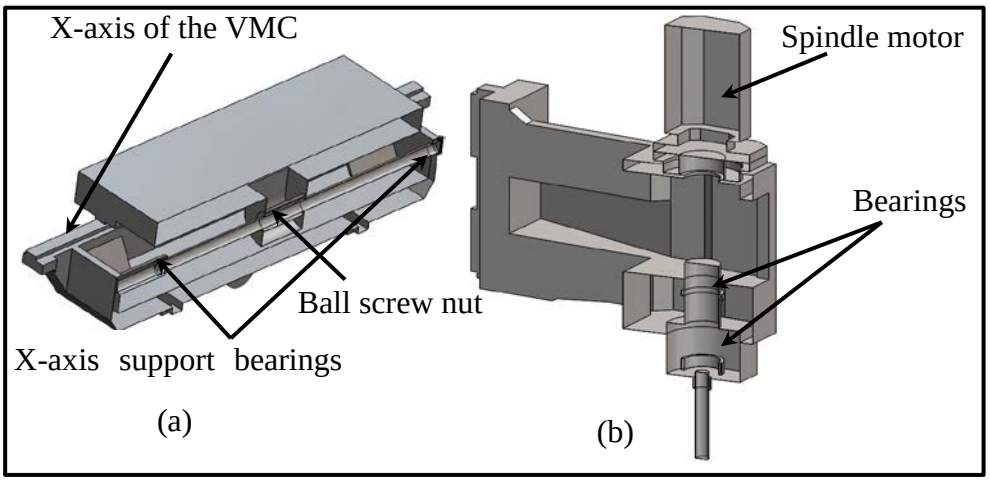

Figure 4-11 Location of modelled heat sources in the FEA model in (a) feed drive system

(b) headslide

4.5 Summary

This chapter shows an approach to identify thermal parameters and run FEA simulations to analyse the thermal behaviour of some simplified components, apply the relevant boundary conditions, TCR and validate the approach against hand calculations.

Three dimensional CAD models of all the significant components of a small C-frame VMC were created and assembled using SolidWorks software and the internal heat sources included in order to simulate the thermal characteristics offline transiently, the details of which will be explained in the next chapter.

Chapter 5

5 Machine tool thermal testing and offline modelling

In this research, two types of tests were carried out on a small VMC to excite the main heat sources: feed drive duty cycle and spindle duty cycle. Experiments were conducted to obtain the thermal characteristics of the feed drive system and the spindle separately so as to isolate the internal heat sources. These were in accordance with the ISO 230 Part 3 standard for thermal testing as described in Chapter 3. The heat power of the X-axis feed drive system were identified using two techniques; the general prediction technique based on formulae provided by OEMs and the energy balance method which has never been applied to parameter identification on the feed drive system of a machine tool. These two methods are described in Section 3.6. The parameters obtained from both techniques were applied in the FEA model of the machine feed drive system and validated against experimental results. The setup of the tests, data analysis, model configuration and simulation results are described in this chapter.

5.1 Feed drive system duty cycle

Recirculating ball screw systems are commonly used in machine tools and are one of the major heat sources which can cause considerable thermal drift, particularly on cost sensitive small to medium sized CNC machine tools that, utilise rotary encoder feedback for position control. Finite Element Analysis (FEA) has been used successfully in the past to model the thermal characteristics of such machine tool axes with promising results. Since FEA predictions are highly dependent on the efficacy of numerical parameters including the surrounding boundary conditions, this study focuses on an efficient modelling technique to obtain optimised numerical parameters for acquiring a qualitative response from the feed drive system model.

5.1.1 Experimental set-up

The ball screw of a small VMC horizontal X-axis was chosen as a typical representative low cost feed drive system, a schematic of which is shown in Figure 5-1. It consists of the ball screw shaft, front and rear bearings, ball screw nut and table. The ball screw shaft is axially constrained and radially supported by a pair of single row angular contact ball bearings at the driven end, while the other end is only radially supported to allow free expansion of the ball screw as it heats up. The bearings are mounted in housings located inside the supporting saddle structure. An AC motor is used to drive this system. The specifications of the ball screw feed drive system are listed in Table 5-1 [77].

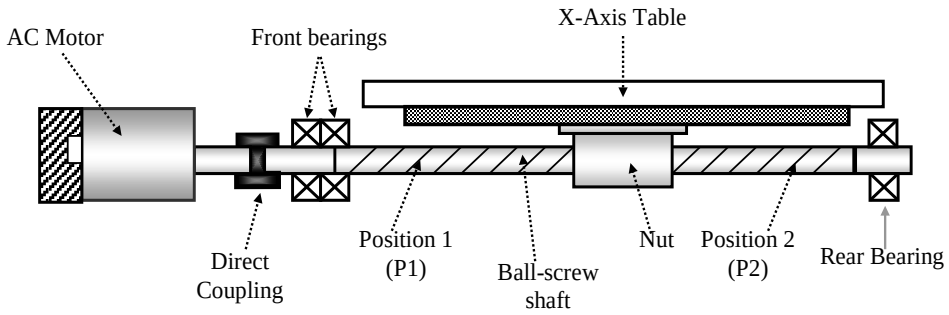

Figure 5-1 Schematic of the ball screw feed drive system

Table 5-1 Specification of the ball screw feed drive system [77]

Ball screw specifications			
Parameters	Value	Parameters	Value
Maximum speed	267 ±10 rpm	Nominal outer diameter of ball screw shaft	20 ± 0.1 mm
Axis stroke	500 ± 1 mm	Lead	10 ± 0.1 mm
Nut length	100 ± 1 mm	Mass of the saddle	122 Kg
Preload of nut using oversized ball	585 ± 20N	Mass of table	105 Kg
Nut type	Single	Bearing type	7204B (NSK)

Throughout the experiment, the temperature change and thermal deformation were recorded by the thermal imaging camera and laser interferometer respectively. Figure 5-2 shows the actual set up of the experiment. The initial temperature for the feed drive system was measured to be 23 ± 0.5 °C.

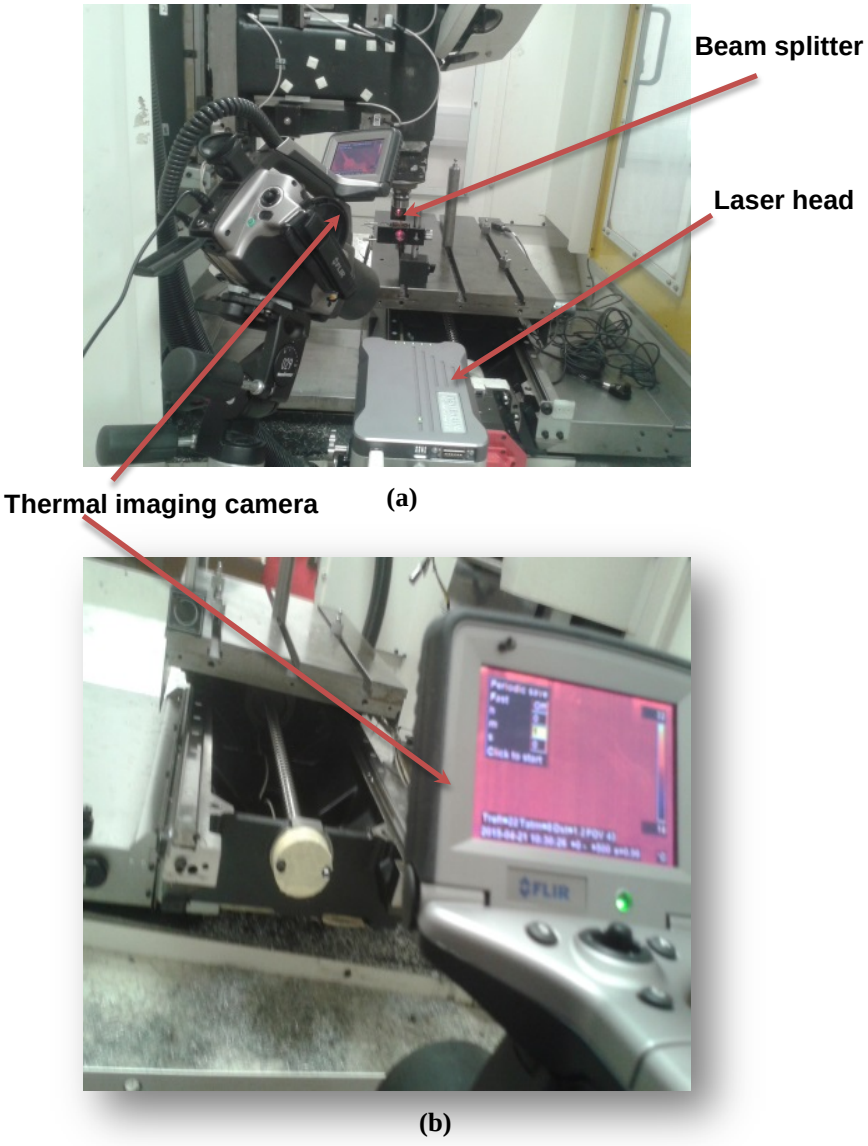

Figure 5-2 Experimental set up: (a) Front view. (b) Rear view.

The table movement was along the x-axis having a full traverse of 500 mm in the X-axis. The temperatures of feed drive heat sources, which are front bearings, rear bearings and ball screw nut, were measured at equal intervals of 10 sec using thermal imaging camera, see Figure 5-3. Two target positions were selected close to the end point of axes travel, due to which, the start and the end positions of the X-axis traverse were selected for the measurement of thermal error, the measurement method explained in Section 1.5.1. Over the 2 hour heating cycle, the table was traversed over its full range ten times at a rapid feed rate of 21 m /min which is 70 % of maximum [9]. At the end of each of these duty cycles, a

slower measurement cycle (feed rate of 2 m/min) with two stop positions at either end of the traverse range was performed, during which the displacement data was recorded. The cooling cycle lasted for 1 hour, during which, the table was rested for 60 sec before it moved to the measuring positions P1 and P2 to record the displacement data, see Figure 5-4.

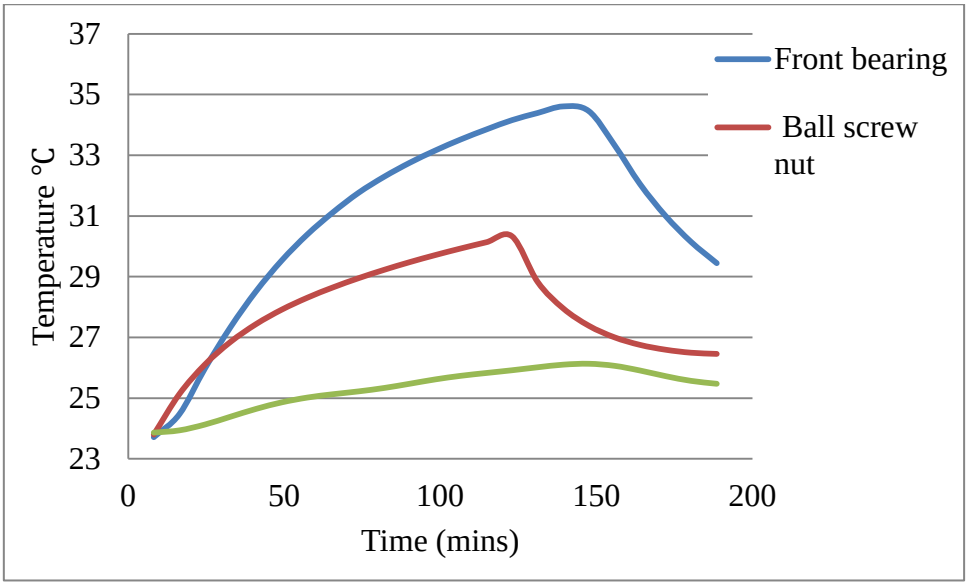

Figure 5-3 Temperature gradient of ball screw nut, front and rear bearings

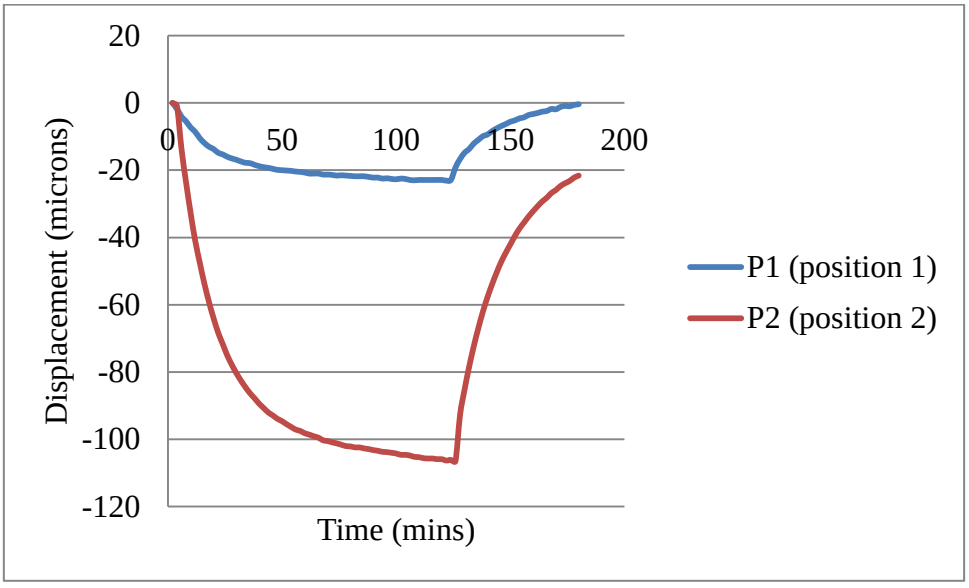

Figure 5-4 Displacement of the feed drive system at two positions

5.2 Thermal model

A FEA model of the ball screw feed drive system was created using the SolidWorks simulation software, as depicted in Figure 5-5. The aforementioned simplifications were applied to the model. The savings in mesh density around small features can be significant, while not adversely affecting, the thermal characteristics. In order to obtain good calculating precision, more mesh elements were assigned to elements representing heat power sources and adjacent areas [71]. A total of 40147 nodes and 22926 contact elements were selected for the FEA model. To visualise the density of the mesh, it is shown in Figure 5-6. The figure also shows the fixture location at the bottom of the saddle which corresponds to the Y-axis guideways. The rigid connection is a simplification but the temperature at the base of the saddle does not change significantly therefore negligible expansion occurs which negates the need for spring connectors representing the rolling elements.

Thermal Contact Resistance (TCR) between bolted joints was considered in the FEA model. The TCR is mainly determined by contact pressure, contact medium, material properties on both sides of the joint, and roughness of the surfaces. The clamping force of the oiled bearings, which tighten by screws of M12, is 80 KN [78], due to which, the TCR of 0.0002 (m^2.℃)/W was applied, as explained in Section 3.7. Due to complicated surface contact of ball screw shaft and ball screw nut, different magnitude of TCR of 0.028 (m^2.℃) /W was obtained experimentally, please refer to Section 3.8. The TCR figure was employed in the FEA simulations.

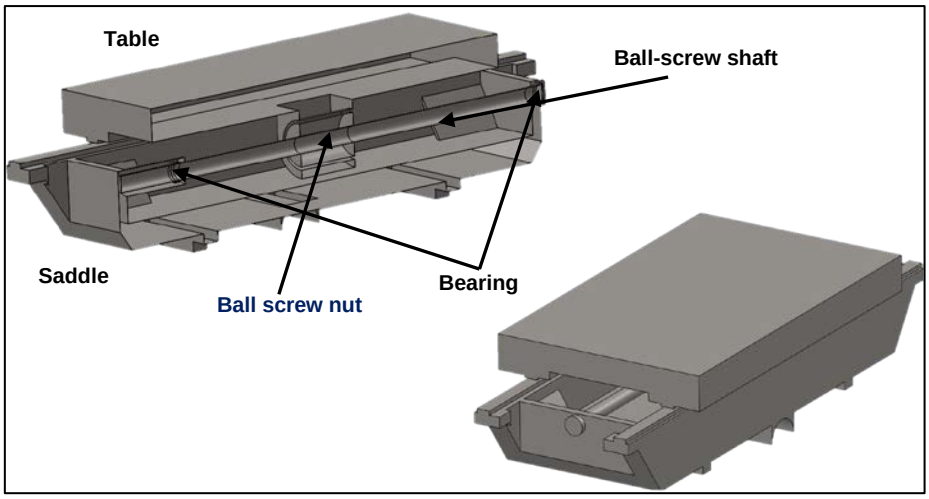

Figure 5-5 Solid model of the ball screw system

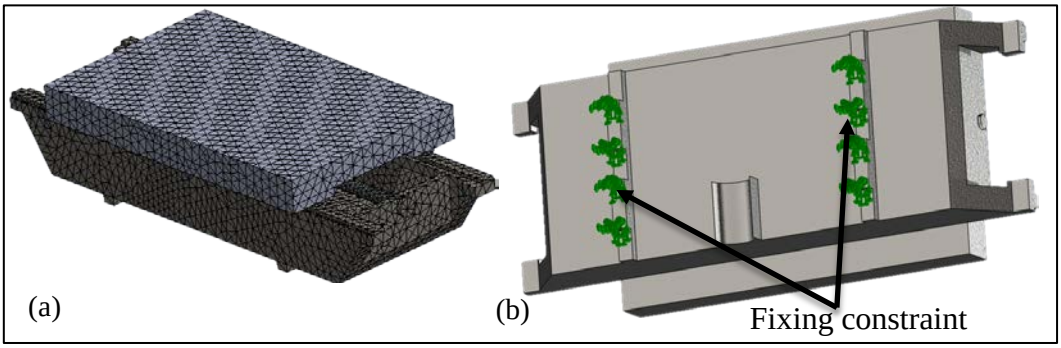

Figure 5-6 (a) Finite element analysis the ball screw system model;

(b) Fixing constrain position

The following assumptions are made in order to simplify the thermal model:

- The screw shaft is simplified to be a solid cylinder [55].
- The radiation term can be neglected as the temperatures involved are relatively low.
- During the measurement runs, the convective heat transfer coefficient was assumed to be steady during the cooling phase since the movement axis traverse rate was very slow (2000 mm/min).
- The TCR for the support bearing and the ball nut interfaces was the same

5.3 Computation of the convection coefficient of heat transfer

As the ball screw rotates, the resulting air flow means that forced convection must be considered for accurate modelling. The forced convection coefficient can be computed by heat transfer equations of air flow along a horizontal cylinder [63]. Refer to Section 3.5 for more detail on the associated calculations.

In order to use the equations associated with convection, some parameters should be obtained from previous literature. At normal temperatures, the Prandtl number of air is 0.701, the kinematic viscosity of the air is $16*10^{-06}$ m^2/s, m=0.5 and c= 0.683 [63]. Using these equations, the convection coefficient was calculated to be 12 $W/m^2.℃$ which was applied throughout the rapid traverse feed rate part of the simulation. In contrast, since the table movement during the measurement runs is very slow, the airflow was assumed to be close to natural, therefore, the natural convective coefficient of 6 $W/m^2.℃$ determined by Mian et al [13] was applied to the moving elements.

5.4 Heat generation

There are three heat sources in this feed drive system;

- Heat generated between the nut and screw shaft.
- Heat generated by support bearings due to the friction between the balls and races.
- Heat generated by the guideway.

In this study two different techniques are used to obtain the heat power parameters which later on are compared. These are aforementioned “formulae method” and “energy balance method” described in Section 3.6.

5.4.1 Formulae method

5.4.1.1 Heat generation due to friction between ball screw shaft and nut

The rolling (or running) torque required to overcome friction in the ball screw and nut system depends on a number of factors such as size, lubrication, types of seals and preload. To maintain accuracy and high rigidity, suitable preload must be applied to the ball screw nut system. Consequently, additional heat will be generated due to friction caused by preload between the ball screw shaft and nut. The heat generated is proportional to this torque and the rotational speed. Equations that are used to obtain heat generated by between ball screw shaft and nut are listed in Section 3.6.1.1. The heat power generated due to friction between the ball screw nut and ball screw shaft was found to be 25 ± 0.75 W. There can be uncertainties in formulae method calculation which can eventually lead to the formulae method giving lower accuracy, especially when the condition of the heat sources changes. The structural uncertainties were in machine component measurements and their specifications due to the fact that the manufacturer's drawings and specifications were not available.

5.4.1.2 Bearing heat generation

As with the ball screw, heat generated in the angular contact rolling element support bearings is due to friction which is influenced by speed, preload, and lubricant and can be calculated by equations listed in Section 3.6.1.2.

The specification of bearings can be found in Table 5-2 [79]. For the front, axial constrained support bearing, opposing pair of these are used while at the rear, only one is used.

Table 5-2 Bearing specification

Bearing	**Front/rear**
Contact angle	40^{o}
Inner diameter	20 ± 0.1 mm
Outer diameter	47 ± 0.1mm
Mean diameter	33.5 ± 0.1 mm
Width	14 ± 0.1 mm
Lubrication mode	Oil spot

The heat power generated due to friction between the front bearings, rear bearing and the ball screw shaft found 4.5 W ± 0.75 and 2 ± 0.75 W respectively. It was found that more heat was generated by front bearings as they provide support axially and radially while rear bearing provide only radially support. These calculations might have some uncertainties as the bearings are not visible and manufacture's drawing not available.

5.4.1.3 Heat generated by the guideway

The guideways are also one of the possible heat sources in the machine tool, particularly for high speed machining and where hydrostatic systems are used. In this case, for common rolling element bearings, heat generation of the guideways can be calculated by equation stated in Section 3.6.1.3.

Equation 3.19 was used to calculate generated heat by guideways, it was found that the heat power on each side of table slides is 1.25 ± 0.75 W for velocity of 21 m /min and a friction

coefficient of 0.12 [55]. The temperature of the guideways was measured using the thermal imaging camera, see Figure 5-7, which showed no significant increase in temperature. Masking tape was used to increase the emissivity of part of the guideways to ensure the readings were as accurate as possible. The lack of heat generation could be due to the fact that this small VMC has small sized guideways (≈20 mm^2) and the highest feed rate of this machine is still relatively low and therefore not sufficient to generate heat flow across guideways as compared to other machine tools with high speed systems. The data also correlates with work completed on another machine which also showed negligible guideway temperature even after significant weight was added to the table.

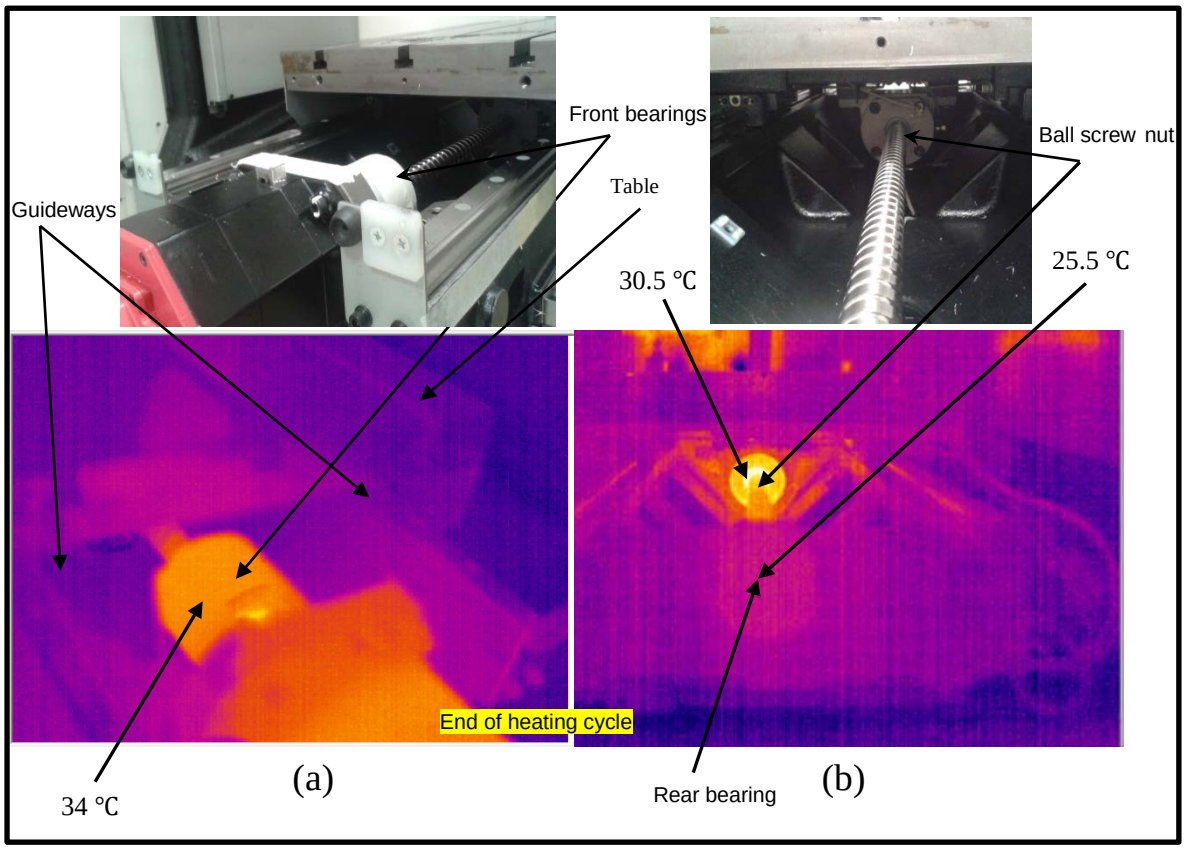

Figure 5-7 Main structure and thermal image of ball screw feed drive system: (a) Front view (b) Rear view

5.4.2 Energy Balance method

Heat power of all sources in the ball screw feed drive system can be calculated using equation 3.23 based on temperature data from a thermal imaging sequence and estimates of the convective heat transfer coefficient. The practical implementation of this requires the heat sources, which are front bearing, rear bearing and ball screw nut, of the feed drive system to be imaged periodically (every 10 s) utilising the thermal imaging camera. There must be consideration for parts of the machine which are difficult to see with the camera which require. This is more often than is typically required to track temperature change but this oversampling was useful to mitigate the fact that the table moves forward and backward, making it difficult to have all the thermal images of the heat sources. However, it was possible to have reasonable temperature gradient of the heat sources despite some missing data. The detail spatial information from the thermal images is also used to monitor the heat flow across the boundaries of the material sections selected for the energy balance calculation. As discussed in the literature review, this existing method has some uncertainty due to conduction, the reduction of which is part of the additional novel work in chapter 6.

The heat flow in the feed drive system structure due to heat sources excited can be identified from thermal images, Figure 5-7. The mass and area of each heat source are needed to calculate the heat power value of each heat sources. This can be done by selecting the specific feed drive system structure volume which is near to the heat source and the thermal images show heat flows in it, see Figure 5-8. The obtained heat powers are shown in Table 5-3.

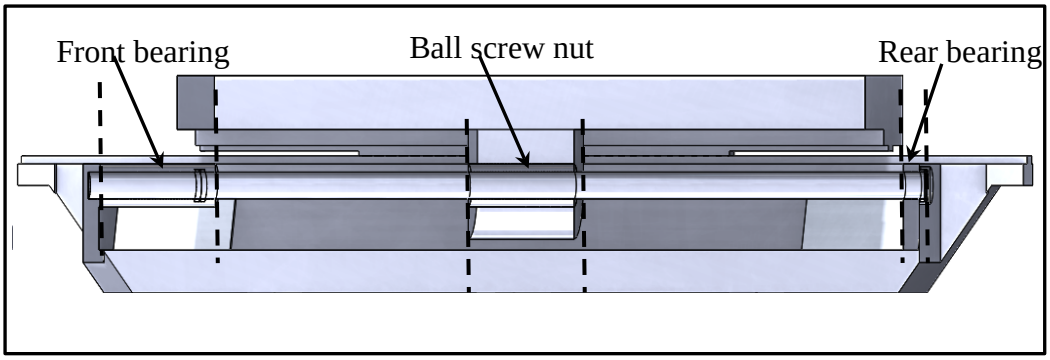

Figure 5-8 Selected specific volume of feed drive system heat sources

Table 5-3 Heat power of the significant heat sources

Heat sources	**Heat power (W) formula method**	**Heat power (W) balance method**
Front bearing	4.5	7 ± 0.75
Rear bearing	2	4 ± 0.75
Ball screw nut	25	27.5 ± 0.75
Guideways of table	1.25	Negligible

From Table 5-3, one can observe the difference in heat power obtained using both methods. When a machine tool is brand new, the formulae method and the balance method may be more likely to give similar results of heat power since the machine tool is in its ideal condition and the components are closer to specification (although in reality the OEM specifications often have large uncertainty factors). However, in the case of a used machine tool, the energy balance method is probably more accurate as the machine elements efficiency decreases due to many reasons such as wear, misalignments and low efficiency

clamping system force. The small VMC under consideration is at least five years old therefore, in its current condition, the balance method would be ideal to obtain more reliable and accurate behaviour of the temperature and displacement compared to the formulae method. This is validated in the following section.

5.5 Thermal simulation of the feed drive system

Transient studies for each simulation were conducted for the same duration as the experiments (described in 5.1.1), (3 hours: 2hrs heating and 1hrs cooling). The numerical parameters calculated for the heat sources shown in Table 5-3 and boundary conditions were applied to the respective elements in the FEA model. These include convective heat transfer coefficients applied to the table, ambient conditions and fixed geometry constraints to the saddle to treat it as fully constrained at the base, as depicted in Figure 5-6.

The FEA model of the feed drive was simulated while the table is stationary which is different from the actual experiment. In order to address this simplification and reduce the effect on the simulation results, the total heat power, which is generated due to friction between balls and ball screw shaft at one side and the other side between balls and body of ball screw nut, (see Figure 5-9) was applied to a small intermediate body representing the ball bearings. This was attached to ball screw nut body at one side and the other side to the ball screw shaft. This can simulate the actual heat transfer in the experiment as the heat conducts to both the body of ball screw nut, and the ball screw shaft.

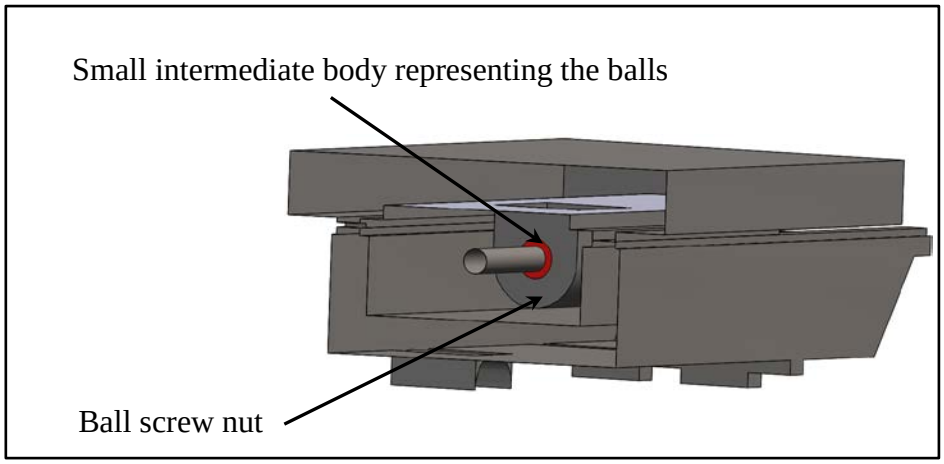

Figure 5-9 Ball screw nut details

Furthermore, in the experiment due to the movement of the ball screw nut, the temperature gradient of the ball screw shaft is more uniform; therefore, the total expansion is the total uniform expansion of its elements. This is not the case in the simulation because the table is stationary which means the heat is more localised. This problem was overcome by applying the total heat power to the intermediate body which makes the elements under and adjacent to the nut expand more but the other element expand less with the resulting expansion remaining accurate.

This can be validated by simulating a shaft which has same dimension and specification of the ball screw shaft of the feed drive system. The shaft was divided in to 6 parts in order to apply heat power to some of these parts. The TCR at parts connection was considered to be zero to represent heat flow in one part of the shaft, see Figure 5-10.

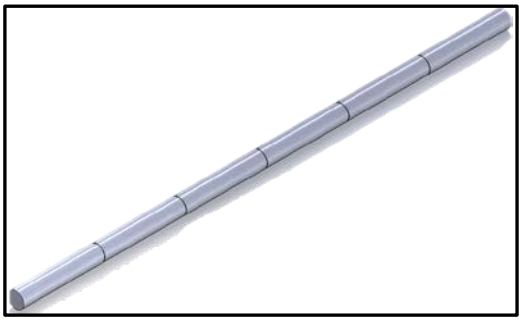

Figure 5-10 Assembled shaft

The gradient of shaft temperature was simulated twice: the first one, heat power of 2 W was applied to all parts in order to have uniform temperature gradient and the second simulation doe by applying heat power of 6 W to two middle parts. The second simulation is similar to feed drive system simulation, see Figure 5-11.

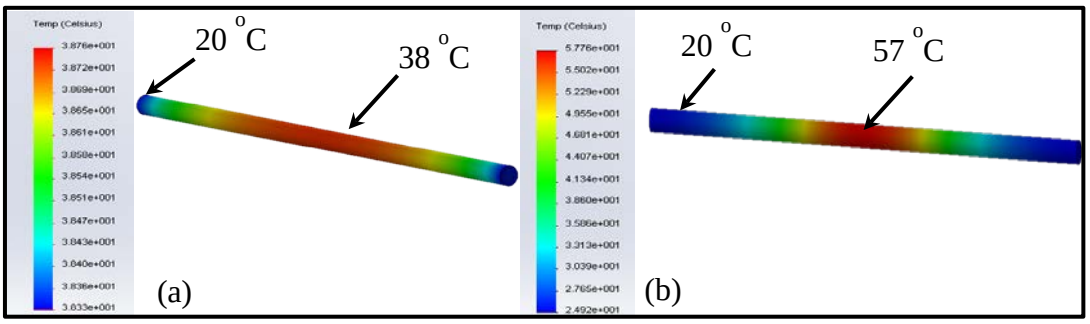

Figure 5-11 Assembled shaft simulation: (a) Heat power applied uniformly

(b) Heat power applied to the middle

In order to obtain the total shaft displacement one side of the assembled shaft was fully constrained which represents the fixed-free bearing support, then simulated displacement data was probed from a node positioned at the other end of the assembled shaft. Figure 5-12 shows that the total displacements, which are probed at the free end of the shaft, have negligible difference.

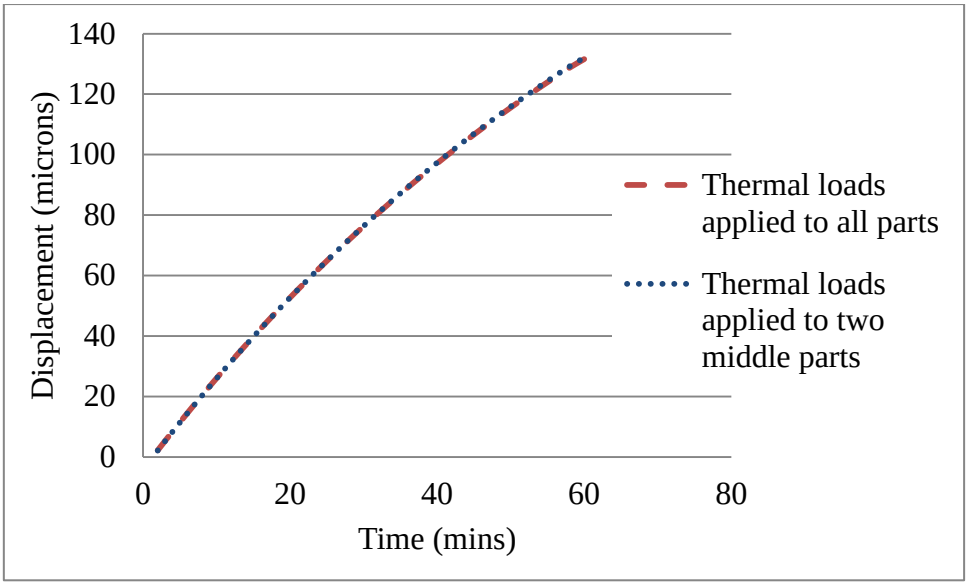

Figure 5-12 Simulation of ball screw shaft using different heat power distribution

The simulation result of the temperature gradient of the feed drive system is shown in Figure 5-13. There is a small temperature increase in the table due to the effects of heat generated at the ball screw nut and bearings.

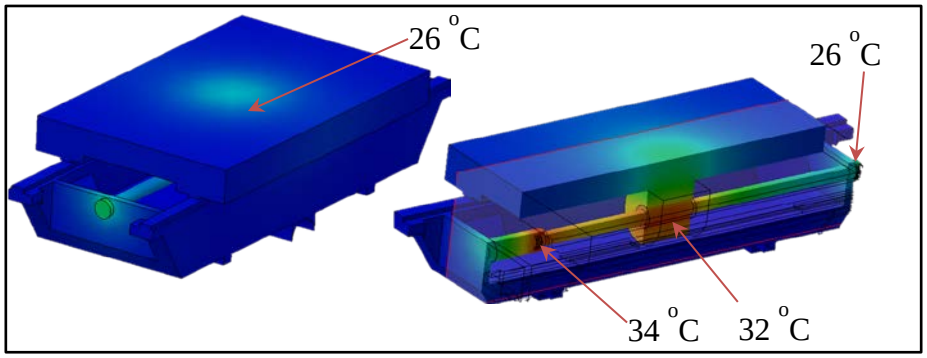

Figure 5-13 Temperature distribution of feed drive system

Figure 5-14 and Figure 5-15 show a significant temperature change in the ball screw nut and front bearings and a smaller temperature increase of the rear bearing as depicted in Figure 5-16. This is expected because the rear bearing is smaller (only one race) and only supports the ball screw shaft radially which reduces the amount of load applied on it compared to front bearings. Simulated temperature data was compared with experimental

data using both methods. The correlation between simulated and experimental data at various locations around the systems was good, with averages of 70 % and 80 % for the formula and balance methods respectively.

It was discussed in Section 5.4.2 the possible reasons behind the energy balance method providing improved results compared to the formulae method. However, it can be noticed that the simulated temperature gradient profiles obtained from the energy balance method do not fit perfectly with the experiment data and are usually lower in magnitude than the experimental temperature gradient profile. Upon analysis, this can be justified for the following reasons: the specification (detailed drawings) of the machine tools structure was not available. Therefore, the material was assumed to be cast carbon steel for which typical property values were assumed. The component dimensions were therefore also not available; consequently they were measured manually which indicates uncertainty in CAD component dimensions. Furthermore, the convective coefficient was averaged to be 6 $W/m^2.k$ across all surfaces of the machine tool elements which might be able to be lower than the actual value as many of the machine surfaces due to their orientation and also the air movement around the machine from moving axes, fans and surrounding activity. An underestimation here would contribute to the underestimation of the results.

The next stage is to correlate the simulated displacement data with the experimental displacement data. The bottom surface of the saddle was constrained to simplify the model at the Y-axis interface which is not part of the simulation. The simulated error was measured from nodes positioned at the actual displacement sensor positions utilised to observe the displacement of the feed drive system as discussed in the experiment set up. Figure 5-17 shows the simulated and experimental displacement data in the X-axis using heat rates from formulae and energy balance method.

It can be observed that the simulation results from the energy balance method correlate more closely with the experimental data than the results from the formulae method. The remaining thermal error in X-axis at position 2 (P2) is approximately 30 ± 0.01 µm using the formulae method while it can be decreased to less than 18 ± 0.01µm using the energy balance method from 106 ± 0.01 µm. At position 1 (p1) the thermal error was reduced to approximately 6 ± 0.01 µm using formulae method whereas it was decreased to 4 ± 0.01 µm using the energy balance method from 20 ± 0.01µm. Figure 5-18 summarises the differences between the models and experiments.

It can be noticed that more thermal error at the P2 than P1 as P2 is near to fixed end of the ball screw shaft and it is the start point of table movement while the p1 is near to the free end point and the end point of the table movement.

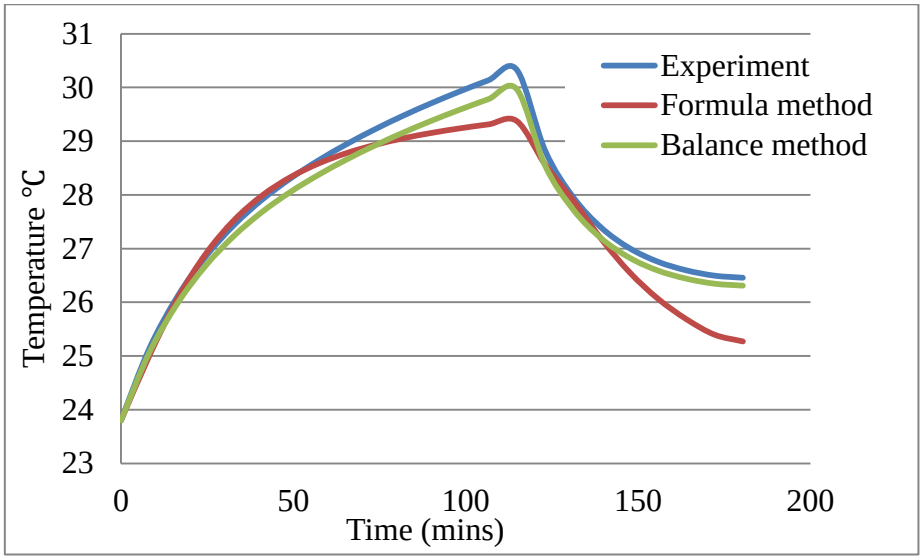

Figure 5-14 Experimental and simulated ball screw nut temperature comparison

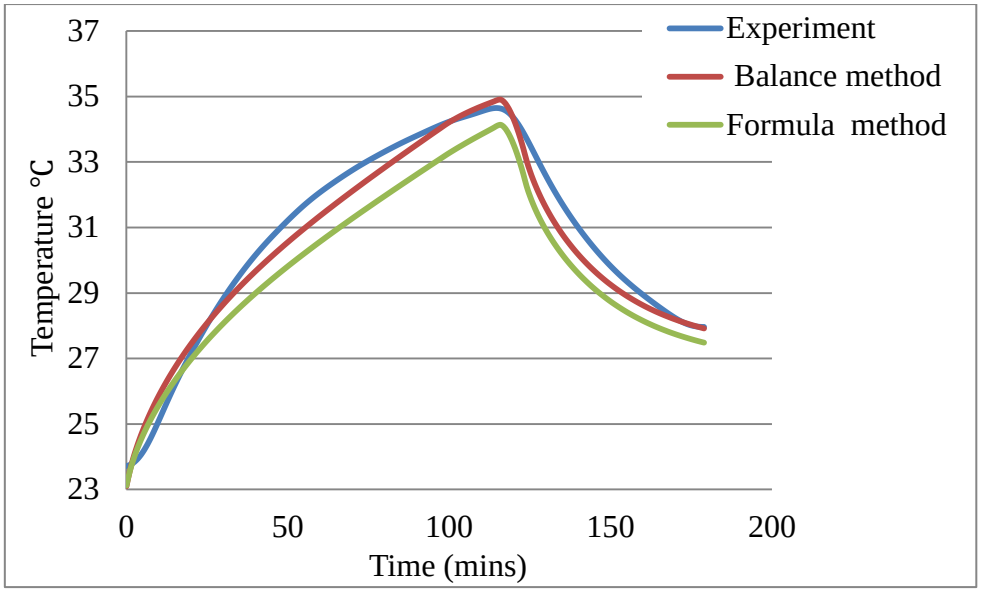

Figure 5-15 Experimental and simulated front bearing temperature comparison

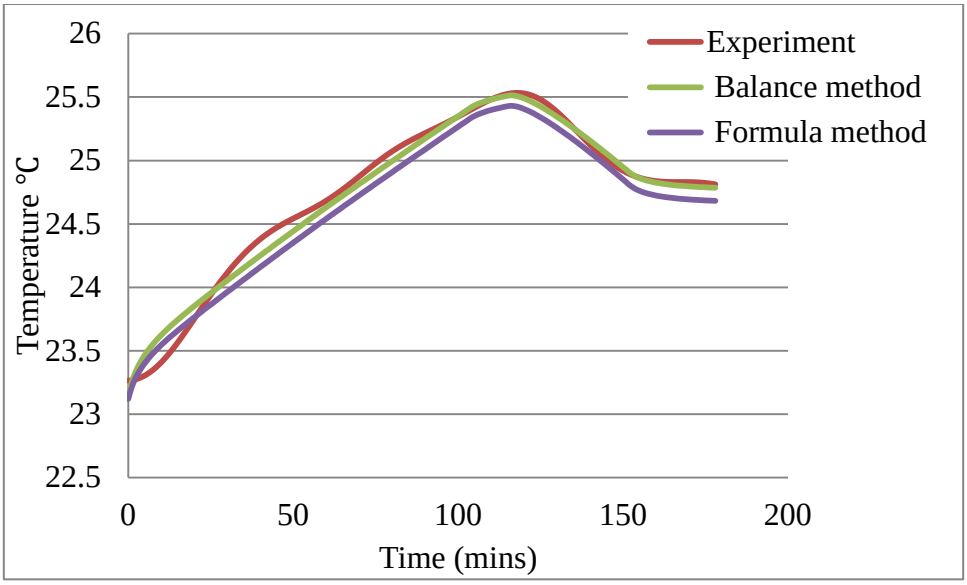

Figure 5-16 Experimental and simulated rear bearing temperature comparison

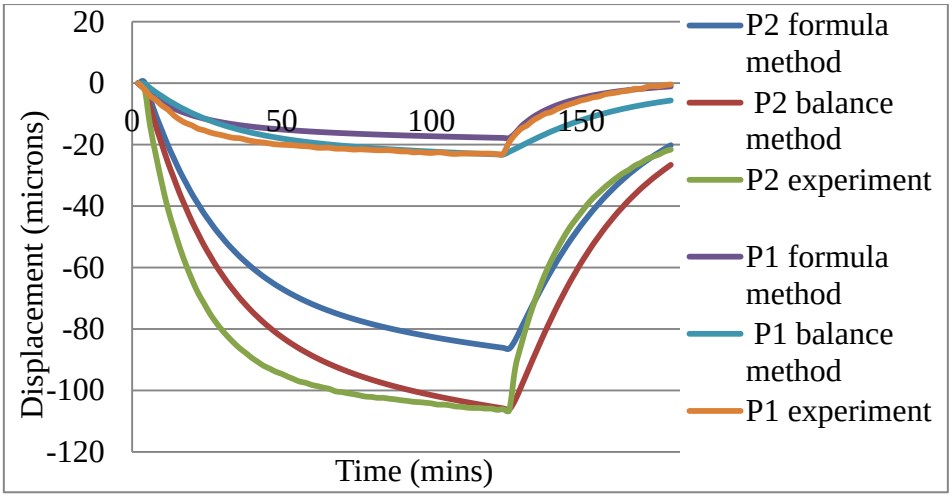

Figure 5-17 Experimental and simulated displacement comparison at two positions

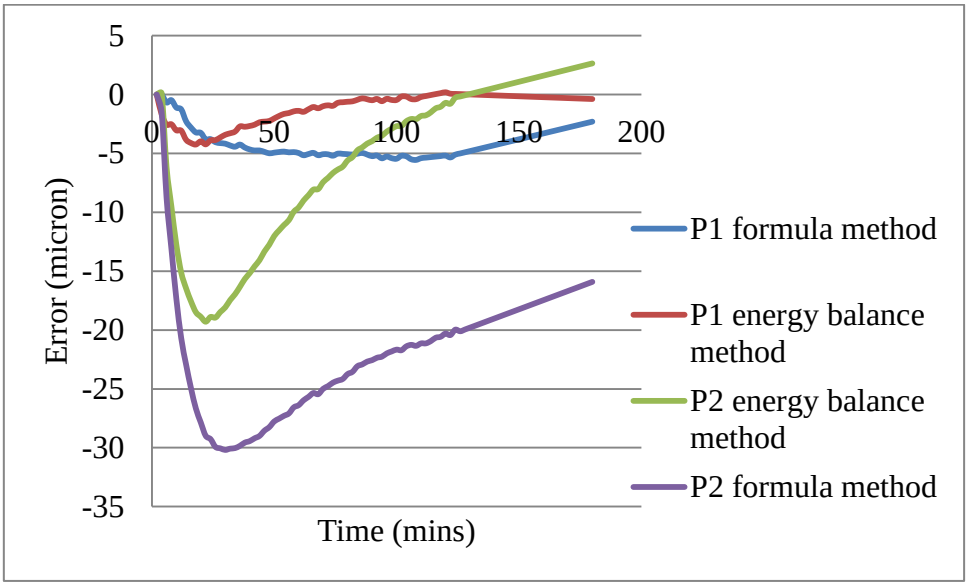

Figure 5-18 Residual error of feed drive system

In order to further validate the performance of FEA model on another set of data, a much long-term and more random duty cycle was conducted on the same machine as follows: The duty cycle took 6 hours and 15 minutes, 1.5 hours heating cycles with feed rate of 21 m /min, it followed by 1 hour cooling down, then 2 hours heating up at feed rate of 15 m /min and 1 hour and 45 minutes cooling down at the end. During the experiment, the ball screw nut and bearings temperature gradient was recorded periodically by thermal imaging camera and the thermal errors were measured by the laser interferometer.

In order to validate the FEA model on the experimental results from a complex duty cycle, the same heat power values listed in Table 5-3 was utilised at the same duty cycle test time.

Although the displacement results are the most important from a performance perspective, the following temperature comparisons are also included for information on how well the extended simulation matches the experiment.

Figure 5-19, Figure 5-20, Figure 5-21 and Figure 5-22 show duty cycle of experimental and simulated data of temperature gradient and thermal errors profiles.

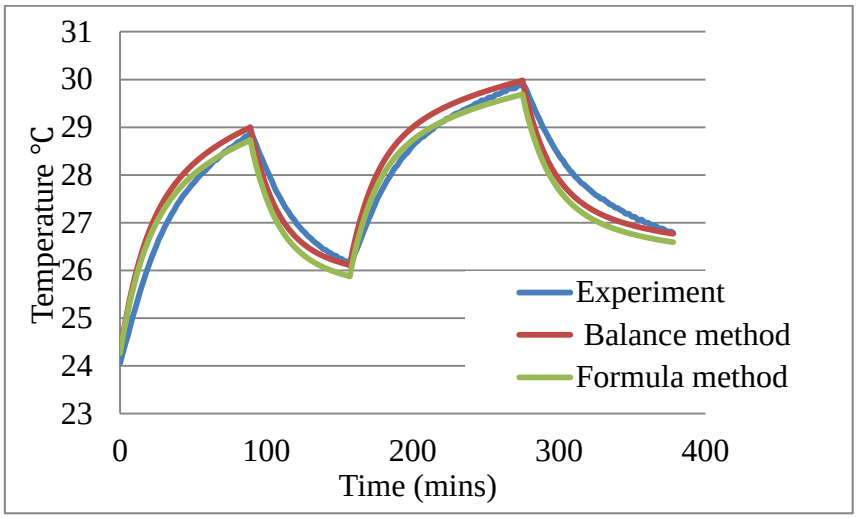

Figure 5-19 Duty cycle test profile of experimental and simulated ball screw nut temperature comparison

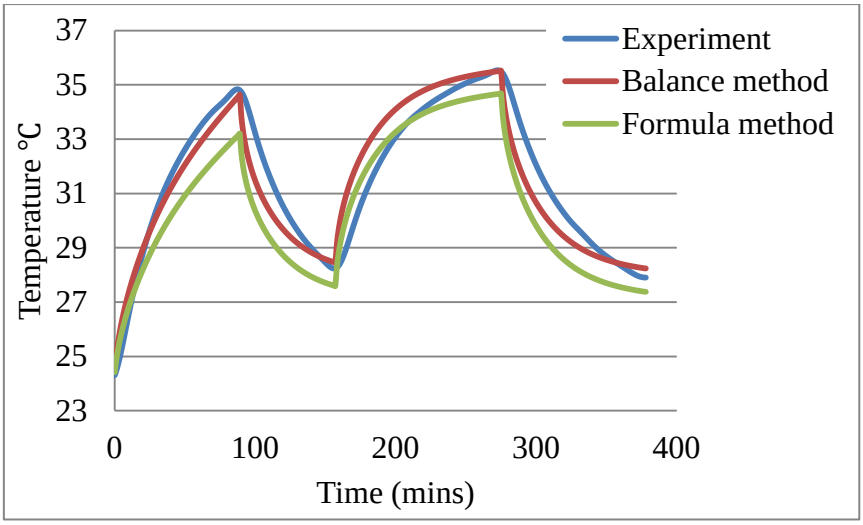

Figure 5-20 Duty cycle test profile of experimental and simulated front bearings temperature comparison

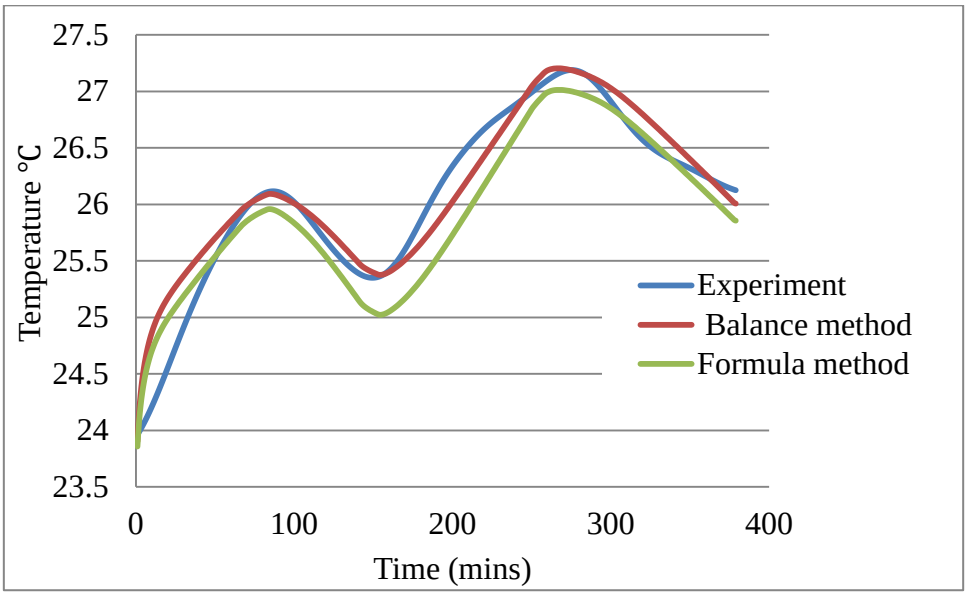

Figure 5-21 Duty cycle test profile of experimental and simulated rear bearing temperature comparison

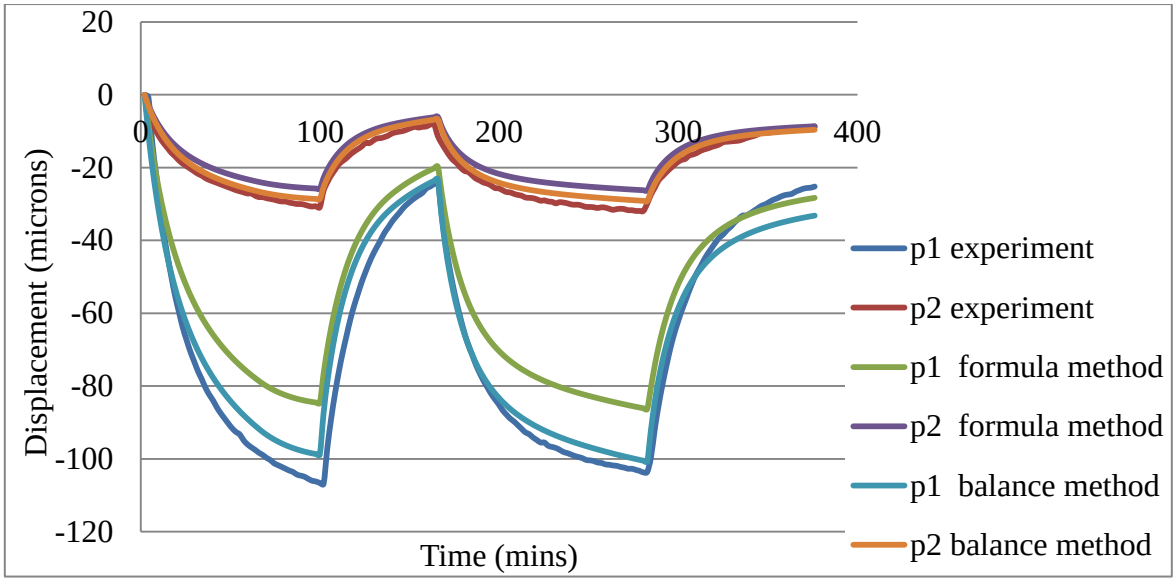

Figure 5-22 Duty cycle test profile of experimental and simulated displacement comparison at two positions

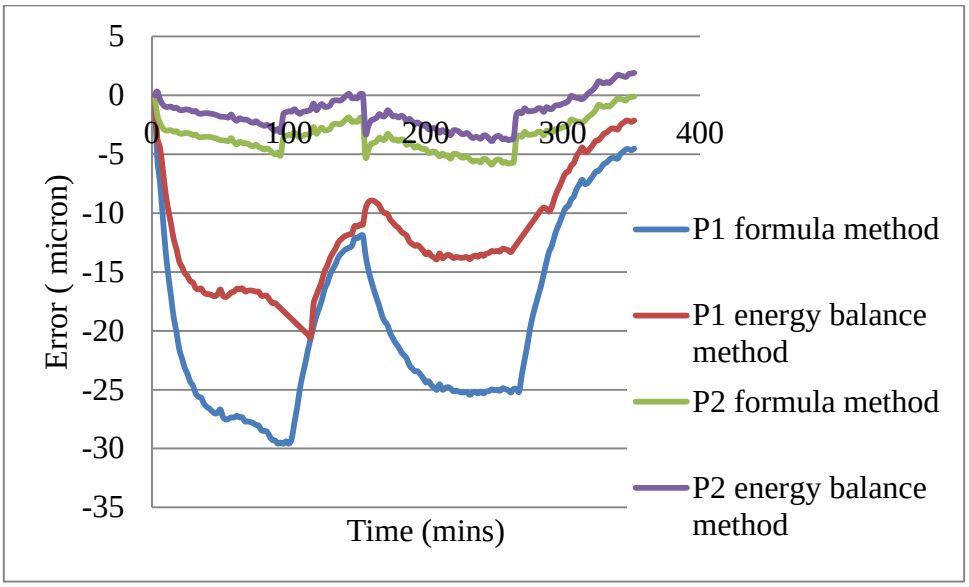

Figure 5-23 Residual error of feed drive system

From the extended duty cycle test results, it can be again noticed that the simulation results from the energy balance method had a better agreement with the experimental data than the results from the formulae method.

The duty cycle test also reveals that he remaining thermal error in X-axis at position 2 (P2) is approximately 30 ± 0.01 µm using the formulae method while it reduced to 20 ± 0.01 µm using the energy balance method from 106 ± 0.01 µm. At position 1 (p1) the thermal error was reduced to approximately 6 ± 0.01 µm using formulae method whereas it was decreased to 4 ± 0.01 µm using the energy balance method from 20 ± 0.01 µm. Figure 5-23 summarises the model differences.

From the results, the energy balance method appears to be more suitable than the formula method for accurate simulation which may be expected as the small VMC tested is not brand new. The subsequent spindle thermal characteristics test is conducted by energy balance method and elaborated in the next section.

5.6 Spindle heating test

The main spindle is the component of a machine tool that typically contributes the most to the total thermal errors due to the significant heat generated from its high rotational speeds, hence the concentration of past research, reviewed in Section 2, on this part of the machine. Thermal deformation studies of the spindle are therefore necessary in order to significantly reduce the total thermal errors. This research will analyse the existing energy balance method on the test machine which has a different kind of spindle to previous research and will provide a basis to build on with a novel solution to improve simulation accuracy which is discussed in the Chapter 6. The boundary conditions are calculated according to measured parameters including, temperatures of machine structure, heat transfer coefficients and ambient temperature. Of particular importance is the heat power of the heat generating components in the spindle which are the motor, upper and lower bearings. These parameters vary with machine use and are calculated using energy balance calculations and thermal imaging data. The FEA simulated results were obtained and are in close correlation with the experimental results. Such accurate FEA simulations permit offline assessments to be made

of temperature gradients and displacements in machine tools structures, reducing the need for expensive on-line testing. Furthermore, correlation coefficient analysis is employed to validate the simulated model temperature.

5.6.1 Experimental set-up

During the experiment the thermal imaging camera was used to monitor the heat flow through the machine structure while the spindle rotates at 8000 rpm (close to its maximum speed) for two hours heating and stopped one hour to cool down. The camera location was chosen so that the heat flow into the spindle, head slide and motor can be monitored. The accuracy of the thermal image was improved by applying masking tape (with identified emissivity of (0.95) to areas of thermal interest and averaging the images to decrease noise [66]. Eddy current NCDTs were used to measure the spindle deformation in X, Y and Z-axes. The stated accuracy of the NCDTs is ± 2 µm. Although not precisely controlled, the ambient temperature of the workshop remained fairly constant between 21 ± 0.5 ^{o}C and 22 ± 0.5 ^{o}C throughout the experiment. Figure 5-24 shows the thermal characteristics test set up.

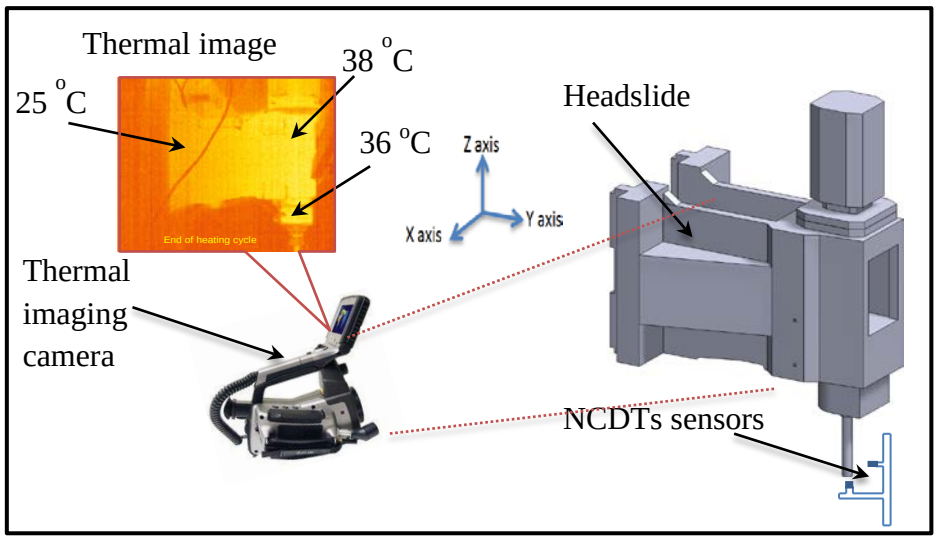

Figure 5-24 Thermal characteristics test platform

5.6.2 Development of the FEA simulation model

The FEA model of the machine tool spindle system was developed using SolidWorks to study and predict the thermal characteristics. Figure 5-25 shows the three dimensional (3D) model. Heat loss from the back of the headslide through the vertical axis guideways is negligible as the heat sources are relatively far away, therefore it was assumed that the heat transfer by conduction was negligible and no boundary condition was applied.

As before, some unimportant structural details were simplified during 3D model creation. This helps to reduce mesh elements that would otherwise affect the computational time for FEA simulation [71;76]. The FEA model was partitioned to 86166 elements. Three internal heat sources of the spindle were considered; spindle motor, upper and lower spindle bearings. The bearings are located close to the spindle nose and the top of the spindle system respectively.

The spindle system is primarily made using three materials, and these material properties were assigned to their corresponding structures in the FEA analysis software. The spindle and associated rotational parts are made of steel, the test bar from aluminium and the rest of the spindle system structure from grey cast iron. The material properties are presented in Table 5-5 [75].

Table 5-4 Machine tool material properties

Material	**Grey cast iron**	**Steel**	**Aluminium**
Density (kg/m3)	7200	7800	2700
Specific heat (j/kg.oC)	510	500	960
Thermal conductivity (W/m.K)	45	30	120
Thermal expansion coefficient(m/m/°C)	$1.2*10^{-5}$	$1.2*10^{-5}$	$2.5*10^{-5}$

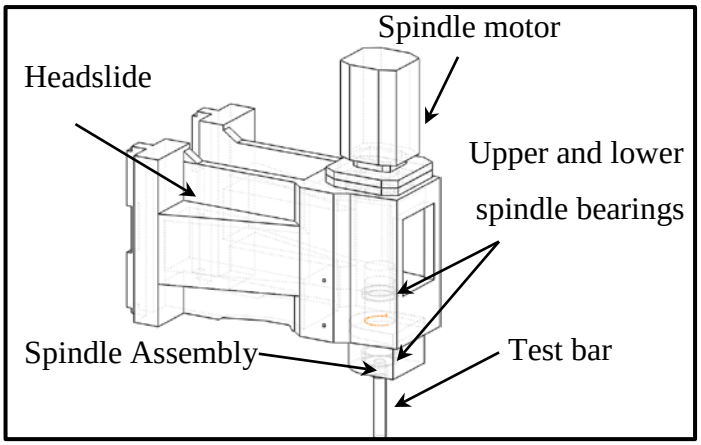

Figure 5-25 CAD model of the spindle system

5.6.3 Definition of the boundary conditions

The simulation accuracy depends on accurate determination of the initial conditions and boundary conditions based on the characteristics of the spindle system structure and the thermal properties [67;80]. These conditions are: (1) initial conditions analysis such as the initial temperature, the ambient temperature, and the thermal parameters for the various materials from which the machine tool components are made. (2) Thermal contact resistance

at spindle system joints (3) heat power calculation of heat sources such as spindle motor and bearings in this case (4) convective heat transfer coefficient calculations such as the natural convection between the static surfaces of the machine tools and the air and the forced heat transfer coefficients between the rotating surfaces of the test bar and the air. These conditions will be explained in detail as follows:

5.6.3.1 Thermal Contact Resistance (TCR)

For the various joints where components are bolted together, the effect of thermal contact resistance was applied. Its value is 0.0002 (m^2.℃)／W explained in Section 3.7.

5.6.3.2 Heat power calculation of heat sources

Heat power, which can be called thermal loads, of heat sources of the spindle system was calculated using energy balance method described in Section 5.4.1.2.

By using the thermal imaging data, material specifications and equations mentioned, the motor and the spindle bearings heat power of the spindle system are shown in Table 5-6. The formulae method was not considered to be used in this section as the energy balance method gives more accurate heat power in this case.

Table 5-5 heat power magnitude of headslide heat sources

Heat sources	**Heat power (W)** **Energy balance method**
Motor	50 ± 0.75
Lower spindle bearing	12 ± 0.75
Upper spindle bearing	8 ± 0.75

5.6.3.3 Determination of convective heat transfer coefficient

Natural and forced heat transfer convective coefficients were applied for spindle system components throughout the FEA simulations. As in the previous simulation on the machine axis, a natural convective coefficient of 6 W/(m^2.^{o}C) was applied around stationary surfaces such as the headslide and a forced convective coefficient of 92 W/(m^2.^{o}C) was applied around the rotating parts that are exposed to the air, such as test bar when the spindle is active and a value of 6 W/(m^2.^{o}C) applied while the spindle is not rotating, these figures were determined empirically by Mian [13].

5.6.4 Thermal simulation of the spindle system

Simulation of the spindle system was performed using transient thermal analyses available within the SolidWorks software. The initial temperature for the spindle system structure was set to 21 ± 0.5 °C and the duration of the transient analysis was set to 3 hours, which matches the experiment time. Heat powers obtained previously were applied to the FEA model to obtain the temperature field of the spindle system, see Figure 5-27.

In order to obtain the spindle system displacement, the correlation of the simulated stabilization period data with the experimental stabilization period data was conducted. The

back of the headslide was fixed as constrained. Thermal deformations of the spindle system in Y and Z axes were obtained. Results for the X-axis were neglected as error in this direction is negligible due to the machine symmetry.

Figure 5-26 shows the simulated temperature (a) and displacement field (b) of the FEA model. The simulated displacement data were obtained from the nodes located at the same displacement sensor positions used to monitor Y and Z axes. The residual errors from the simulation results (see Figure 5-22 and Figure 5-23) can be observed as 5 ±2 μm in the Y-axis and 10 ±2 μm in the Z-axis.

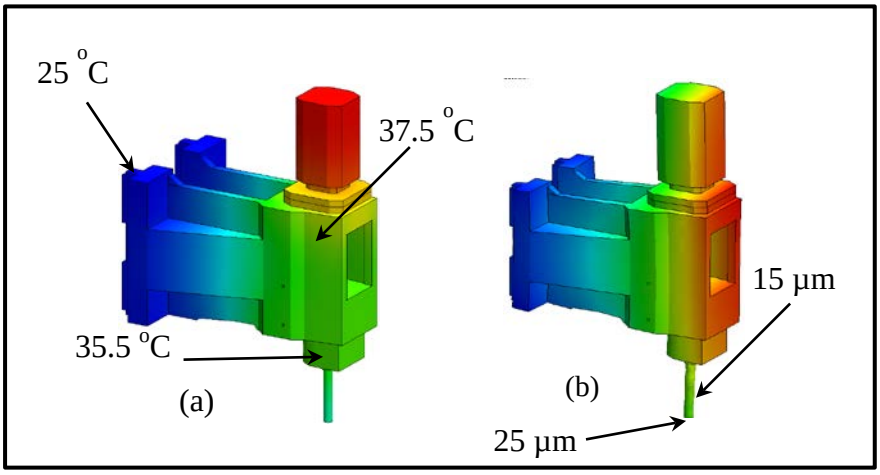

Figure 5-26 Thermal simulation results for the spindle system:

(a) Simulated temperature of the headslide (b) Simulated displacement of headslide

The results show that the simulated data and the experimental data are in good agreement. The simulation error was less than 30 %. It shows that the thermal characteristics simulation model proposed by this study is reasonably reliable. Further analysis of the correlation of the result to the experimental data is presented in the next section.

5.6.5 Correlation coefficient

Correlation coefficient is one of the standard statistical coefficients. It signifies the closeness of two arbitrary variables (X and Y) and its formula is showed as follows.

$$r = \frac{\sum_{i=1}^{n}((x_i - \bar{x})(y_i - \bar{y}))}{\sqrt{\sum_{i=1}^{n}(x_i - \bar{x})^2 \sum_{i=1}^{n}(y_i - \bar{y})^2}} \qquad 5.1$$

Where x and y are the experimental values of temperature or displacement and y the simulated values respectively.

As *r* approaches 1, it indicates that the two variables increasingly relate to each other [81]. Based on thermal imaging camera data and simulation results of the spindle system of VMC model, correlation coefficients of experiment and simulated data calculated at places close to the heat sources and spindle system of VMC axes are more than 80 %. See Figure 5-27, Figure 5-28 and Figure 5-29.

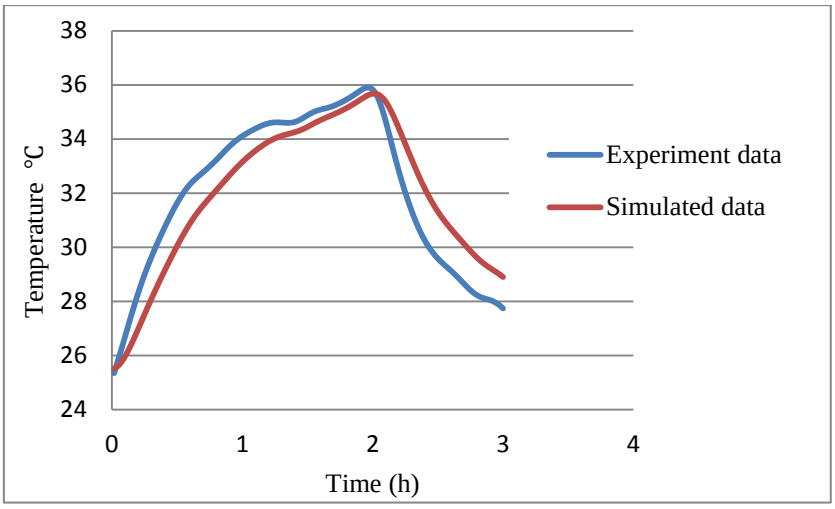

Figure 5-27 experiment and simulated temperature at spindle nose

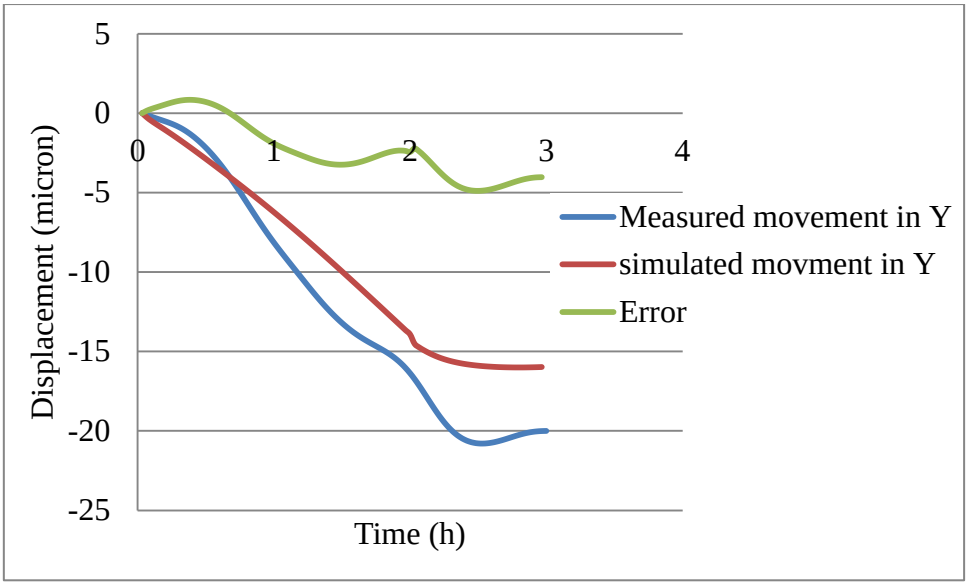

Figure 5-28 Displacement in Y axis

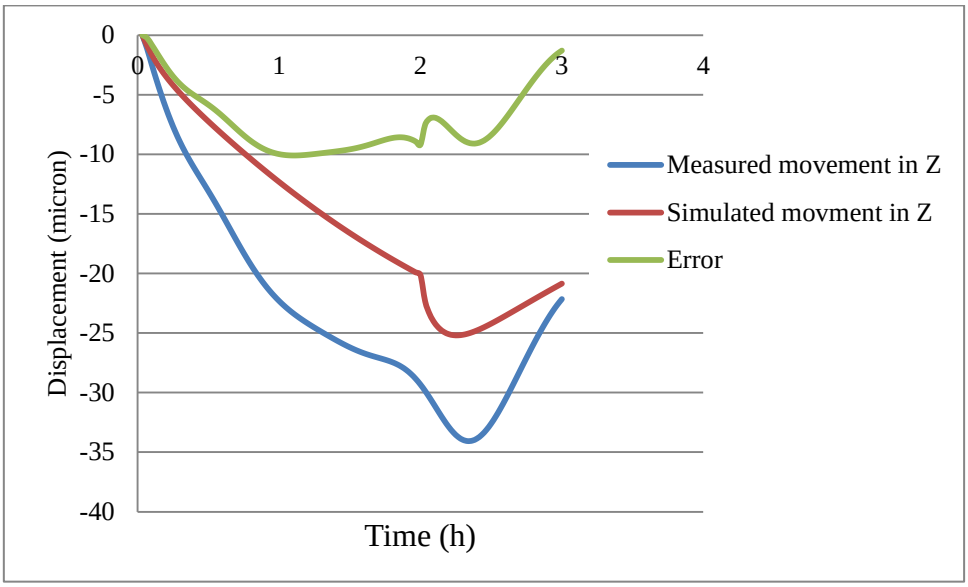

Figure 5-29 Displacement in Z-axis

The thermal error in Z-axis is larger than in Y-axis. This is because much heat is generated in the spindle bearings, which is near to the test mandrel; due to complexities in machine tools bearings such as variation in pre-load, viscosity of lubrication etc. It can be also as a result of test mandrel expansion as it has free end and simple structure. Displacement in Y-axis is small as it occurs as a result of machine bending due to different temperature gradient at

different machine tool structure such as different temperature gradient at spindle assembly and region near to spindle motor.

Furthermore, the temperature of various parts on the side of the carrier (from thermal imaging) was correlated with the same carrier surface on the model as indicated in Figure 5-30. The correlation coefficient of selected spots, area and axes displacement is indicated in Table 5-6 and Table 5-7.

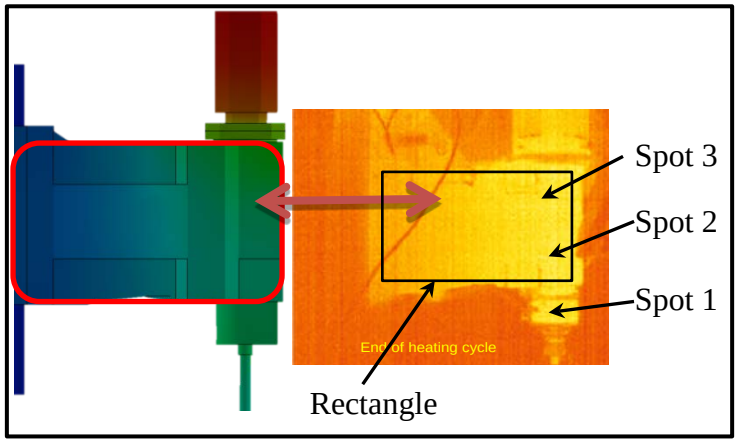

Figure 5-30 The selected area on the head slide model and thermal image

Table 5-6 Correlation coefficient at points of interest

Places on the carrier	Spot 1	Spot 2	Spot 3	The rectangle
Correlation Coefficient	0.92	0.91	0.91	0.90

Table 5-7 Axes displacement correlation coefficient

VMC Axes	X-axis	Y-axis	Z-axis
Correlation Coefficient	0.97	0.98	0.98

It is clear from the correlation coefficient values that the experiment and simulated results are close to each other. An additional comparison was made using measurement of temperature over an area of the surface, not just at a specific point. This will help indicate total energy input. An average temperature of the rectangle shown in Figure 5-30 taken from the thermal camera images was compared with the same area of the surface model temperature nodes. The result in Figure 5-31 shows they correlate by 80 %.

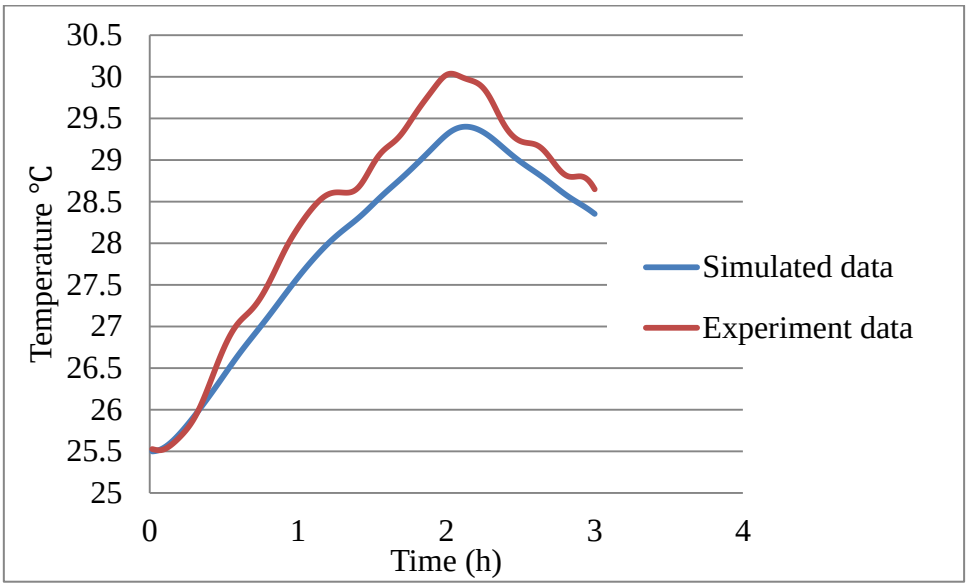

Figure 5-31 Headslide side temperature correlation

The simulated and the experimental profiles are in good agreement; however, the residual displacement error is about 30 %. This implies that the existing method for calculating some of the thermal parameters requires improvement and it is already known that there are some uncertainties associated with defining the regions of the structure where negligible conduction is assumed to occur and in the TCR and convections coefficients.

5.7 Summary

In this chapter, an efficient approach to identify thermal parameters and study the thermal characteristics of a three axis small VMC during varying operating conditions is presented and discussed.

Thermal error of the feed drive system of spindle system of machine tool were studied and analysed experimentally and the effects of internally generated heat sources on the positioning error of a ball screw feed drive system were predicted offline using the FEA model. To ensure accurate FEA predictions, the boundary conditions such as the heat transfer convective coefficients were calculated analytically. The heat power of the feed drive system of heat sources were calculated using two different methodologies; the formulae and the energy balance methods and compare them for their effectiveness. A longer term random duty test was conducted to validate the effectiveness of the FEA model. The residual displacement errors from simulation employing parameters calculated using the energy balance method was smaller than the formulae method. This can be justified as the machine under consideration was not new and it is known that the characteristics of wear items such as bearings change with use and therefore deviate from specification; therefore, the energy balance method has been proved to be more realistic and effective for assessing the current thermal status of the feed drive system.

Likewise, experimental work was conducted to obtain the thermal behaviour of the machine structure by running the main spindle. Heat power of the spindle heat sources were calculated by energy balance method. The predicted temperature rise and displacement data from the simulations fit the experimental data well. The correlation coefficient of experimental and simulated temperature of various parts on the side of the carrier and points of thermal interest was calculated at to validate the effectiveness of the FEA model. Differences in the simulation results were observed and assumed to be primarily a result of uncertainties in the energy balance and TCR calculations therefore a novel optimisation method is presented in the next chapter to fine tune the parameters and improve the accuracy of thermal error simulation.

Chapter 6

6 Thermal parameters optimisation

This chapter presents development and application of a novel 2D optimisation technique to find the optimal heat power of an object subject to multiple heat sources based on thermal imaging data. The concept grew from the use of thermal imaging to identify some of the boundary conditions as described so far in the thesis. However, as the structural complexity increases and/or where there are multiple heat sources that are sufficiently close that they interact in a complex manner, uncertainty in the energy balance method increases. This is due to temperature gradients across boundaries of the regions use to calculate the specific heat capacity. By analysing the change in the gradients across the surrounds surfaces over time, it was anticipated that the interaction between heat sources could be better understood and the associated heat power parameters more accurately determined.

A test rig of known heat power was assembled incorporating a plate, which is heated using small electrical heaters. The plate surface temperature gradient was recorded periodically by thermal imaging camera. Details of the test rig are included in the following section.

A 2D heat transfer model, representing the plate, was created in Matlab to calculate the same surface temperature gradient in order to be compared with real data from the plate test rig.
An optimisation function was used to minimise the sum-of-the-squares error between the experimental data (thermal images data) and model data to obtain the heated plate heat power which are validated against the power of the heater elements, calculated from the known heater resistance and measured current.
This method was then applied on the headslide side of small machine tools in order to optimise the heat power values of the headslide. The optimised thermal parameters will be

used in the machine FEA simulation and compared with the non-optimised energy balance method.

6.1 Plate test rig set up

Three 70 W electric heaters (Type A-3-DBK) were attached to the rear side of the plate, the dimensions of which are 340 mm x340mm x 20 mm depth. Multiple heaters were used to prove the methodology and the reliability of predicting heat power of multiple, interacting heat sources. The heater powers are controlled by current adjustable power supplies and the temperature monitored by temperature controllers and thermocouple sensors. The adopted (on-off) temperature controllers are mains supplied therefore relays circuits were incorporated to controller can cut off or give power to the heater through the relay.

Thermal imaging camera was used to measure and image the front side of the plate. The front side of the plate was covered by masking tape to increase the uniformity and magnitude of the emissivity. The test set up is depicted in Figure 6-1.

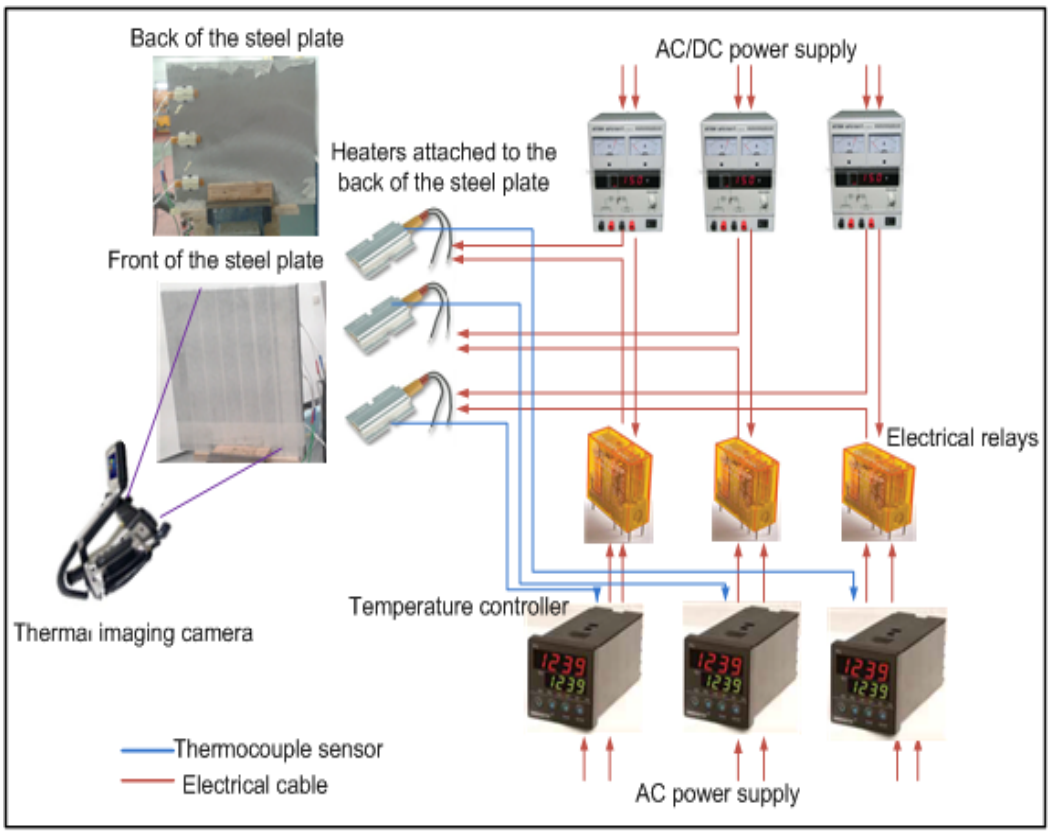

Figure 6-1 Heated plate test rig set up.

6.1.1 Plate surface temperature measurement

The set-point for the temperature controllers was set to 40 ^{o}C to represent a typical increase in temperature of a running spindle bearing. The heaters are securely attached to the plate with reasonable pressure using screws and heat transfer compound in the interface to help maintain a consistent heat transfer coefficient across the heater surface. The experiment was conducted using 3 different input configurations: using 1 heater on, then 2 heaters on and 3 heaters on. At each time the temperature rise of the plate surface was recorded by the thermal imaging camera, see Figure 6-2.

The heat power of each heater is simply calculated from the product of the voltage and current (equation 6.1) which is displayed on the Direct current (DC) power supplies. Table 6-1 shows the test rig parameters.

$$P=I*V \qquad 6.1$$

Where P is the heat power (W), I is the current (Amps), V is the voltage (V).

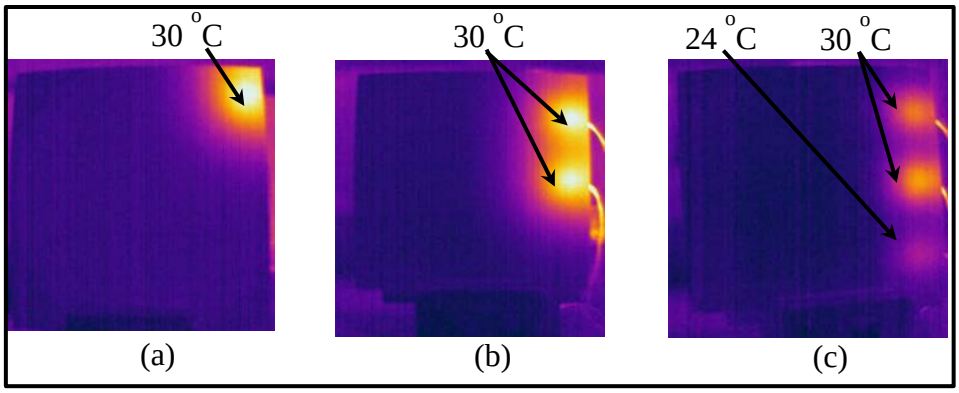

Figure 6-2 Thermal images of the plate: (a) 1 heater on, (b) 2 heaters on, (c) 3 heaters on

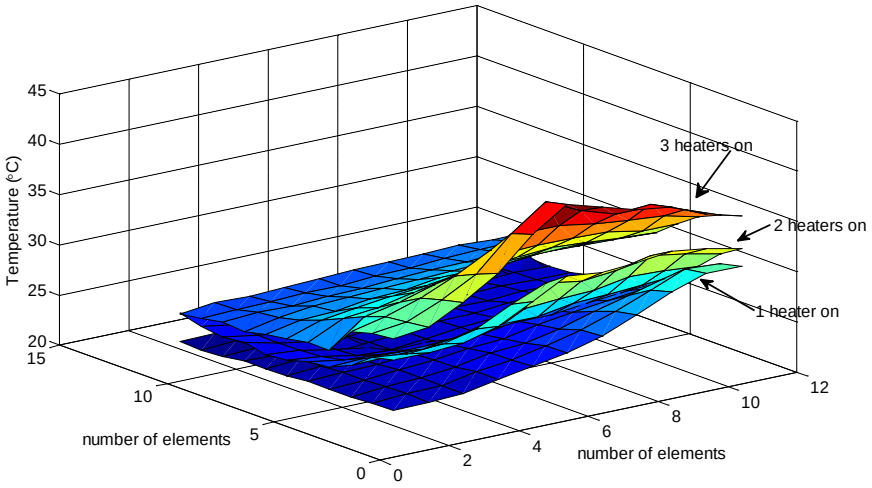

Figure 6-3 Plate surface temperature at end of 30 minute heating cycle

Table 6-1 Test rig parameters

Heaters	Ambient temperature	Current (Amps)	Voltage (Volt)	Heat power (W)
Heater 1	24 ^{o}C	2	12	24
Heater 2		2	12	24
Heater 3		1	8	8

Heat power of the heater 1 and 2 was higher than the heat power of heater 3. This is because of lower current input was used for heaters 3.

The thermal simulation of the plate was carried out to validate the correct application of the thermal parameters and determine the accuracy of the thermal simulations compared to experimental data. A FEA model of the plate and heaters was created using SolidWorks software.

In order to perform accurate simulations, the heat power and boundary conditions should be identified. The power of the heaters is obtained from the power supply, see Table 6-1 and the natural heat transfer convective coefficient of 6 W/m^2.K was obtained from previous work and experiments conducted in a workshop confirmed that there was no forced air flow or draft. The remaining unknown boundary condition is the heat transfer rate between the heater and the plate which is dependent on a large number of factors as described in Section 3.7.

A method for determining the thermal contact resistance (TCR) between heaters' surface and the plate was therefore required. The heaters and the plate are not manufactured with very high precision therefore, surfaces roughness and flatness is relatively poor, and specific to

this application therefore finding values from existing literature was not possible, the pressure applied by the M6 fixing screws is relatively low compared to typical machine tool mechanical joints. Consequently, the TCR values at the joints are expected to be high but completely unknown. In order to reduce the TCR value at joints, thermally conductive paste was applied. It was considered that the magnitude of the TCR could be identified using a CAD parameter optimisation technique which in SolidWorks is called a Design Study. Initially, the TCR was estimated to be 0.1 m^2.K/W for the simulation and then it was linked to a Design Study in order to be optimised. The heat power, initial temperature of the plate, convection coefficient and ambient temperature were constants in the design study while the TCR was set as the optimisation target. In order to find the TCR, the design study was made sensitive to the difference in temperature between the heater and the plate close to the heater. The goals of the design study, in order to optimise the TCR, was to minimise the difference between four spots temperature values obtained from thermal images of the heated plate and of the values from corresponds nodes on the FEA model at the end of a heating cycle of 30 minutes. Figure 6-4 shows the locations of the temperature readings. The optimised TCR was found to be 0.075 $m^2.^oC$ / W.

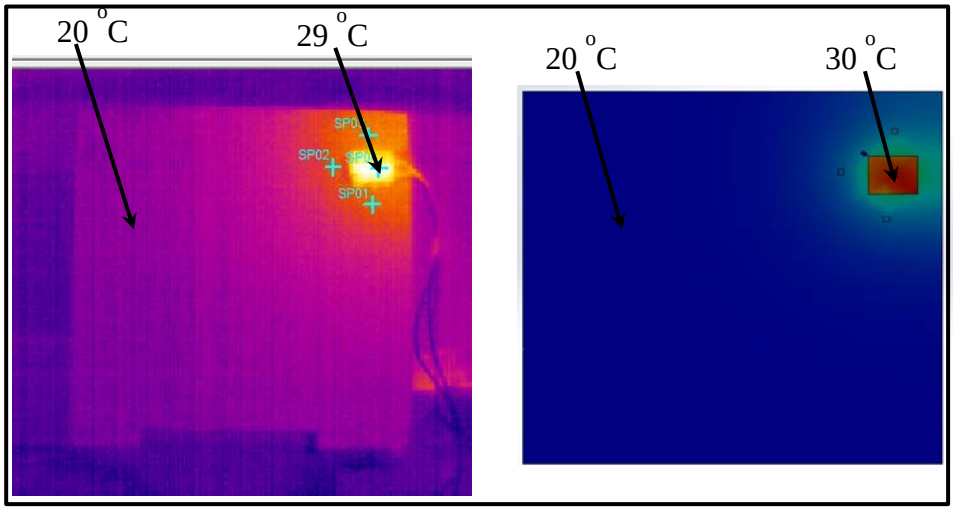

Figure 6-4 Places of goal temperature spots in the design study

The obtained boundary conditions were applied to the FEA model of the plate to check the accuracy of the simulation under different conditions. Three transient simulations, designed to match a 0.5 hour experiment, were conducted to consider1 heater on, 2 heaters on and 3 heaters on, as shown below in Figure 6-5.

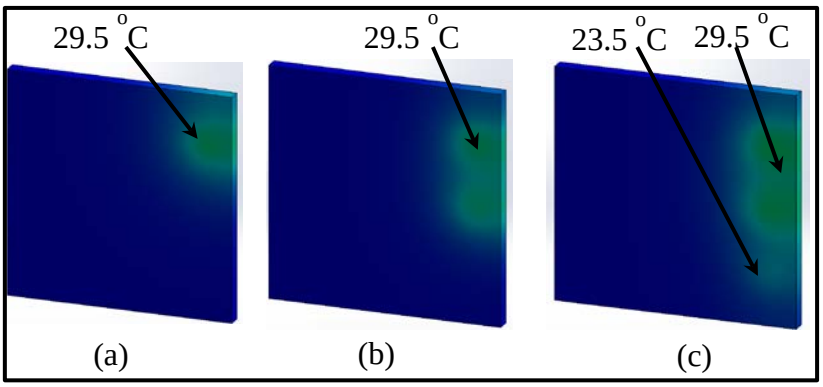

Figure 6-5 Simulations of the plate (a) 1 heater on, (b) 2 heaters on, (c) 3 heaters on

The high temperature areas of the plate in experiment and simulation were chosen for data extraction and results comparison. The experimental and simulated data of the temperature profile during the three experiments were compared. The correlations of 90 % between experimental and simulated results were obtained. The comparison is shown in Figure 6-6, Figure 6-7, Figure 6-8. It can be observed that the simulated temperature profile agrees well with the measured temperature. The maximum temperature difference of about 0.5 ^{o}C, which is very small, was revealed. This is due to fact that the real heat power and boundary conditions from the experiments were used.

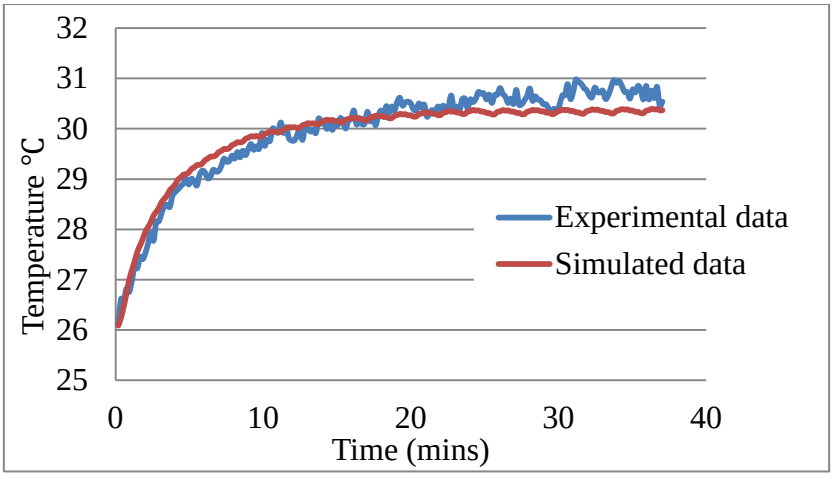

Figure 6-6 Temperature profile comparison (1 heater on)

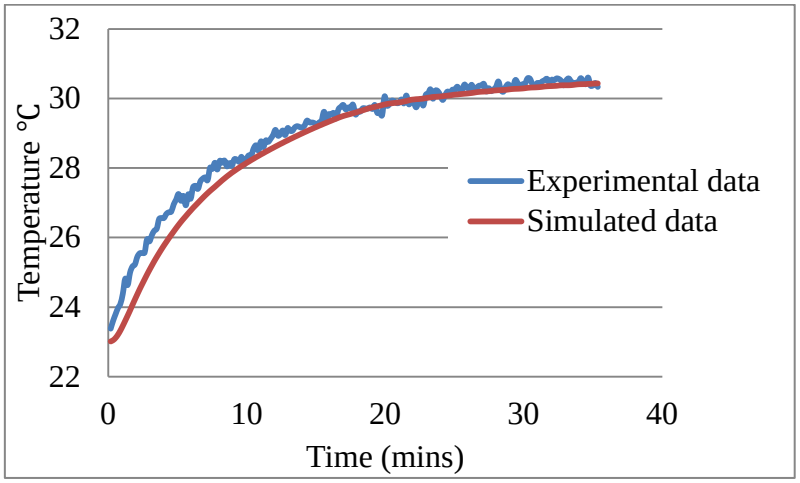

Figure 6-7 Temperature profile comparison (2 heaters on)

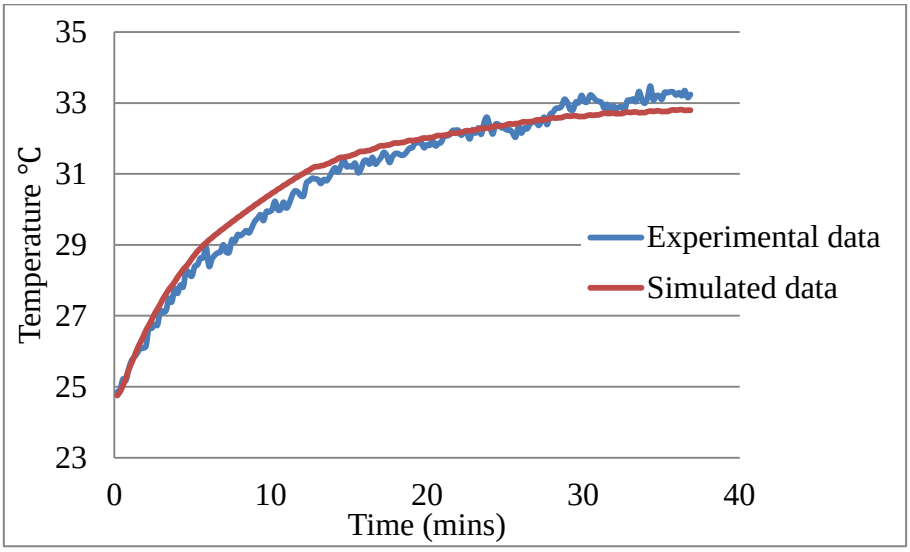

Figure 6-8 Temperature profile comparison (3 heaters on)

6.2 Two Dimensional (2D) optimisation model establishment

The heat power of the plate can be obtained using an optimisation technique based on thermal imaging data. The design study in SolidWorks for optimisation method is not practical if huge amount of thermal imaging data are used. Therefore, a method of thermal parameters optimising based on arrays of temperature data extracted from thermal imaging data and a Matlab function.

A reduced 2D heat transfer model of the square surface of the front side of the plate was created in MATLAB in order to simulate the front side of plate surface temperature throughout the heating cycle and optimise the heat power.

This technique enabled a relatively large number of points from the thermal images to be compared against the simulated temperature profile as described in Section 6.3. In order to compute the heat power for the different heat sources of the 2D model, differential equations of the second order, see equation 6.2 [63], were used to describe the process of heat flow in the plate and solved using numerical methods. The numerical methods convert exact differential equations into approximate algebraic equations. The first step to create a 2D model was to divide the component shape, which has the same dimensions of the plate, into small elements. See Figure 6-9,

$$\frac{\partial^2 \mathrm{T}}{\partial^2 \mathrm{x}} + \frac{\partial^2 \mathrm{T}}{\partial^2 \mathrm{y}} + \frac{\mathrm{Q}}{\mathrm{k}} = \frac{1}{\alpha}\frac{\partial \mathrm{T}}{\partial \mathrm{t}} \tag{6.2}$$

$$\alpha = \frac{\mathrm{k}}{\rho \mathrm{c_p}} \tag{6.3}$$

Where α is the thermal diffusivity (m^2 /s), k is the thermal conductivity (W /(m.K)), C_p is the specific heat (j /kg.^{o}C), Q is the heat power (W), T is the temperature (^{o}C), X, Y are the axes.

To solve the partial differential equation in 6.2 the finite differences method was chosen. This method resembles the physical heat flow development, where each observed element is

calculated periodically (small period) enabling accurate interaction with the adjacent elements. This is based on the four known temperatures at the neighbouring elements, the temperature at the next time increment is calculated.

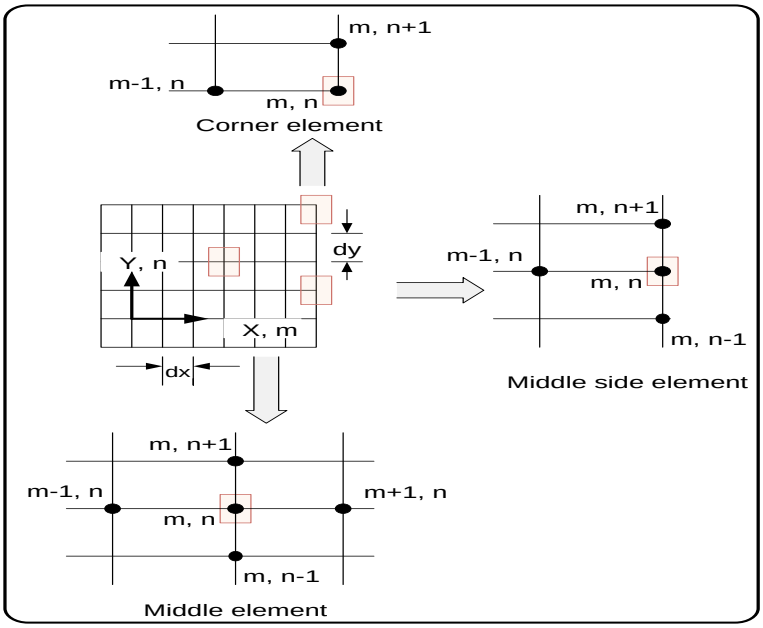

Figure 6-9 Element network of 2D model

The approximate solution of the partial differential equation in 6.2 results in the following equations [63].

$$\frac{\partial^2 T}{\partial^2 x} \approx \frac{T_{m+1,n} + T_{m-1,n-} 2T_{m,n}}{(\Delta x)^2} \tag{6.4}$$

$$\frac{\partial^2 T}{\partial^2 y} \approx \frac{T_{m,n+1} + T_{m,n-1} + 2T_{m,n}}{(\Delta y)^2} \tag{6.5}$$

The heat flow in the front side elements of the plate (m, n) are also influenced by convective exchange with the air and this exchange may be viewed as happening along the front, back and sides of the plate. The total convection rate Q_c of the middle elements may be expressed as

$$Q_c = 2h(dydx)(T_{surface} - T_{air}) \tag{6.6}$$

The total convection of the side elements may be expressed as

$$Q_c = 2hdydx\left(T_{surface} - T_{air}\right) + h\,(dy) * depth\left(T_{surface} - T_{air}\right) \quad (6.7)$$

Where Qc is the heat lost by convection, dy is the element length in Y-axis (m), dx is the element length in X-axis (m), h is the convective coefficient (W/(m^2.^{o}C)), m is the mass (kg), $T_{surface}$ is the surface temperature, T_{air} is the air temperature.

The 2D model is comprised of the same three heat sources (1 heater on, 2 heaters on, 3 heaters on), and steel thermal properties. Figure 6-10 shows the temperature distribution calculated by the 2D model of the plate after the 3 heaters have been active for 30 minutes. The Matlab code containing the main functions described above is shown in Appendix B.

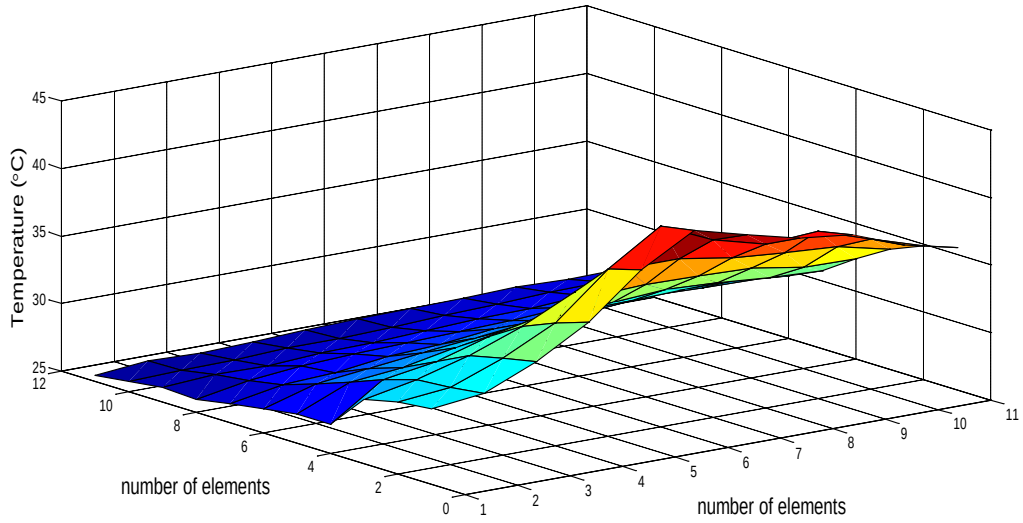

Figure 6-10 Temperature rise model of plate

6.3 Thermal parameters optimisation of the plate

Based on the measured surface temperature distribution on the plate and the modelled temperature distribution, the heat power may be obtained by an optimisation technique. In this case, a MATLAB optimisation function utilising the Nelder–Mead method [82] was used to minimise the sum-of-the-squares error between the experimental data (thermal images data) and simulated data. This is a commonly applied numerical method used to find the

minimum or maximum of an objective function in a many-dimensional space and therefore suited to finding a number of heat source parameters.

The initial and final temperatures at the end of a heating cycle were extracted as an 11×11 array from the thermal images of the plate with the varying heater configurations as shown in Figure 6-11. This array size provided a good compromise between spatial resolution and the run time of the Matlab function. This data was used to fit the 2D model simulated data, which was run using the same set of heater configurations, in order to optimise the heat power; see Figure 6-12, Figure 6-13, Figure 6-14 for the comparison between the experimental and simulated temperature array. The maximum temperature difference between the experimental and simulated arrays was about 0.3 ^{o}C. Table 6-2 shows the heat power of the plate heat sources obtained from current and voltage and after using the preliminary optimisation process.

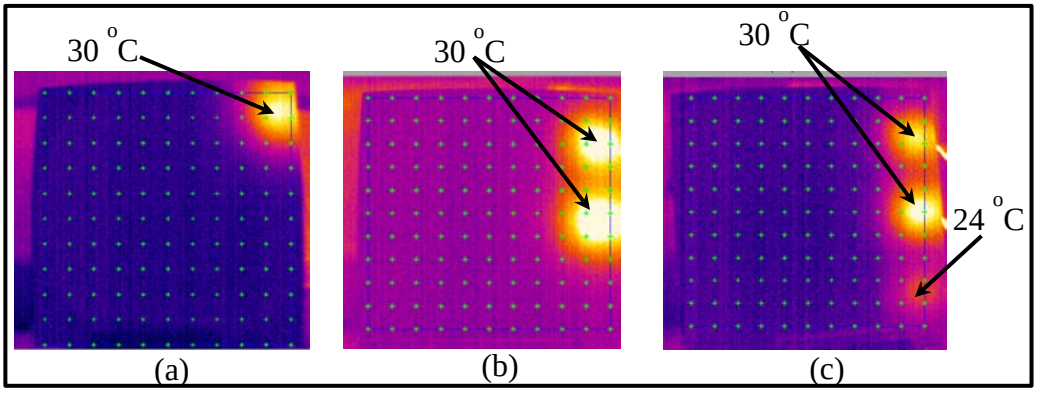

Figure 6-11 Experiment temperature data extraction from IR image, (a) 1 heater on, (b) 2 heaters on, (c) 3 heaters on

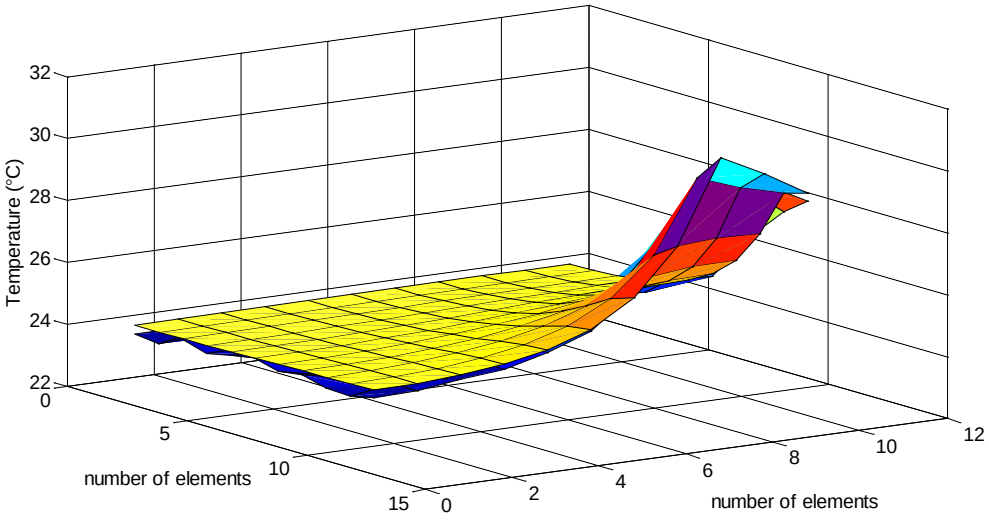

Figure 6-12 Experimental and model temperature data fit (1 heater on)

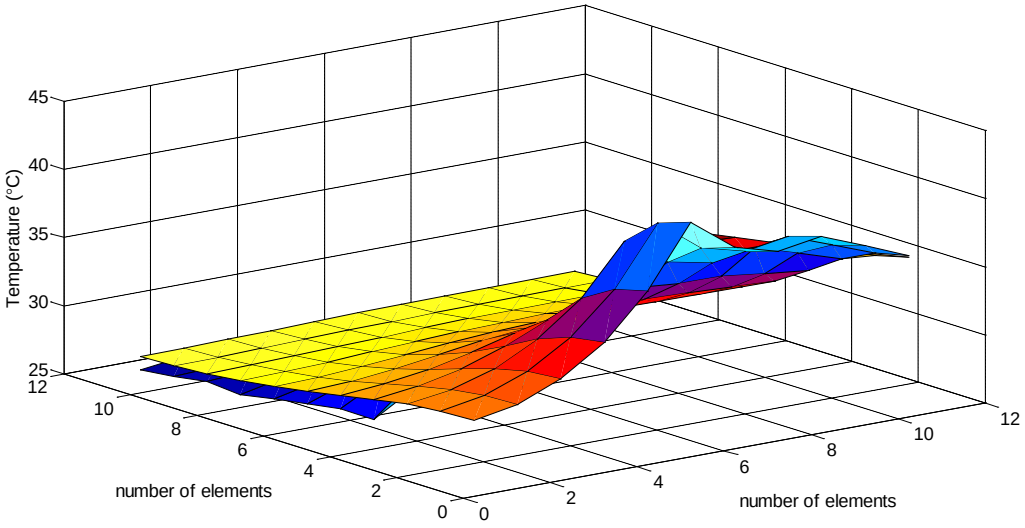

Figure 6-13 Experimental and model temperature data fit (2 heaters on)

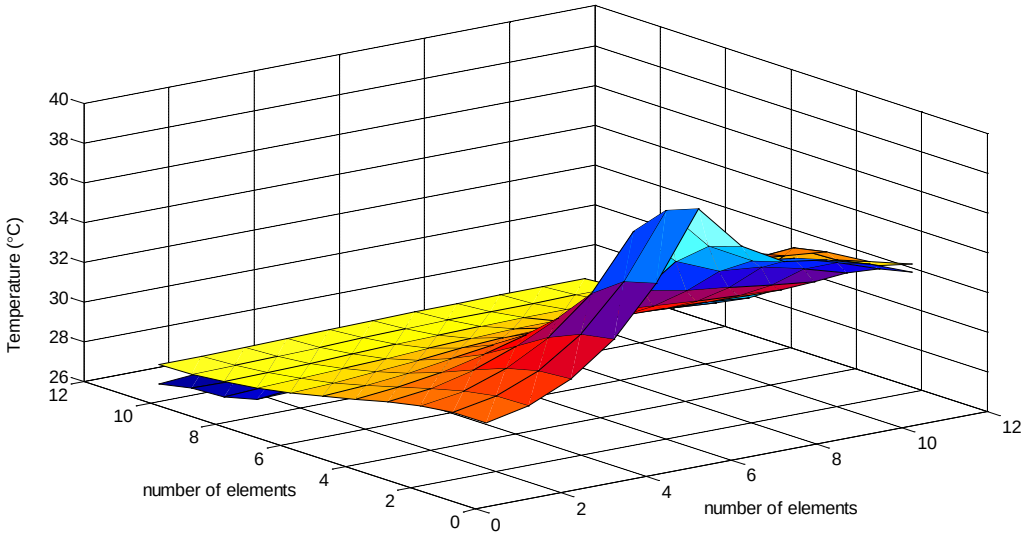

Figure 6-14 Experimental and model temperature data fit (3 heaters on)

Table 6-2 Heat power magnitude

Heat sources	Heat power (W) Based on current and voltage	Heat power (W) Optimisation technique
Heater 1	24	23.3
Heater 2	24	22.7
Heater 3	8	7.2

The optimised heat power values were used in the FEA model in order to more accurately simulate the thermal behaviour of the plate assembly. Figure 6-15, Figure 6-16 and Figure 6-17 show comparisons of experimental and simulated data for the displacement.

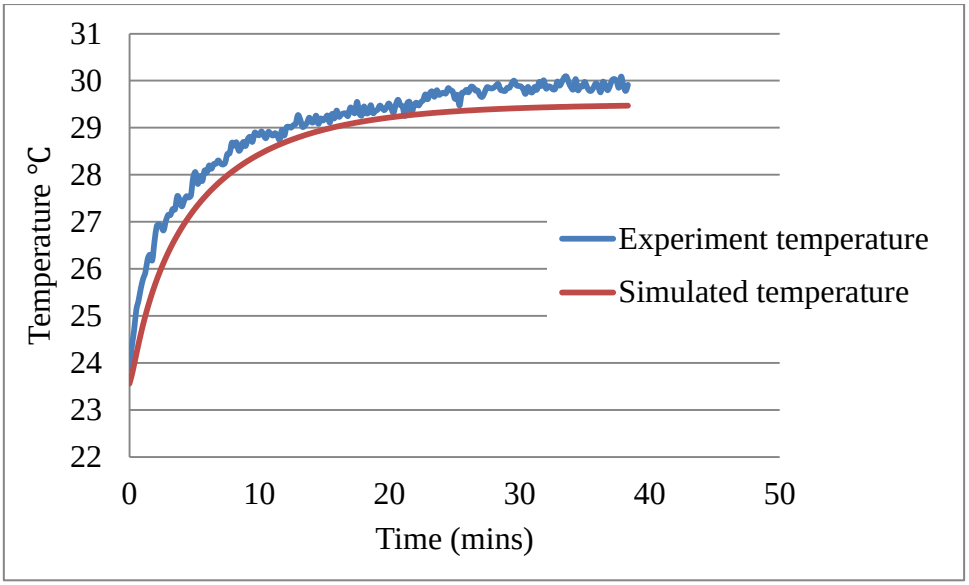

Figure 6-15 Temperature profile of plate using optimised heat power (1 heater)

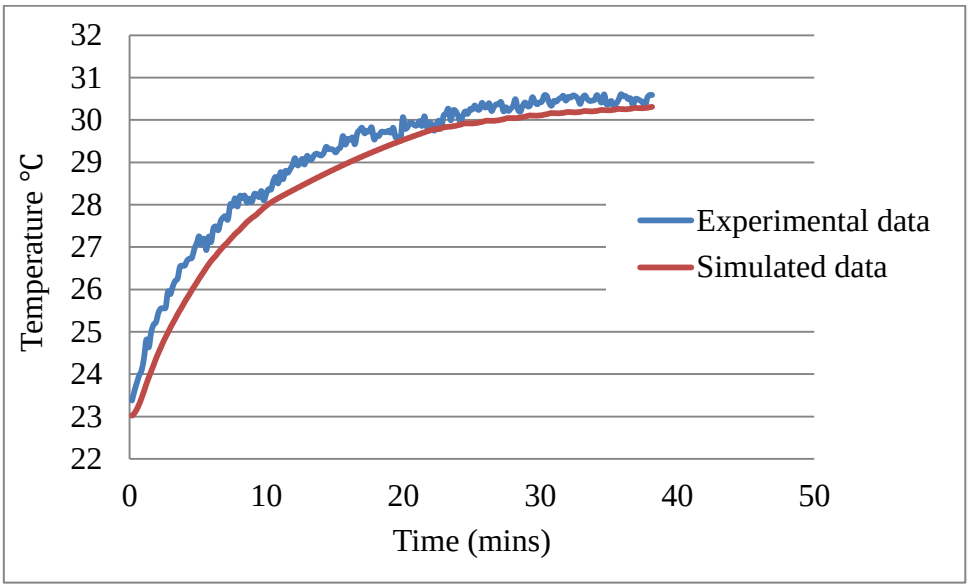

Figure 6-16 Temperature profile of plate using optimised heat power (2 heaters)

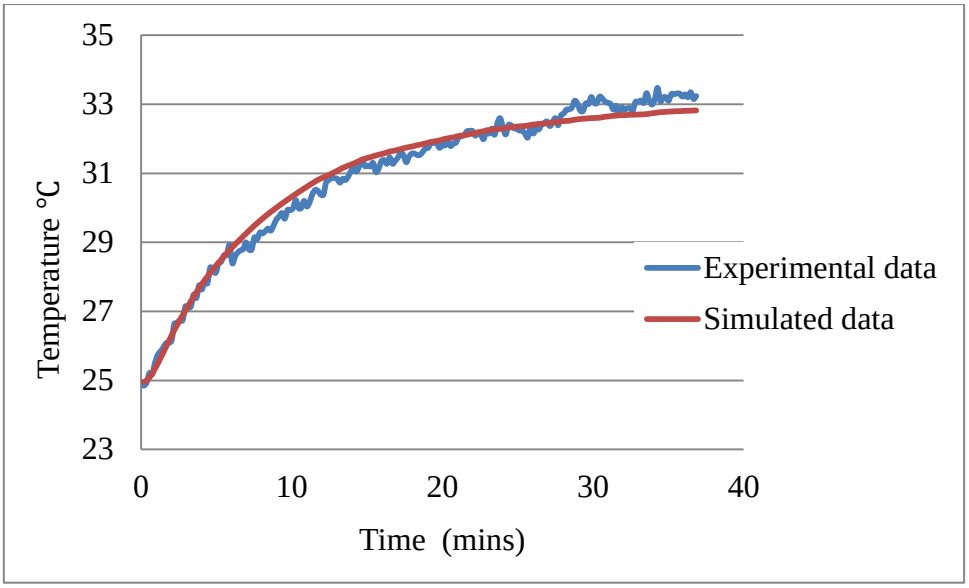

Figure 6-17 Temperature profile of plate using optimised heat power (3 heaters)

The results show that the proposed optimisation technique can be an efficient technique to predict the heat power. It can be observed that the magnitude of the residual errors is about 0.5 ^{o}C using the optimisation technique. This preliminary validation shows that the proposed optimisation technique can enhance the model's prediction capability by approximately 90 % for this relatively simple structure.

6.4 Employing the proposed optimisation method on a machine tool

The proposed optimisation method was then applied to optimise the heat power of the headslide of the small VMC, described in Section 4.2. The headslide temperature gradient was obtained using the thermal imaging camera as explained earlier in Section 5.6.1.

The same steps applied to the bench tests on the plate were followed to optimise the heat power values of the machine heat sources which in this case were the motor and spindle bearings. A reduced 2D heat transfer model of the rectangular surface of the side of the headslide was created in MATLAB. This enabled a relatively large number of points from the thermal images to be compared against the simulated temperature profile as described in 6.4.1. The model is comprised of the same three heat sources (motor and upper and lower

bearings) and thermal properties. In order to compute the heat power for the different elements of the 2D model, equations used to establish 2D during heat cycle explained in Section 6.2. Figure 6-18 shows the temperature profile from the 2D model of the headslide.

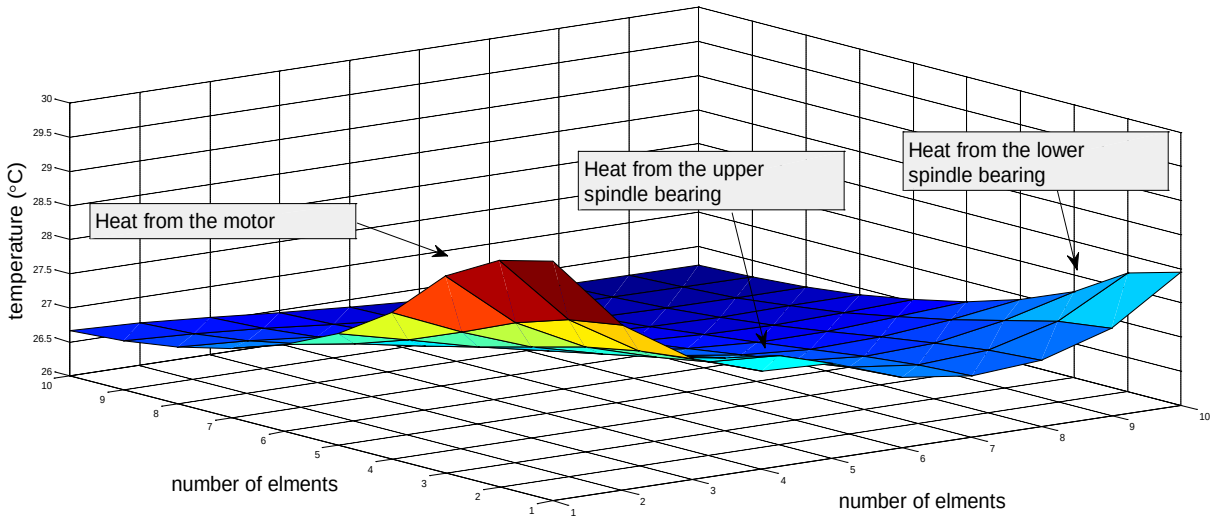

Figure 6-18 2D temperature rise model of headslide

6.4.1 Thermal parameter optimisation on a machine tool headslide

In order to determine optimal thermal parameters over the previously defined case of the headslide simulation problem (Section 5.6.4), the same MATLAB optimisation function used to optimise the heat power values of the plate was used with this case.

Initial and final temperatures at the end of heating cycle were extracted as an 11×11 array from the thermal images of the headslide as shown in Figure 6-19. This data was used to compare with the 2D model simulated data in order to optimise the head slide heat power. Figure 6-20 shows the comparison between the experimental and simulated temperature array. Some differences still exist of about 0.5 ^{o}C which are estimated to come from the noise in the thermal imaging data and 2D filtering at each selected time frames. Table 6-3 shows the heat power of the spindle system heat sources before and after the preliminary optimisation process.

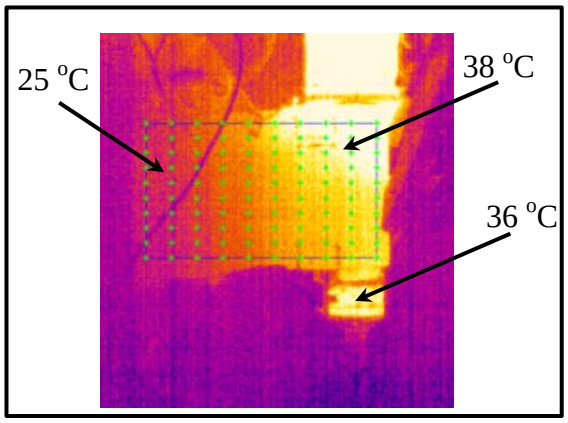

Figure 6-19 Experiment temperature data extraction from IR image

Table 6-3 Heat power magnitude of headslide heat sources

Heat sources	Heat power (W) Energy balance method	Heat power (W) Optimisation method
Motor	50 ± 0.75	46 ± 0.75
Lower spindle bearing	12 ± 0.75	15 ± 0.75
Upper spindle bearing	8 ± 0.75	10 ± 0.75

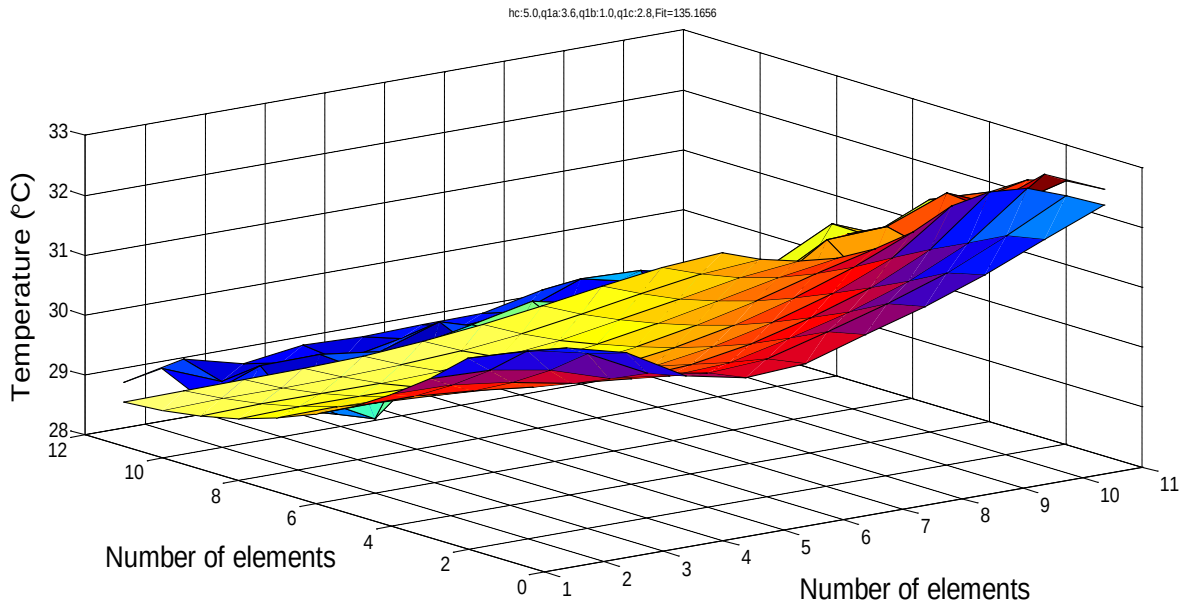

Figure 6-20 Experimental and model temperature data fit of headslide

6.4.2 Results and discussion of optimised headslide heat power figures

The optimised heat power values were used to simulate the FEA model of spindle system of small VMC, see Section 5.6.4, in order to obtain the optimised thermal behaviour of the headslide. Figure 6-21and Figure 6-22 show a comparison of experimental and simulated data for the displacement. It is important to note that the Solidworks simulation software allows time varying boundary conditions. This was used to change the heat power values to zero to represent the transition from heating to cooling in the experiments.

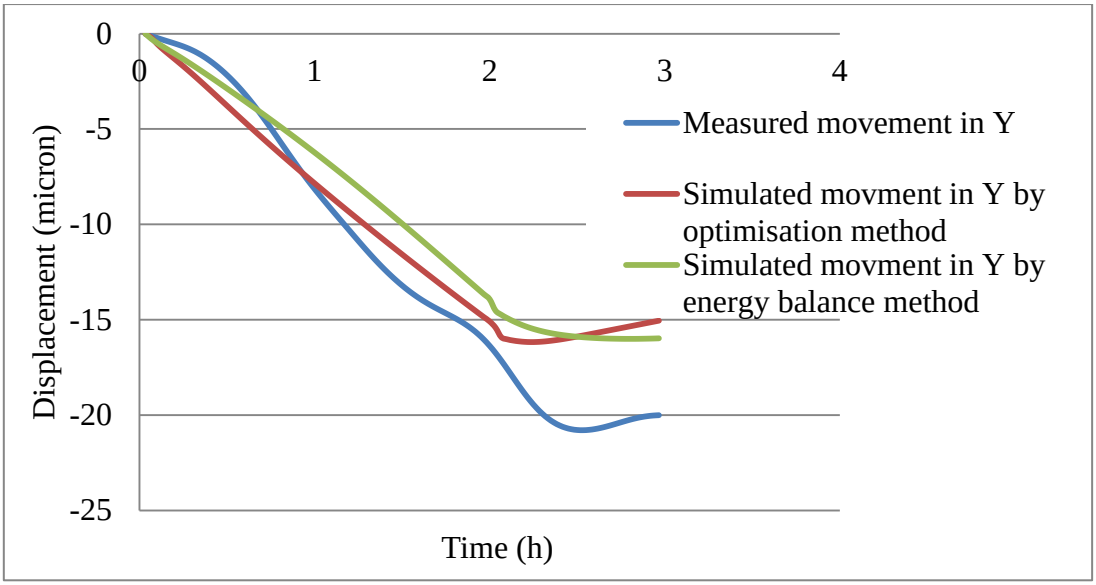

Figure 6-21 Displacement of the headslide in Y-axis

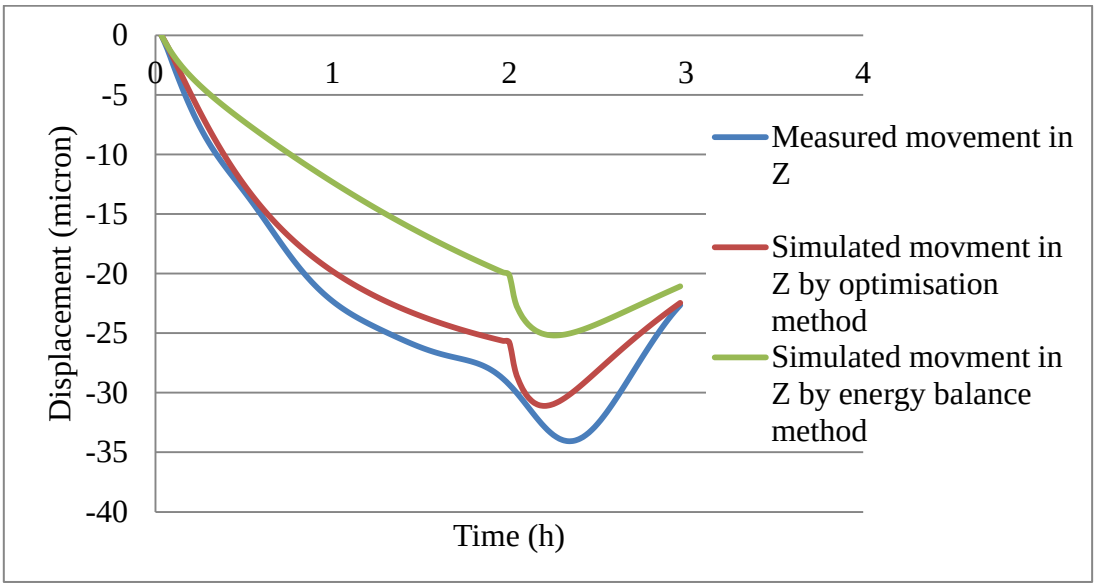

Figure 6-22 Displacement of the headslide in Z-axis

The results show that there is an improvement in the headslide accuracy using the proposed optimisation technique. It can be observed that the amount of the residual thermal error in both the Y and Z-axes has been reduced using the optimisation technique to 15 % when compared to the energy balance method explained in Section 5.6.4. This validation shows that the proposed optimisation technique can enhance the model's prediction capability by approximately 15 %. Further improvements are anticipated if the simplified optimisation

model of the structure can incorporate the 3D effects (mainly hysteresis) of varying material thickness in more detail.

6.5 Summary

In this chapter a novel approach was presented to carry out accurate and efficient determination of the heat power of multi heat sources using an optimisation function incorporating a 2D finite difference model and spatially rich data from thermal imaging sequences. To help develop and validate the proposed approach, a relatively simple square plate was heated with three small electric heaters that have a known heat power. By comparing the actual and optimised heat power values and subsequent comparison between FEA and experimental results, it was validated that the proposed optimisation method is able to predict the heat power of such heat sources with good accuracy with the difference in temperature at key points on the plate being about 0.5 ^{o}C. The accuracy of the proposed method is was within experimental error.

In addition, the proposed optimisation method was validated by applying it to the prediction of the heat powers of heat sources in the headslide of small VMC. The displacement results were compared to experimental ones and it reveals that the proposed optimisation technique can improve the model's prediction capability by approximately 15 % compared to the energy balance method.

Chapter 7

7 Conclusion and future work

7.1 Conclusion

Thermal errors on machine tools are caused by a variety of internal and external heat sources and their combined effect can result in deformation of the machine structural that often occurs in a complex manner due to the non-linear behaviour and interaction across the machine structural elements.

Modelling of the thermal error can be a convenient and cost-effective method for minimising machine tool thermal error and therefore attracts the attention of many researchers around the world.

This research on thermal parameter optimisation for accurate FEA based on simulation of thermal characteristics on machine tools, set out to find a novel and efficient method which can be implemented easily for finding and optimising thermal parameters associated with machine components, such as spindle bearings, that are hard to characterise. The reason and motivation for this is to improve the accuracy of machine tools by utilising accurate FEA models as a design aid or for error compensation which can be much less costly than prototyping or additional services used for controlling temperature. This research has highlighted the following points:

- Thermal parameter calculation utilising energy balance method which was found to be more accurate, especially for used machine tools, than formula method which most previous research employed.
- An in-line method was applied to calculate TCR across machine tool joints which are a practical and relatively easy way to determine the values as some surfaces and interfaces

are complicated or difficult to characterise therefore a methodology utilising simple experiments was presented to calculate the TCR at these joints.

- A novel 2D temperature gradient model was presented to optimise thermal parameters and obtain more accurate thermal characteristics of machine tools.

These novelties contribute considerably for the forthcoming of efficient thermal model development to enable widespread industrial application of thermal modelling and compensation.

This research looked over a number of techniques for modelling of thermal errors such as regression and neural networks techniques. It was noticed that these methods may be complicated to implement, often involving a significant amount of training time and can be affected by the high variability in the different ways that machine tools are used, the environments in which the machine tools are located and also the performance of temperature sensors or rather the difficulty of installing sensors in sensitive locations. Finite element analysis has also been used widely in modelling of the thermal error of machine tools. However, the review shows that determining the heat transfer coefficients using FEA was not very accurate. Consequently, this research focuses on how to obtain optimal heat transfer coefficients of machine tools to improve the accuracy of FEA modelling.

FEA is used to simulate the thermal characteristics of the feed drive system of small VMC using SolidWorks software. The model of the feed drive system assembly was generated using the CAD facility in the software. Thermal error of feed drive system were studied and analysed experimentally and the effects of internally generated heat on the positioning error of a ball screw feed drive system were predicted offline using the FEA model. To ensure accurate FEA predictions, the boundary conditions such as the heat transfer convective coefficients were calculated analytically. The heat power of the feed drive system heat

sources was calculated using two different methodologies; the formula; and the energy balance and compare them for their effectiveness. The methodology was validated by recalculating the heat power of heat sources using long term test data and simulates the FEA model.

A study was also carried out to find out the amount of heat flow across structural joints (i.e. ball screw shaft and ball screw nut). Therefore, TCR values at different mechanical joint were needed. TCR at complicated surface contact was obtained as well experimentally and at other joints was calculated based on thermal imaging data. Employing TCR magnitude in FEA model simulation ensures realistic thermal behaviour across assembly joints.

The correlations between the experimental and FEA simulated results of the feed drive system simulation revealed 70 % for the formulae method and 80 % for the energy balance method. In terms of the residual error, the comparison revealed the error of 30 µm using the Formulae method and 18 µm using the energy balance method from 106 µm. The improvements in the FEA results are evident that the energy balance method has provided optimised parameters representative of the real state of the machine. Another important highlight is that the energy balance method is an easy to implement and a quicker method to apply for obtaining the thermal behaviour for any feed drive system. Moreover, since the machine under consideration was not new, the energy balance method has been proved to be more realistic and effective for assessing the current thermal status of the feed drive system.

This was followed by the investigation of the thermal behaviour of the spindle of machine tools due to both internal heat and external environmental fluctuations using FEA. Heat power of spindle heat source was calculated using energy balance method. The predicted temperature rise and displacement data from the simulations fit the experimental data well. The correlation coefficient was calculated at points of thermal interest to obtain the closeness

between the experiment and simulated data which was calculated to be more than 80 %. Thermal error could be reduced to just 4 µm in the Z-axis and Y-axis directions from 35 and 20 µm respectively.

The FEA prediction of thermal characteristics of machine tools was improved utilising an optimisation method to optimise the heat power of heat sources of machine tools. A proposed method for optimising the heat power of machine tool spindle and headslide on a small VMC was presented. A 2D model of surface temperature gradient created in Matlab software in order to be compared with real data of surface temperature rise. To validate the correct application of the heat power identifications, a surface temperature gradient of plate was compared to the 2D model data. In addition, to validate the simulation accuracy, FEA model of the plate and heaters created in the SolidWorks software in and simulated for the temperature gradient using real and optimised heat power.

An FEA model of machine tool was simulated using the optimisation technique method, utilising heat power obtained from optimisation method. Accuracy and effectiveness of the thermal error model and optimisation technique was also evaluated.

The optimised heat power parameters improved the FEA model prediction results and obtain its accuracy compared to simulation using parameters obtained by energy balance method. Results from simulating the resulting displacement show correlation with the actual movement of the tool in the spindle up to 85 %.

7.2 Suggestions for future work

This work has highlighted some potential areas for research. These areas are

- The energy balance method was applied to calculate the heat power of machine tool spindle and X-axis feed drive system heat sources and the philosophy and methodology validated. The technique should be applicable to any machine tool mechanical feed drive

system but additional determination of the Z-axis and Y-axis thermal behaviour would give a complete picture of the main thermal errors of the machine tool. These additional axes are typically identical or very similar in design, perhaps with different traverse lengths, therefore it is expected that the method will be just as applicable and accurate.

- The optimisation function developed in this research was capable of optimising the heat sources in both spatial and temporal domains using simulated data on the bench tests but it was not fully validated on a more complex structure with time varying heat sources due to time constraints of the project. There are potentially many uses for an efficient method of determining time varying heat power values for robust simulation work beyond just machine tools and this would be valuable further work to determine the accuracy of the method.
- The technique was applied to axes using rotary encoder feedback. Further work would be required to determine the effectiveness of the modelling method to axes using a linear scale for position feedback. Linear scales can be fitted to most machine tools based on the customer specification request but the additional cost of a machine tool with linear scale fitted can be much higher than machines utilising the existing rotary encoder fitting to axis drive motors. Although thermal errors are typically much lower on machines employing linear scales, they can still be significant. Figure 7-1 below shows the error on the X-axis of machine similar to the one tested in Chapter 5 except employing such a linear scale. In this case, the error is predominantly position dependent which means the scale is varying in length due to the internally generated heat. On the same machine but this time on the Y-axis, the error shown in Figure 7-2 is again significant but this time predominantly position independent i.e. caused predominantly by the movement of the scale reader head in relation to the tool. Modelling of these errors using FEA would contribute to design optimisation and error compensation.

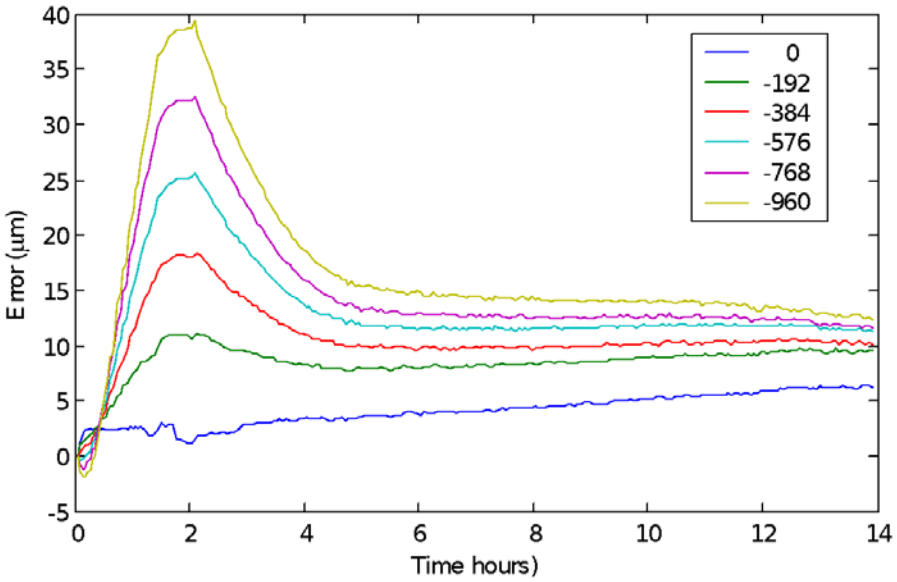

Figure 7-1 Positioning error with linear scale feedback example

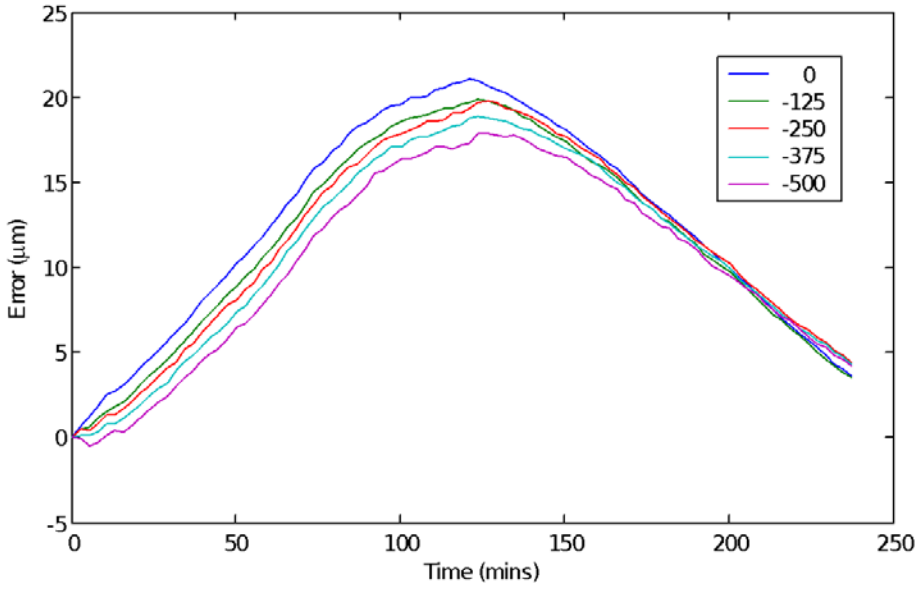

Figure 7-2 Positioning error with linear scale feedback example

- The new optimisation technique presented can be used to optimise the thermal parameters of heat sources on a machine tool. However, in the scope of this work, only one Matlab optimisation function which uses the Nelder-Mead method was applied. Due to the large number of parameters associated with the different including multiple heat sources across

multiple time periods meant that the optimisation routine was quiet time consuming and did not always find a solution unless the initial conditions were quite close, which was usually the case as the energy balance method provided good initial estimates. As a future step it would be interesting to use different optimisation functions to optimise the thermal parameters and compare the results. One possible method that is suited to large numbers of parameters is the Genetic Algorithms optimisation method.

- In some cases the array of temperature data extracted from the surfaces of heat sources was difficult to obtain due to the lack of line of sight i.e. ball screw nut, consequently, a different optimisation technique or methodology should be applied. For example, it is possible to use the inverse heat transfer method with discrete temperature sensors only.
- The thermal behaviour of different machine tools could be modelled using the new technique and the simulated data compared with experimental data for verification of FEA model robustness. Machine structure and spindle designs vary on, for example, horizontal machining centres or machine tools for specific applications such as Numerical Control (NC) lathes.
- The machining process also was not the scope of this work. A future step for the thermal simulation of machining process should be added in as there will be more heat sources affecting the thermal behaviour of the machine tool such as swarf and friction between workpiece and tool. Furthermore, machining variety of workpiece material specification as the friction between cutting tool and workpiece changes with different material type and therefore, more heat is generated.

List of references

[1] Ramesh, R., M. Mannan, and A. Poo. 2000. *Error compensation in machine tools—a review: Part I: geometric, cutting-force induced and fixture-dependent errors.* International Journal of Machine Tools and Manufacture, Vol. **40**(9): p. 1235-1256.

[2] ISO 230-3. 2007. *Test code for machine tools- part 3: Detemination of thermal effects, .*

[3] Kiridena, V. and P. Ferreira. 1994. *Parameter estimation and model verification of first order quasistatic error model for three-axis machining centers.* International Journal of Machine Tools and Manufacture, Vol. **34**(1): p. 101-125.

[4] Ferreira, P. and C.R. Liu. 1993. *A method for estimating and compensating quasistatic errors of machine tools.* Journal of Manufacturing Science and Engineering, Vol. **115**(1): p. 149-159.

[5] Fletcher, S., 2001, *Computer aided system for intelligent implementation of machine tool error reduction methodologies*, in *Center for Precicion Technology*. University of Huddersfield.

[6] Jorgensen, B.R. and Y.C. Shin. 1997. *Dynamics of machine tool spindle/bearing systems under thermal growth.* Journal of Tribology, Vol. **119**(4): p. 875-882.

[7] De Lacalle, N.L. and A.L. Mentxaka, *Machine tools for high performance machining*. 2008: Springer Science & Business Media.

[8] Uhlmann, E. and J. Hu. 2012. *Thermal modelling of a high speed motor spindle.* Procedia CIRP, Vol. **1**: p. 313-318.

[9] Hatamura, Y., T. Nagao, M. Mitsuishi, K. Kato, S. Taguchi, T. Okumura, G. Nakagawa, and H. Sugishita. 1993. *Development of an intelligent machining center*

incorporating active compensation for thermal distortion. CIRP Annals-Manufacturing Technology, Vol. **42**(1): p. 549-552.

[10] Wiele, H., H. Groppe, and R. Horn. 1985. *Comparison Between the Thermically Caused Deformations of a Cast Iron and a Concrete Lathe Bed.* The University of Birmingham, Department of Mechanical Engineering, Vol.: p. 357-361.

[11] Okafor, A.C. and Y.M. Ertekin. 2000. *Vertical machining center accuracy characterization using laser interferometer: part 1. Linear positional errors.* Journal of Materials Processing Technology, Vol. **105**(3): p. 394-406.

[12] Renishaw. *http://www.renishaw.com/en/machine-calibration-and-optimisation--6330*.

[13] Mian, N.S., S. Fletcher, A.P. Longstaff, and A. Myers. 2011. *Efficient thermal error prediction in a machine tool using finite element analysis.* measurement science and technology, Vol. **22**(8): p. 85-107.

[14] Li, Y., W. Zhao, S. Lan, J. Ni, W. Wu, and B. Lu. 2015. *A review on spindle thermal error compensation in machine tools.* International Journal of Machine Tools and Manufacture, Vol. **95**: p. 20-38.

[15] Postlethwaite, S., J. Allen, and D. Ford. 1999. *Machine tool thermal error reduction—an appraisal.* Proceedings of the Institution of Mechanical Engineers, Part B: Journal of Engineering Manufacture, Vol. **213**(1): p. 1-9.

[16] Leatham-Jones, B., 1986, *Introduction to computer numerical control*. Pitman New York.

[17] Xu, Z.-Z., X.-J. Liu, C.-H. Choi, and S.-K. Lyu. 2013. *A novel high speed/high precision ball screw.* International Journal of Precision Engineering and Manufacturing, Vol. **14**(1): p. 165-167.

[18] Xu, Z., X. Liu, H. Kim, J. Shin, and S. Lyu. 2011. *Thermal error forecast and performance evaluation for an air-cooling ball screw system.* International Journal of Machine Tools and Manufacture, Vol. **51**(7): p. 605-611.

[19] Jedrzejewski, J. 1988. *Effect of the thermal contact resistance on thermal behaviour of the spindle radial bearings.* International Journal of Machine Tools & Manufacture, Vol. **28**(4): p. 409-416.

[20] Bryan, J. 1990. *International status of thermal error research, .* Annals of the CIRP, Vol. **vol 39**(number 2): p. pp 573-645.

[21] Allen, J., S. Postlethwaite, and D. Ford. 1997, *Practical application of thermal error correction-4 case studies*.

[22] Chen, J.-S. 1997. *Fast calibration and modeling of thermally-induced machine tool errors in real machining.* International Journal of Machine Tools and Manufacture, Vol. **37**(2): p. 159-169.

[23] Yang, M. and J. Lee. 1998. *Measurement and prediction of thermal errors of a CNC machining center using two spherical balls.* Journal of Materials Processing Technology, Vol. **75**(1): p. 180-189.

[24] Chen, J. and G. Chiou. 1995. *Quick testing and modeling of thermally-induced errors of CNC machine tools.* International Journal of Machine Tools and Manufacture, Vol. **35**(7): p. 1063-1074.

[25] Chen, J.-S. 1996. *A study of thermally induced machine tool errors in real cutting conditions.* International Journal of Machine Tools and Manufacture, Vol. **36**(12): p. 1401-1411.

[26] El Ouafi, A., M. Guillot, and A. Bedrouni. 2000. *Accuracy enhancement of multi-axis CNC machines through on-line neurocompensation.* Journal of Intelligent Manufacturing, Vol. **11**(6): p. 535-545.

[27] Chen, J.-S. 1995. *Computer-aided accuracy enhancement for multi-axis CNC machine tool.* International Journal of Machine Tools and Manufacture, Vol. **35**(4): p. 593-605.

[28] Chen, J., J. Yuan, J. Ni, and S. Wu. 1992. *Thermal error modeling for volumetric error compensation.* ASME PROD ENG DIV PUBL PED., ASME, NEW YORK, NY(USA), 1992, Vol. **55**: p. 113-125.

[29] El Ouafi, A., M. Guillot, and N. Barka. 2013. *An integrated modeling approach for ANN-based real-time thermal error compensation on a CNC turning center*. in *Advanced Materials Research*. : Trans Tech Publ.

[30] Huang, Y., J. Zhang, X. Li, and L. Tian. 2014. *Thermal error modeling by integrating GA and BP algorithms for the high-speed spindle.* The International Journal of Advanced Manufacturing Technology, Vol. **71**(9-12): p. 1669-1675.

[31] Vanherck, P., J. Dehaes, and M. Nuttin. 1997. *Compensation of thermal deformations in machine tools with neural nets.* Computers In Industry, Vol. **33**(1): p. 119-125.

[32] Weck, M. and U. Herbst. 1998. *Compensation of thermal errors in machine tools with a minimum number of temperature probes based on neural networks*. in *Proceedings of the ASME DSC*.

[33] Yang, H. and J. Ni. 2005. *Dynamic neural network modeling for nonlinear, nonstationary machine tool thermally induced error.* International Journal of Machine Tools and Manufacture, Vol. **45**(4): p. 455-465.

[34] Ahn, K. and D. Cho. 1999. *In-process modelling and estimation of thermally induced errors of a machine tool during cutting.* The International Journal of Advanced Manufacturing Technology, Vol. **15**(4): p. 299-304.

[35] Tseng, P.-C. and S.-L. Chen. 2002. *The Neural-fuzzy Thermal Error Compensation Controller on CNC Machining Center*. JSME International Journal Series C, Vol. **45**(2): p. 470-478.

[36] Ramesh, R., M. Mannan, A. Poo, and S. Keerthi. 2003. *Thermal error measurement and modelling in machine tools. Part II. Hybrid Bayesian Network—support vector machine model.* International Journal of Machine Tools and Manufacture, Vol. **43**(4): p. 405-419.

[37] Chen, J., J. Yuan, and J. Ni. 1996. *Thermal error modelling for real-time error compensation.* The International Journal of Advanced Manufacturing Technology, Vol. **12**(4): p. 266-275.

[38] Li, J., W. Zhang, G. Yang, S. Tu, and X. Chen. 2009. *Thermal-error modeling for complex physical systems: the-state-of-arts review.* The International Journal of Advanced Manufacturing Technology, Vol. **42**(1-2): p. 168-179.

[39] Lingjærde, O.C. and K. Liestøl. 1998. *Generalized projection pursuit regression.* SIAM Journal on Scientific Computing, Vol. **20**(3): p. 844-857.

[40] Yang, J., Y. Ren, and Z. Du. 2002. *An application of real-time error compensation on an NC twin-spindle lathe.* Journal of Materials Processing Technology, Vol. **129**(1): p. 474-479.

[41] Pahk, H. and S. Lee. 2002. *Thermal error measurement and real time compensation system for the CNC machine tools incorporating the spindle thermal error and the feed axis thermal error.* The International Journal of Advanced Manufacturing Technology, Vol. **20**(7): p. 487-494.

[42] Qianjian, G. and Y. Jianguo. 2011. *Application of projection pursuit regression to thermal error modeling of a CNC machine tool.* The International Journal of Advanced Manufacturing Technology, Vol. **55**(5-8): p. 623-629.

[43] Huang, S.-C. 1995. *Analysis of a model to forecast thermal deformation of ball screw feed drive systems.* International Journal of Machine Tools and Manufacture, Vol. **35**(8): p. 1099-1104.

[44] Tseng, P.-C. and J.-L. Ho. 2002. *A study of high-precision CNC lathe thermal errors and compensation.* The International Journal of Advanced Manufacturing Technology, Vol. **19**(11): p. 850-858.

[45] Li, Y., W. Zhao, W. Wu, B. Lu, and Y. Chen. 2014. *Thermal error modeling of the spindle based on multiple variables for the precision machine tool.* The International Journal of Advanced Manufacturing Technology, Vol.: p. 1-13.

[46] Zverev, I.A., I.-U. Eun, W.J. Chung, and C.M. Lee. 2003. *Thermal model of high-speed spindle units.* KSME International Journal, Vol. **17**(5): p. 668-678.

[47] Sun, M.-L., Z.-Y. Yang, W.-Q. Li, Q. Liu, and J.-H. Guo. *2010. An improved thermal simulation model for the spindle of CNC machine tool*. in *Mechanic Automation and Control Engineering (MACE), International Conference on*: IEEE.

[48] Moriwaki, T., K. Yokoyama, and C. Zhao. 1991. *Improving Machining Accuracy in Turning With Use of Tool Holder Made of Super-invall.* International Mechanical Engineering Congress, Sydney, Vol. **vol 1**: p. pp 88-92.

[49] Han, J., L.P. Wang, and L.Q. Yu. 2010. *Modeling and Estimating Thermal Error in Precision Machine Spindles*. in *Applied Mechanics and Materials*. Trans Tech Publ.

[50] Haitao, Z., Y. Jianguo, and S. Jinhua. 2007. *Simulation of thermal behavior of a CNC machine tool spindle.* International Journal of Machine Tools and Manufacture, Vol. **47**(6): p. 1003-1010.

[51] Creighton, E., A. Honegger, A. Tulsian, and D. Mukhopadhyay. 2010. *Analysis of thermal errors in a high-speed micro-milling spindle.* International Journal of Machine Tools and Manufacture, Vol. **50**(4): p. pp 386-393.

[52] Zhu, R., S. Dai, Y. Zhu, X. Wu, and Y. Guo. 2008. *Thermal error analysis and error prediction modeling on a machine tool*. IEEE.

[53] Yang, A., S. Cai, S. Hsieh, T. Kuo, C. Wang, W. Wu, W. Hsieh, and Y. Hwang. 2013. *Thermal deformation estimation for a hollow ball screw feed drive system*. in *Proceedings of the world congress on engineering*. London, U.K.

[54] Kim, S. and D. Cho. 1997. *Real-time estimation of temperature distribution in a ball-screw system.* International Journal of Machine Tools and Manufacture, Vol. **37**(4): p. 451-464.

[55] Min, X. and S. Jiang. 2011. *A thermal model of a ball screw feed drive system for a machine tool.* Proceedings of the Institution of Mechanical Engineers, Part C: Journal of Mechanical Engineering Science, Vol. **225**(1): p. 186-193.

[56] Wu, C.-H. and Y.-T. Kung. 2003. *Thermal analysis for the feed drive system of a CNC machine center*. International Journal of Machine Tools and Manufacture, Vol. **43**(15): p. 1521-1528.

[57] Gostimirovic, M., P. Kovac, and M. Sekulic. 2011. *An inverse heat transfer problem for optimization of the thermal process in machining.* Sadhana, Vol. **36**(4): p. 489-504.

[58] Fletcher, S. and D.G. Ford, 2003. *Measuring and modelling heat transfer and thermal errors on a ballscrew feed drive system*, in *Lamdamap*. Uk.

[59] Wang, L., F. Yu Xu, and W.X. Song. 2012. *Analysis of thermally induced machine tool errors of a crank press.* Proceedings of the Institution of Mechanical Engineers, Part B: Journal of Engineering Manufacture, Vol. **226**(9): p. 1465-1478.

[60] Mian, N.S., S. Fletcher, A.P. Longstaff, and A. Myers. 2012. *Efficient estimation by FEA of machine tool distortion due to environmental temperature perturbations.* Precision Engineering, Vol. **37**: p. 372-379.

[61] Huo, D., k. Cheng, D. Webb, and F. Wardle. 2004. *A Novel FEA Model for the Integral Analysis of a Machine Tool and Machining Processes.* Key Engineering materials, Vol. **Vol 257-258**: p. pp 45-50.

[62] Kim, J.-J., Y.H. Jeong, and D.-W. Cho. 2004. *Thermal behavior of a machine tool equipped with linear motors.* International Journal of Machine Tools and Manufacture, Vol. **44**(7): p. 749-758.

[63] Incropera, F.P., D.P. Dewitt, T.L. Bergman, and A.S. Lavine, 2007. *Introduction to Heat Transfer*. 5th ed. , United States of America: John Wiley & Sons.

[64] Mian, N., 2010. *Efficient machine tool thermal error modelling strategy for accurate offline assessment*, in *centre precision of technology*, University of huddersfield: Huddersfield

[65] Hugen, K.D., 1999. *Heat transfer with application*. Upper Saddle River, N.J.

: Prentice Hall.

[66] Fletcher, S., A.P. Longstaff, and A. Mayers. 2007. *Measurement methods for efficient thermal assessment and error-compensation.* Proceedings of the Topical Meeting: Thermal Effects in Precision Systems – Maastricht., Vol.

[67] Li, D., P. Feng, J. Zhang, Z. Wu, and D. Yu. 2014. *Calculation method of convective heat transfer coefficients for thermal simulation of a spindle system based on RBF neural network.* The International Journal of Advanced Manufacturing Technology, Vol. **70**(5-8): p. 1445-1454.

[68] Tenjitus, W. 2004. *Solution for heating of ball screw and environmental engineering.* Key Compon. CNC Mach. Tool,, Vol. **3**: p. 65-67.

[69] Picazo-Rodenas, M., R. Royo, J. Antonino-Daviu, and J. Roger-Folch. 2013. *Use of the infrared data for heating curve computation in induction motors: Application to fault diagnosis.* Engineering Failure Analysis, Vol. **35**: p. 178-192.

[70] Holman, J.P., 2010. *Heat transfer*. Boston [Mass.]: McGraw-Hill.

[71] Min, X., J. Shuyun, and C. Ying. 2007. *An improved thermal model for machine tool bearings.* International Journal of Machine Tools and Manufacture, Vol. **47**(1): p. 53-62.

[72] Attia, M. and L. Kops. 1980. *Importance of contact pressure distribution on heat transfer in structural joints of machine tools.* ASME Journal of Engineering for Industry, Vol. **102**: p. 159-167.

[73] White, A., 2000. *Experimental Thermal Error Analysis and Correction applied to CNC Machine Tools*, in *Center for Precision Technology*. Huddersfield

[74] Guevarra, D.S., A. Kyusojin, H. Isobe, and Y. Kaneko. 2002. *Development of a new lapping method for high precision ball screw (2nd report): design and experimental study of an automatic lapping machine with in-process torque monitoring system.* Precision Engineering, Vol. **26**(4): p. 389-395.

[75] Lienhard IV, J.H. and J.H. 2008. Lienhard V, *A heat transfer textbook.* Cambridge,Massachusetts, U.S.A: Phlogiston press.

[76] Barkanov, E. 2001. *Introduction to the finite element method.* Institute of Materials and Structures Faculty of Civil Engineering Riga Technical University, Vol.

[77] NSK, 2008. *Ball screw specifications manual.*, in *SA series (finished shaft end).*

[78] ISO 898-1. 2013. *Mechanical properties of fasteners made of carbon steel and alloy steel Part 1: Bolts, screws and studs with specified property classes – Coarse thread and fine pitch thread.*

[79] NSK. *Rolling bearings manual*

[80] Zhang, J., P. Feng, C. Chen, D. Yu, and Z. Wu. 2013. *A method for thermal performance modeling and simulation of machine tools.* The International Journal of Advanced Manufacturing Technology, Vol. **68**(5-8): p. 1517-1527.

[81] Yang, L. and Z. Wanhua. 2012. *Axial thermal error compensation method for the spindle of a precision horizontal machining center*. IEEE.

[82] Lagarias, J.C., J.A. Reeds, M.H. Wright, and P.E. Wright. 1998. *Convergence properties of the Nelder--Mead simplex method in low dimensions.* SIAM Journal on optimization, Vol. **9**(1): p. 112-147.

Appendix A - CAD modelling of machine structural parts

The components of the machine tool were created separately before the assembly took place. The parts are as follows:

headslide	Test bar
Column	Guideways
Table	Spindle
Base	Spindle Motor
Saddle	Bearings

Machine tool complements were simplified by removing unnecessary details such as fillets, chamfers etc. vents in machine tool structure are included as they might have effect on cooling down the machine tool structure. See the following figures.

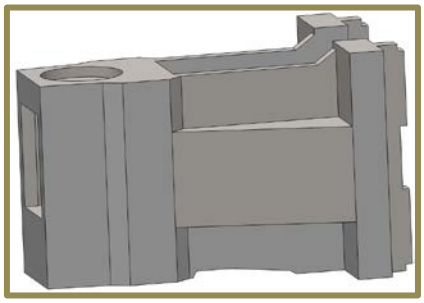

Figure 1-A Machine headslide

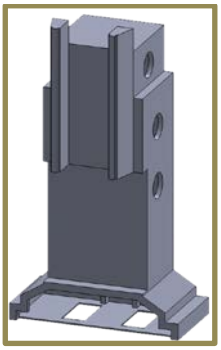

Figure 2-A Machine column

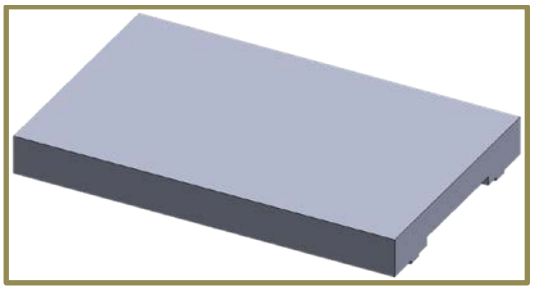

Figure 3-A Machine table

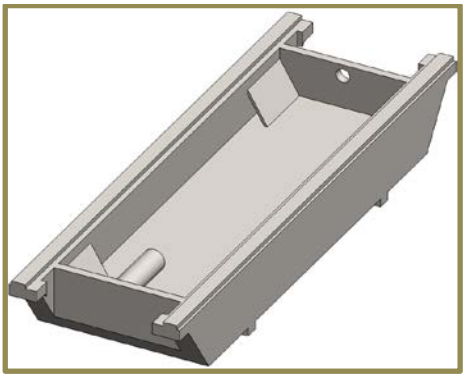

Figure 4-A Machine saddle

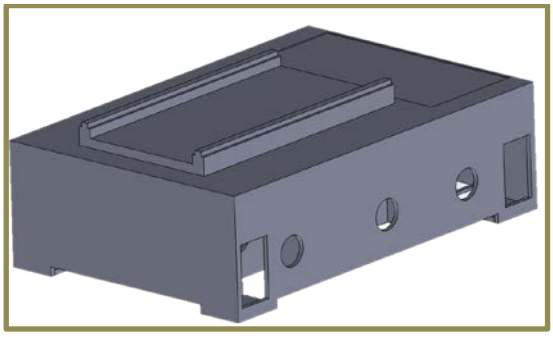

Figure 5-A Machine base

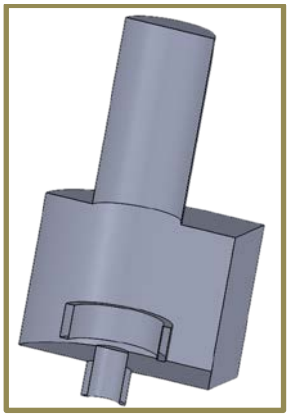

Figure 6-A Machine spindle

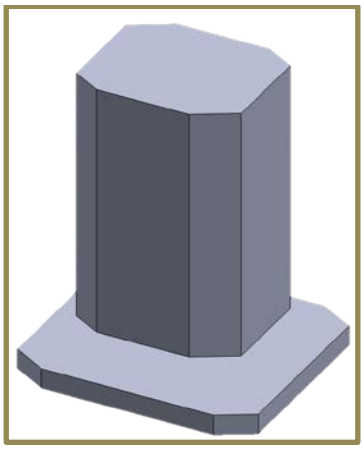

Figure 7-A Spindle motor

Appendix B - Matlab function

This program creates 2D model of plate based on its properties such as material, environment temperature and heat power of heaters which are known based on the applied current and coil resistance. Figure 1-B shows 2D model of plate where 2 heaters are switched on and Figure 2-B shows 2D model where one heater switched on.

Matlab function of the plate where two heaters switched on

```
%----------------initial variables-------------------------------------

hc=6;         % convective coefficient, double for both sides

qstartI=1;
timeIncs=3;   % Number of sets of data at different times

Xh=0.34;      % bar length in x dimension's unit is m
Xv=0.34;      % bar length in Y dimension's unit is m
A=Xh*Xv;      % Area of the part m^2
Mh=11;        % number of elements in horizontal axis
Mv=11;        % number of elements in vertical axis
M = Mh*Mv;    % total grid number for x-axis
dxh = Xh/Mh;  % width of the grid in horizontal
dxv=  Xv/Mv;  % width of the grid in vertical

T1 = 24;      % initial temperature of the plate °C
Ta=24 ;       % air temperature
k = 30;       % thermal conductivity, unit is W/m*K
D=7800;       % density of cast carbon steel kg/m^3
Cp=500 ;      % specific heat  J/kg.k
depth=0.02;   % m
v=depth*A;    % m^3
Av=dxv*depth; % Area for conductance across elements
Ah=dxh*depth; % Area for conductance across elements

m= D * v;     % mass Kg
mi=m/M;       % element mass
Ai=A/M;       % element area
s=2289;       % Total time
tsi=1;        % time increment
C=11;         % number of columns
R=11;         % number of rows
heatedElementNumber1=[1,4 1,5 1,6 1,7; 2,4 2,5 2,6 2,7;3,4 3,5 3,6 3,7];   %round(C/2);
heatedElementNumber2=[1,8 1,9 1,10; 2,8 2,9 2,10; 3,8 3,9 3,10];
```

```
elementsPerHeater=8;
T=[23.0464  23.1117 23.3422 23.4422 24.2786 25.2147 24.0727 23.8745 24.3874 23.5237
23.1126  23.0598  23.0773  23.1521  23.4665  24.5117  25.9907  24.1216  23.7852  24.899
23.9425  23.1826  23.1665  23.0813  23.1489  23.3169  23.7583  23.9095  23.5243  23.4797
23.539   23.2233  23.0706  23.2606  23.1431  23.051   23.1054  23.2011  23.1327  23.3421
23.3087  23.2777  23.223   23.3107  23.1359  23.0674  23.0912  23.1927  23.121   23.2518
23.2038  23.3245  23.2256  23.2743  23.129  23.3764  23.1914  23.2035  23.2282  23.1735
23.1749  23.2289  23.3184  23.269   23.0873  23.0579  23.0155  22.9716  22.9722  22.9622
22.9235  22.9916  23.0435  23.0893  23.0492  23.1529  22.9247  23.2685  23.1533  23.0727
23.2441  23.0451  23.1078  23.2619  23.1007  23.1593  23.1683  23.2822  23.0291  23.0694
23.2169  23.1491  23.1323  23.1947  23.1465  23.1455  23.3114  23.2442  23.249  23.0171
23.2607  23.3301  23.2093  23.1471  23.2073  23.1856  23.2558  23.2457  23.2305  23.1913
23.0949  23.1913  23.1751  23.1746  23.0758  23.2516  23.1087  23.1875  23.1241  23.2294
23.2563];
EI=2;
dataI=1;
numIncs=floor(s/tsi);
t_last=0;
doCompare=0;
ii=1;
w=[10 24 10 10 24 10 10];
for E=1:numIncs-1
   t=E*tsi;  % Time since test start (s)

   % Time dependent parameters:
   for i=1:R
      for j=1:C
   q1=0; q2=0; q3=0; q4=0; q5=0; q6=0; q7=0; q8=0; q9=0; q10=0;    q11=0; q12=0; q13=0;
q14=0; q15=0; q16=0; q17=0; q18=0; q19=0; q20=0;
 if i==heatedElementNumber1(1,1) && j==heatedElementNumber1(1,2)
    q1=w(3)/elementsPerHeater;
  end
 if i==heatedElementNumber1(1,3) && j==heatedElementNumber1(1,4)
     q2=w(2)/elementsPerHeater;
  end
 if i==heatedElementNumber1(1,5) && j==heatedElementNumber1(1,6)
      q3=w(3)/elementsPerHeater;
  end
 if i==heatedElementNumber1(1,7) && j==heatedElementNumber1(1,8)
      q4=w(3)/elementsPerHeater;
  end
 if i==heatedElementNumber1(2,1) && j==heatedElementNumber1(2,2)
      q5=w(3)/elementsPerHeater;
  end
 if i==heatedElementNumber1(2,3) && j==heatedElementNumber1(2,4)
       q6=w(2)/elementsPerHeater;
  end
 if i==heatedElementNumber1(2,5) && j==heatedElementNumber1(2,6)
        q7=w(3)/elementsPerHeater;
  end
```

```
 if i==heatedElementNumber1(2,7) && j==heatedElementNumber1(2,8)
       q8=w(3)/elementsPerHeater;
  end
 if i==heatedElementNumber1(3,1) && j==heatedElementNumber1(3,2)
       q9=w(3)/elementsPerHeater;
   end
  if i==heatedElementNumber1(3,3) && j==heatedElementNumber1(3,4)
       q10=w(2)/elementsPerHeater;
   end
  if i==heatedElementNumber1(3,5) && j==heatedElementNumber1(3,6)
       q11=w(3)/elementsPerHeater;
    end
        qa=q1+q2+q3+q4+q5+q6+q7+q8+q9+q10+q11;

   if i==heatedElementNumber2(1,1) && j==heatedElementNumber2(1,2)
        q12=w(3)/elementsPerHeater;
     end
   if i==heatedElementNumber2(1,3) && j==heatedElementNumber2(1,4)
        q13=w(5)/elementsPerHeater;
  end
 if i==heatedElementNumber2(1,5) && j==heatedElementNumber2(1,6)
        q14=w(7)/elementsPerHeater;
  end
 if i==heatedElementNumber2(2,1) && j==heatedElementNumber2(2,2)
        q15=w(6)/elementsPerHeater;
  end
 if i==heatedElementNumber2(2,3) && j==heatedElementNumber2(2,4)
        q16=w(5)/elementsPerHeater;
  end
 if i==heatedElementNumber2(2,5) && j==heatedElementNumber2(2,6)
        q17=w(7)/elementsPerHeater;
  end
 if i==heatedElementNumber2(3,3) && j==heatedElementNumber2(3,4)
        q18=w(6)/elementsPerHeater;
    end
  if i==heatedElementNumber2(3,5) && j==heatedElementNumber2(3,6)
        q19=w(5)/elementsPerHeater;
    end
        qb=q10+q11+q12+q13+q14+q15+q16+q17+q18+q19+q20;
        Te=T(i,j);          % Temperature of current element;          Qconv=hc*Ai*2*(Te-
Ta);          % Convection (double for both sides)
        if i==1 && j==1             % Corner section
     QL=((T(i,j+1)-Te)*k*Av)/(dxh);      % Conduction from/to left element
           Qb=((T(i+1,j)-Te)*k*Ah)/(dxv);
           u=QL+Qb;
        elseif i==1 && j<C              % bottom edge
        QL=((T(i,j-1)-Te)*k*Av)/(dxh);  % Conduction from/to left element
        Qb=((T(i+1,j)-Te)*k*Ah)/(dxv);
        QR=((T(i,j+1)-Te)*k*Av)/(dxh);
        u=QL+Qb+QR;
```

```
      elseif i==1 && j==C                % Corner section
      QL=((T(i,j-1)-Te)*k*Av)/(dxh);  % Conduction from/to left element
      Qb=((T(i+1,j)-Te)*k*Ah)/(dxv);
      u=QL+Qb;
      elseif i>1 && i<R && j==1          % left edge
      QL=((T(i,j+1)-Te)*k*Av)/(dxh);  % Conduction from/to left element
      Qb=((T(i-1,j)-Te)*k*Ah)/(dxv);
      QT=((T(i+1,j)-Te)*k*Ah)/(dxv);
      u=QL+Qb+QT;
     elseif i>1 && i<R && j>1 && j<C     % Middle section
      QL=((T(i,j-1)-Te)*k*Av)/(dxh);  % Conduction from/to left element
      Qb=((T(i-1,j)-Te)*k*Ah)/(dxv);
      QR=((T(i,j+1)-Te)*k*Av)/(dxh);
      QT=((T(i+1,j)-Te)*k*Ah)/(dxv);
      u=QL+Qb+QR+QT;
     elseif i>1 && i<R && j==C          % right edge
      QL=((T(i,j-1)-Te)*k*Av)/(dxh);  % Conduction from/to left element
      Qb=((T(i-1,j)-Te)*k*Ah)/(dxv);
      QT=((T(i+1,j)-Te)*k*Ah)/(dxv);
      u=QL+Qb+QT;
     elseif i==R && j==1                % Corner section
      QL=((T(i,j+1)-Te)*k*Av)/(dxh);  % Conduction from/to left element
      Qb=((T(i-1,j)-Te)*k*Ah)/(dxv);
      u=QL+Qb;
     elseif i==R && j>1 && j<C          % top edge
      QL=((T(i,j-1)-Te)*k*Av)/(dxh);  % Conduction from/to left element
      QR=((T(i,j+1)-Te)*k*Av)/(dxh);
      Qb=((T(i-1,j)-Te)*k*Ah)/(dxv);
      u=QL+Qb+QR;
      elseif i==R && j==C                % Corner section
      QL=((T(i,j-1)-Te)*k*Av)/(dxh);  % Conduction from/to left element
      Qb=((T(i-1,j)-Te)*k*Ah)/(dxv);
      u=QL+Qb;
       else
          error
       end
       Q=qa+qb+u-Qconv;                  % total Q
       dT=(Q* tsi)/(mi*Cp);
       T(i,j)=Te+dT;

   end
end

if doCompare
   data=TIdata(dataI).data;
   Te=T-data;
   ff(dataI)=sqrt(sum(sum(Te.^2)));
   Tplot(dataI).T=T;
   dataI=dataI+1;
   doCompare=0;
```

```
    end
   xx=[1:11];
   yy=[1:11];
     surf(xx,yy,T);
    xlabel('number of element')
    ylabel('number of elements')
    zlabel('Temperature (\circC)')
    titlestr=sprintf('Simulation progress - %1.1f%%',(E/s)*100);
    title(titlestr)
    drawnow
end
```

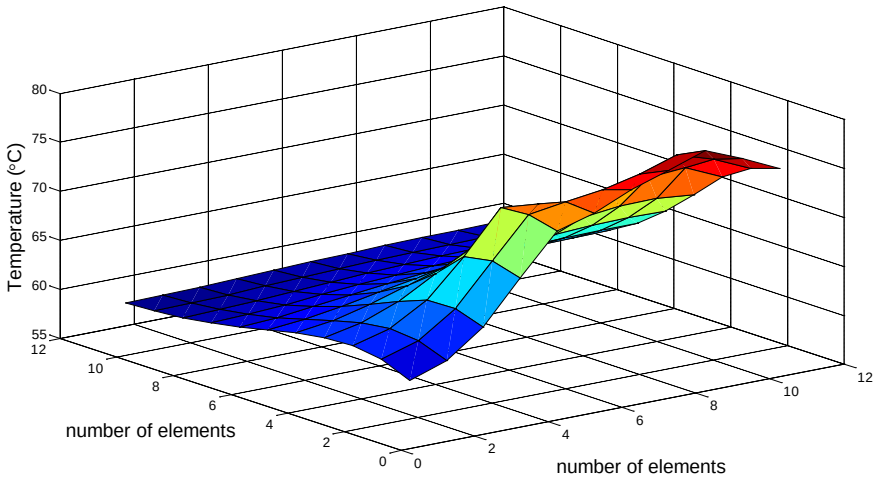

Figure 1-B 2D model of steel pate where two heaters switched on

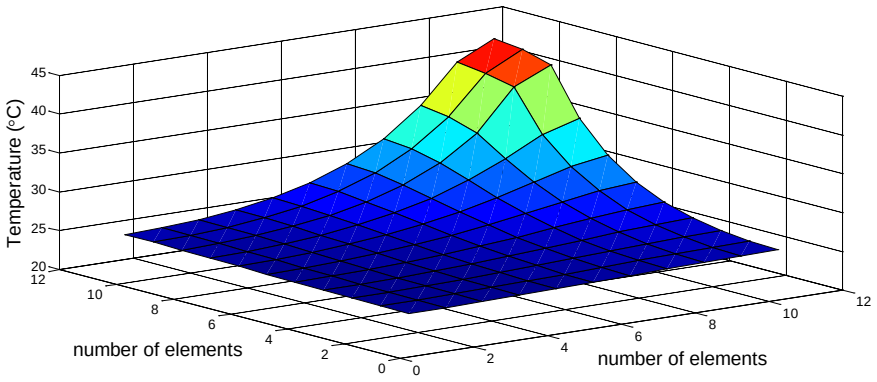

Figure 2-B 2D model of steel pate where one heater switched on